7848-3-Q

HELICAL AND LOG CONICAL HELICAL ANTENNAS LOADED WITH AN ISOTROPIC MATERIAL

Third Quarterly Report
1 August through 31 October 1966

by
George G. Rassweiler

November 1966

A dissertation submitted in partial fulfillment
of the requirements for the degree
of Doctor of Philosophy in
The University of Michigan
1966

Contract No. AF 33(615)-3609
Project 6278, Task 01
O. E. Horton, Project Monitor
AVWE

Air Force Avionics Laboratory
Research and Technology Division
Air Force Systems Command
Wright-Patterson Air Force Base, Ohio

FOREWORD

This is the Third Quarterly Report on a general study of UHF/VHF electrically small antennas. The work includes four tasks involving the following problems.

Task 1: Design of a physically small conical spiral antenna.

Task 2: The use of physically small slot antenna in a 300 MHz array.

Task 3: The use of endfire ferrite rod antennas in the 300 - 1000 MHz frequency range.

Task 4: Study of the feasibility of using new type ferrite antennas at frequencies as low as 30 MHz.

This particular report includes work on Task 1 only. Quarterly Reports 1 and 2 issued under this contract, and future quarterly reports, will treat all four tasks.

PREFACE

The author wishes to express his sincere appreciation to the members of the Doctoral Committee for their helpful criticisms, particularly to the Chairman, Professor John A. M. Lyon for the many hours of helpful advice and encouragement. The author also appreciates the many hours of help from the staff of the Radiation Laboratory, particularly, U. Edward Gilreath for the antenna construction and measurements; Claire F. White for typing the thesis, and Professor Ralph E. Hiatt, Head of the Radiation Laboratory, for making the opportunity possible. Most especially, the author thanks his wife and parents.

HELICAL AND LOG CONICAL HELICAL ANTENNAS LOADED WITH AN ISOTROPIC MATERIAL

George G. Rassweiler

ABSTRACT

The determinental equation for a bifilar tape helix loaded inside with a full core of isotropic material is numerically solved for the complex propagation parameter of the primary current wave as a function of frequency. The results of the tape helix calculation are compared to a simplified slow-wave, inside-loaded sheath helix solution. Both methods show that such an antenna with a small pitch angle ψ has a diameter reduction factor for backward fire radiation of approximately $\sqrt{(1/\mu+1)/(\epsilon+1)}$ where μ and ϵ are the relative permeability and permittivity constants, respectively. Thus, the loading does achieve diameter reduction by slowing the phase velocity of the primary current wave. The log-conical helix is considered as a gradually tapered helix. The effect of dielectric loading is found theoretically to greatly reduce the radiation attenuation rate, making long active zones and small cone angles necessary for complete radiation of the power from the source. The addition of ferrite to the loading causes less reduction in the radiation attenuation, which allows some reduction in antenna length.

Experimental verification with antenna patterns, radiation efficiency, and near field amplitude and phase measurements verify the theoretical diameter and phase velocity reduction calculations; the calculated radiation attenuation rate of a loaded helix is not quantitatively verified experimentally.

TABLE OF CONTENTS

I	INTRODUCTION	1
	1.1 Statement of the Problem	1
	1.2 Loaded Antennas: Review	2
	1.3 Helical Antennas: Review	4
	1.4 Conical Helical Antennas: Review	9
II	LOADED SHEATH HELIX SOURCE-FREE MODES	12
	2.1 Basic Equations: Full Core Loading	12
	2.2 Dispersion Equation Solution	18
	2.3 Asymptotic Cases	18
	2.4 Application to Antennas	23
	2.5 Inside Layer Loading: Sheath Helix	25
	2.6 Limitations of Sheath Solutions	33
III	FULL-CORE-LOADED TAPE HELIX, FREE MODES	34
	3.1 Solution for Constants, Approximate Boundary Conditions	34
	3.2 Resonant Term	41
	3.3 Non-Resonant Remainder	44
	3.4 Numerical Calculation of Tape Dispersion Equation	53
	3.5 Results of the Computer Computation	56
IV	FORMULATION OF A TAPE HELIX WITH A SOURCE	74
	4.1 Formulation of the Inversion Integral	75
	4.2 Contribution of Leaky Wave Poles: Relation to Free Mode Solutions	77
	4.3 Contribution of the Branch Cut Integrals to the Inversion Integral	78
	4.4 Relative Magnitude of Pole Contributions	81
V	EXTENSION TO THE CONICAL HELIX	84
	5.1 Basic Step-wise Approximation: WKB Improvement	84
	5.2 Effect of Antenna Loading on Active Region: Example	85
VI	EXPERIMENTAL RESULTS	87
	6.1 Facilities	87
	6.2 Helix Experiments	89
	6.3 Log-Pyramidal Helix Experiments	104
VII	SUMMARY	115
	7.1 Conclusions	115
	7.2 Original Work Done	116
	7.3 Further Work	117
APPENDIX A: SOLUTION OF TAPE HELIX AMPLITUDE CONSTANTS		118
APPENDIX B: NUMERICAL CALCULATIONS OF MODIFIED BESSEL FUNCTIONS OF COMPLEX ARGUMENT AND INTEGER ORDER		122
APPENDIX C: APPROXIMATE SUMMATION OF A SERIES		129
REFERENCES		131

LIST OF ILLUSTRATIONS

1-1	The Bifilar Log-Conical Helical Antenna	10
2-1	Sheath Helix with a Full Core of Loading Material	13
2-2	k-β Diagram for Helix Antenna	22
2-3	Sheath Helix with an Interior Loading Cylinder	26
2-4	Layer Loading Effectivness	31
3-1	Effect of Dielectric Loading in Dispersion. ψ=12.6°, Δ=. 1, μ=1.	58
3-2	The Effect of Magnetic Loading on Dispersion. ψ=12.6°, Δ=. 1, ϵ=1.	60
3-3	Effect of Dielectric on Dispersion. ψ=12.6°, Δ=. 01, μ=1.	61
3-4	Effect of Magnetic and Dielectric Loading. ψ=12.6°, Δ=. 01.	62
3-5	Effect of Dielectric Loading, ψ=5°, Δ=. 1, μ=1.	63
3-6	Effect of Magnetic and Dielectric Loading. ψ=5°, Δ=. 1.	64
3-7	Effect of Dielectric Loading. ψ=5°, Δ=. 01, μ=1.	65
3-8	Effect of Magnetic and Dielectric Loading. ψ =5°, Δ=. 01.	66
3-9	Effect of Dielectric Loading ψ=25°, Δ=. 1, μ=1.	67
3-10	Effect of Magnetic and Dielectric Loading. ψ=25°, Δ=. 1.	68
3-11	Effect of Dielectric Loading. ψ=25°, Δ=. 01, μ=1.	69
3-12	Effect of Magnetic and Dielectric Loading. ψ=25°, Δ=. 01.	70
3-13	Examples of High Attenuation Leaky Waves Found.	73
4-1	Complex β Plane with Original and Deformed Inversion Contours.	79
6-1	Bifilar 4" dia. Helix with Balsa Wood Core and Cap.	90
6-2	The Bifilar Cylindrical Helix	91
6-3	Loading Diagram: Bifilar Helix No. 213 Layer Loading	92
6-4	Helix with Dielectric Loading. Plots of $\|E_\phi\|^2$	93
6-5	Helix with Dielectric Loading. Plots of $\|E_\theta\|^2$	94
6-6	Helix with Ferrite Loading. Plots of $\|E_\phi\|^2$	95
6-7	Helix with Ferrite Loading. Plots of $\|E_\theta\|^2$	96
6-8	Near Field Amplitude of $\|H_\phi\|$ of Antenna No. 217. Probe Position $\lambda/6$ Above Antenna Surface.	102
6-9	Near Field Amplitude of $\|H_\phi\|$ of Antenna No. 217, with Ferrite Layer. Probe Position $\lambda/5$ Above Antenna Surface	103
6-10	Tapered Loading of Log-Pyramidal Helix No. 223	106
6-11	Tapered Loading on Log-Pyramidal Helix No. 221	107
6-12	Dielectric Loading of Log-Pyramidal Antenna No. 223: Unloaded	109
6-13	Dielectric Loading of Log-Pyramidal Antenna No. 223: Loaded	110
6-14	Measured Phase of Log-Pyramidal Antennas No. 221 and 223 With and Without Loading	112
6-15	Measured Amplitude of Log-Pyramidal Helical Antennas No. 221 and 223 With and Without Loading	113

I

INTRODUCTION

1.1 Statement of the Problem

The problem studied in this dissertation is that of the operation of the bifilar helix and bifilar log-conical antennas fed in 'push-pull' (the current on one wire 180^{o} out of phase with respect to the other wire) and 'loaded' with an isotropic material of arbitrary μ and ϵ. The shape of the loading material is confined to the case of a full-core interior loading and simplified work on interior cylinders of material. The emphasis is on the backward radiation region, where the helix is a useful antenna.

Specifically, it is desired to obtain the current on the loaded antenna. Since the problem at present is too complicated to solve exactly, approximations must be found to the theoretical part and experiments must be performed to verify these results. In the theory, the current on the source-free helix is approximated by a single traveling wave and the problem becomes that of solving for the propagation velocity of this wave, and attenuation of the wave along the helix due to radiation. The conical antenna is treated as a gradually changing helix.

The mathematical models are first used to obtain the source-free mode propagation characteristics of a 'sheath' helix in the presence of the loading material, using asymptotic approximations that are valid only in the waveguide or non-radiating region of operation. An assumption of a straight line k-β characteristic then allows extrapolation into the radiation region. Then the dispersion equation for the more exact tape model is solved, including its complex zeros, which occur in the radiation region and correspond to 'leaky waves'. On the basis of experimental data and previously used theoretical methods, a single leaky current wave is assumed for the purpose of getting the source-free propagation characteristics on the helix. The complex axial propagation constant, β, of this dominant current wave yields both phase and relative amplitude of the current along the antenna, which in turn determines the far field patterns; these patterns are not calculated, but general statements

about them are made from studies of β. Finally, a source problem is formulated which, although not solved exactly, shows the significance of the leaky wave as the dominant pole of an integral expression, and some of the approximations necessary for this representation.

1.2 Loaded Antennas: Review

The term 'loading' is used to refer to the addition of material to an antenna for the purpose of reducing its size while maintaining similar electrical characteristics. In particular it may be desired to preserve the same general far field pattern or perhaps a match of impedance.

A useful concept of the action of such loading material is that the velocity and wavelength of electromagnetic wave propagation are known to decrease in an infinite medium of $\mu\ \epsilon > 1$, where μ and ϵ are relative permeability and permittivity, respectively. This reduction also decreases the dimensions or spacings necessary for various resonances on an antenna in such an infinite medium, as well as in a sufficiently large finite medium. Note that some well-known slow wave structures employ a ferrite or dielectric (Jasik, 1961). For very small antennas compared to a wavelength, the increase of capacitance or inductance by loading forms a more useful concept than the concept of phase velocity.

In reality, the loading medium is finite, and the waves outside the loading material that couple with the antenna cannot be 'loaded' even though the fields inside the material are 'loaded'. Thus, there will be electrical changes for any change in antenna size although a favorable trade-off is possible in some cases. The loading situation can be discussed in three parts, according to whether the antenna is very small, about the same, or much larger than a wavelength.

Loading antennas much smaller than a wavelength is mainly a problem of tuning or cancellation of input reactance, and performance should be compared with that of external tuning with lumped transmission line elements. The loading in this case would be encasement of the antenna by the material. The basic problems of narrow bandwidth and high losses are associated with large reactive

energies stored, regardless of the method of tuning. Loading can also affect radiation resistance to some extent. Radiation resistance is important for small antennas since it must be larger than ohmic losses for reasonable efficiency. Small dipoles loaded by encasement in a material are affected mainly by permittivity, which reduces the radiation resistance, thus making performance worse. Considerable analysis has been made of small loaded dipoles (Adams and Kalafus, 1963; Galejs, 1962; New, 1960; Polk, 1959; Grimes, 1958). Larger dipoles may have a small improvement in radiation resistance due to improved distribution of the current on the dipole. Small loaded loops are mainly affected by permeability, which increases the radiation resistance and thus efficiency (Adams and Kalafus, 1963; Galejs, 1963; New, 1960; Cruzan, 1959; Herman, 1958; Dropkin, 1958; Stewart, 1957; Rumsey and Weeks, 1956; Wait, 1953; Page, 1946). Thus receiving performance can be improved well beyond a dipole of the same size; the ferrite loaded loop is common in transistor radios today. Loading also has been used in cavity-backed slots by simply filling the cavity with material (Adams and Lyon, 1965; Jones, H, 1956; Adams, 1964; Schroeder, 1964; Sharp and Jones, 1962; Brownell and Kendall, 1960; Shanks and Galindo, 1959; Tyras and Held, 1958; Medved, 1957; Angelakos and Korman, 1956; Admiralty Services; Wheeler, 1958). Loading has reduced the resonant size of cavity backed slots, as is easily understood by considering that the TE_{10} mode of an infinitely long rectangular waveguide requires the width of the waveguide to be larger than one-half wavelength in the medium. The wavelength with loading is reduced, thus so may the waveguide size. The cavities are similarly reduced in size by adding material. The far field pattern may be obtained simply by considering the open end of the waveguide as an aperture with an approximately known field. More rigorous analyses in the references cited verify this somewhat intuitive argument. Size reductions of approximately 6 : 1 in each lineal dimension of the cavity, with efficiencies of 25 per cent, have been achieved without severe bandwidth problems (Adams, 1964).

For antennas much larger than a wavelength where high directivities are required, reducing the size while maintaining the same beamwidth requires 'supergain' . Although this is possible, the stored energies increase tremendously which tends to make losses high and bandwidths very small. Hansen (1966) concisely summarizes some of the problems with reducing the size of both very small and large antennas.

For antennas close to a wavelength in at least one dimension, such as helices, loading can vary the size of the antenna without great increase in the reactive stored energy which occurs for the high gain antennas. Therefore, the bandwidths and losses are not greatly increased by loading. In addition, some directivity can still be maintained whereas very small antennas allow no antenna pattern control. In particular, a dimension (such as the helix diameter), which does not affect the antenna pattern greatly, may be made smaller by loading which ensures that the proper phasing of the helix along the axial direction is maintained.

Loading of the broadband antennas such as the helical, log conical helical, log-spiral and log-periodic antennas with material, slow wave structures, or lumped elements, has been reported experimentally (Lyon, et al, 1965a, 1965b, 1965c, 1966; Di Fonzo, 1964; Moore and Beam, 1963; Jones, J., et al, 1960; Stephenson and Mayes, 1963; General Precision, 1962) but little theoretical justification or detailed experimental verification has been made; this report is intended to help fill this gap for material loading of helices and log-conical antennas.

1.3 Helical Antennas: Review

The literature on the helix is very large; only the major bibliographic sources and directly pertinent material will be cited. The literature generally deals with either the waveguide (slow-wave) region of operation or the antenna properties of the helix.

1.3.1 Waveguide (Slow-wave) Approach

Most of the literature deals with the helix as a non-radiating waveguide,

solving the problems of propagation, travelling wave tube interaction impedances, and losses. Good bibliographies appear in Kornhauser (1949); Sensiper (1951, 1955); Harvey (1964); Watkins (1958); Klock (1963) and Walter (1965). The article by Sensiper (1955) is an especially complete, concise, and available review of helical waveguide theory.

The helix is usually approximated by one of three major mathematical models; the 'sheath', the 'tape', or the 'planar' or 'developed' helix models. A little work with a helical coordinate system has also been done. The sheath model assumes a cylinder with an anisotropically conducting surface in the direction of the wire. In other words, current is allowed to flow only in the direction of the wire, and uniformly over the cylindrical surface. No consideration to wire shape or size is given. All modes of propagation are uncoupled due to the uniformity of the boundary conditions in the axial, z, direction. Thus each mode may be considered separately. The sheath helix model has been found to give excellent approximations to the propagation constant of a helix in the slow wave region (Watkins, 1958; Pierce, 1950).

The tape helix model (Sensiper, 1951) replaces the conductor by an infinitely thin, flat tape, of a given small width, S . A round wire size can be approximated by an equivalent tape width; however, wire shape is not considered. In order to satisfy the more difficult boundary conditions of the tape helix, all modes must be used, increasing the difficulty of solution. Because the application of all the boundary conditions leads to very complicated equations, two extremely important steps used in all calculations so far with this model are; to simplify the boundary condition on the tangential electric field, and to assume a current distribution. The simplified boundary condition is either that the tangential E field is required to be zero only on the conductor center line, or a variational expression approximating the boundary condition is used. Both methods are insensitive to the assumed current distribution for narrow conductors.

Methods using an integral equation approach (Klock, 1963; Kogan, 1949, 1959; Phillips, 1950) produce almost the same dispersion equation when similar simplifying assumptions are used. The Russians often use a variation of the tape

model by applying a so-called 'averaged boundary condition' to problems involving thin periodic discontinuities such as this one (Moizhes, 1958; Smirnov, 1958). The method, apparently developed by Kantorovich (1939), replaces the non-uniform boundary conditions with one uniform in z, but includes a term which is logarithmic in the width of the conducting tape. As will be seen later, such a term appears with the other methods of solution as well. The tape model has been found to be more accurate than the sheath helix model for travelling wave tube interaction problems and propagation near the 'forbidden' regions (Klock, 1963; Watkins, 1958, Sensiper, 1951).

The 'plane' or 'developed' helix model is a two-dimensional model where the helix is unwrapped and laid on a plane, with conduction still at an angle $(90^{o}-\psi)$ to the propagation or axial direction, where ψ is the pitch angle. Because of the simplified geometry, more careful investigation of such things as conductor shape (Chu, 1958) and loading (Ash, 1964) may be carried out. The 'planar' or 'developed' helix model appears to be a good approximation when fields are confined to the vicinity of the conductors, as in higher modes or the zeroth mode for helices fairly large with respect to the wavelength. However, in the radiation regions where at least the dominant radiating mode is not at all confined to the conductor region, this model appears to be inaccurate.

Rather than striving for a formal solution to study the problem of a tape helix supporting many modes, Pierce and Tien (1954) have applied the general theory of coupled modes to this problem and successfully showed how the stop bands and pass bands are formed in a wire helix. However, Klock (1963) has shown that the complex leaky mode solutions in the radiation region do not follow this theory, which is basically a waveguide theory.

Although most of the theory of tape helices has been applied to the n=0 mode, there have been a few waveguide studies of the n= -1 mode for travelling wave tubes (Johnson, et al, 1956; Tien, 1954; Jones, E., 1950).

The literature also contains many references on slow wave solutions to the helix problem when a loading material is placed inside or outside. The purpose of this loading was to either support the helices used in travelling wave

tubes, or to slow the axial wave velocity still more than with the helices in air in order to achieve interaction with slow streams of electrons. All three of the major mathematical models of helices have been used in these analyses. These analyses all use the slow wave assumption, which allows the very important simplifying approximation that the radial propagation constants inside and outside the helix are equal. This approximation will be discussed in more detail later. The major differences of the work reported herein is that this approximation is not used for the tape helix, since it is not valid in the fast wave zone.

Solutions for the loaded sheath helix (n=0 mode) have appeared in Johnson (1959); Shestopalov (1958); Unger (1958); Swift and Hook (1958); Morgan (1956); Tien (1963); and Olving (1955). Tape helix solutions with loading material have been studied in Shestopalov (1960); Shestopalov and Kondrat'ev (1959); Shestopalov and Yatsuk (1959); Kirschbaum (1959); Watkins (1954), and Harris (1949). Anisotropic media outside a sheath helix have received considerable attention for attenuators for unwanted travelling wave tubes (Bulgakov, et al, 1960, 1961; Yakimenko and Shestopalov, 1962; Shestopalov and Slyusarskii, 1954; Suhl and Walker, 1954).

1.3.2 Helices as Antennas

The use of the helix as an antenna was developed experimentally quite separately from all the mathematical propagation theories, partly because these theories are waveguide theories, and do not take into account the possibility of radiation. In fact, the so-called 'forbidden' regions of operation in the theory are forbidden only because radiation could take place there, contrary to waveguide assumptions.

There is a basic difference between forward- and backward-radiating helices that is seldom stated in the literature; forward radiation helices are slow-wave antennas that depend upon a truncation to diffract a surface wave into space that would otherwise continue to propagate without radiation. On the other hand, backward wave helical antennas are 'leaky wave' antennas, in that radiation takes place continuously along the antenna causing the current to decay rapidly to zero away from the feed point.

The forward-radiating helix was the first helical antenna developed (Kraus, 1950). Good bibliographies appear in Harvey (1964), Walter (1965), Jasik (1961) and Wong and Thomas (1959). The approach to calculations is either to use experimental data or theoretical helical waveguide formulas to obtain the current phase velocity along the wire (Maclean, 1962; Maclean and Kouyoumjian, 1959; Kraus, 1950). The amplitude of the dominant forward-fire current mode (called T_1 by Kraus) is assumed constant along the helix following considerable experimental evidence (Marsh, 1951). The far fields are then obtained by the usual integral of the current contributions (Fradin, 1961). Similar computations have also been done for a helix loaded with material, while continuing to use the slow wave approximations in the fast wave zone(Shestopalov and Bulgakov, 1961; Shestopalov, et al,1962). Although it will be shown later that higher space harmonics can be represented by these slow wave approximations, the leaky or radiating harmonics cannot be. A more satisfactory mathematical treatment of these far fields of the helices uses a Weiner-Hopf approach (Mikazan, 1960) for a semi-infinite helix; the result is shown to be close to the above methods, however.

Backward wave helices, emphasized in this report, are a more recent discovery, stemming from the wideband log-conical helical antenna. Since the currents of this antenna decay rapidly from the feed point, due to radiation, the methods above fail, since they depended upon a constant current assumption. The rate of decay of the current, as well as its phase velocity, becomes vital in explaining the antenna operation. Again, the basic characteristics of the far field can be predicted from a knowledge of the current; thus far field calculations are not emphasized here.

The important calculations of the backward wave helix antennas in air have been done by Klock (1963) and Patton (1962), with considerable supporting work done in the log-conical helix, to be discussed later. In both of these works, the current decay is not assumed but calculated. Klock's method, which is used in this report, is to numerically find the complex zeros of the determinantal equation which determines the phase velocity of a current wave on the helix. The

zero corresponding to a given current wave then determines the complex propagation constant for this wave, which specifies both amplitude (decay) and phase of this current wave. In all these calculations, the helix line is assumed infinitely long, as in all helical waveguide problems. The complex current wave is then regarded as a 'leaky wave' (to be discussed later) which dominates the near field for some frequencies, including the antenna surface. Patton (1962) solves the Weiner-Hopf problem associated with a semi-infinite bifilar helix in air fed at the end, i.e., the basic source problem. Only the far fields are obtained by this method; the fundamental waves that exist on the helix are not displayed.

1.4 Conical Helical Antennas: Review

The conical helix antenna without loading has been carefully investigated recently; both experimentally (Dyson, 1964; McClelland, 1962; American Electronics Laboratory, 1959; Carrel, 1957; Copeland, 1960) and theoretically (Mittra and Klock, 1966; Timirev, 1958, 1965; Lee, 1960; Hellgren, 1953). Design is still largely based on experimental data. The reference by Mittra and Klock is the most recent of a long series of papers from The University of Illinois which approach the problem as a perturbation of a helix; i. e., a helix with slowly varying diameter as one moves outward on the cone.

To understand why this technique has been successful requires an explanation of the mechanism of radiation of a conical helix. Figure 1-1 shows a typical bifilar (two-wire) conical helix and plots of the near field H (magnetic field) and currents in the conductor. The most important characteristic of this antenna is the active zone, shown in Fig. 1-1; i. e. the region where radiation takes place. Since the radiation of this antenna is in the backward direction with respect to the current phase velocity, the current decays in the forward direction in the active zone due to radiation power loss, as shown in Fig. 1-1. This active zone occurs at roughly one wavelength circumference when no loading is present. As the wavelength is changed, the active zone obviously moves along the conical helix to the new one-wavelength-circumference position.

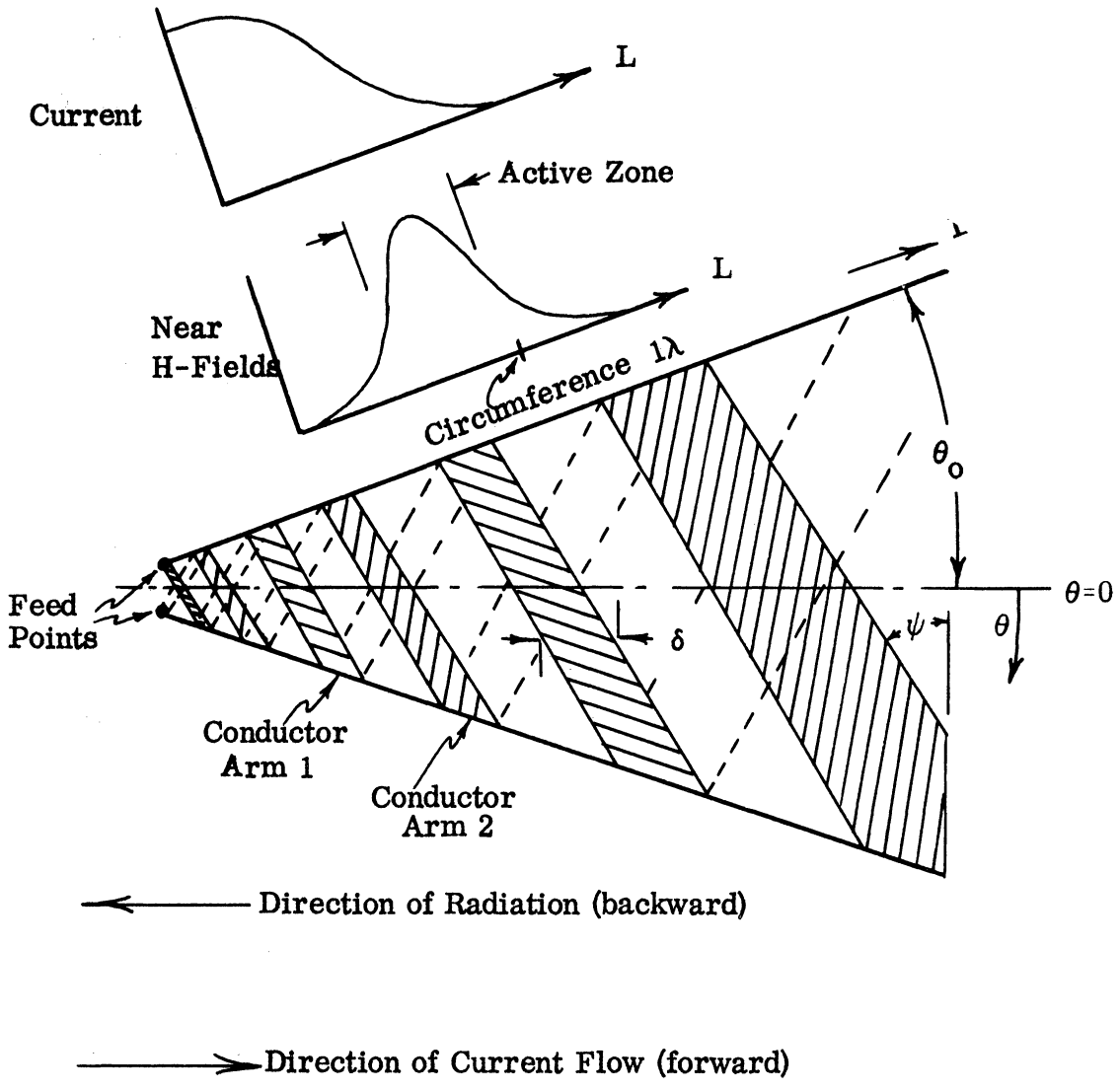

FIG. 1-1: THE BIFILAR LOG-CONICAL HELICAL ANTENNA

This characteristic of 'adapting' to a change in frequency makes possible extremely large bandwidths for this antenna.

It is this active zone region, as contrasted with most antennas that have a fairly uniform current, that makes possible the use of helix antenna theory to explain the conical helix radiation properties. The regions outside the active zone do not contribute to radiation; the active zone is sufficiently short to consider it as a bifilar helix with its backward wave radiation properties. The combination of using a single current wave solution for β and this gradually changing helix concept has successfully explained many of the characteristics of conical helices, even those with large cone angles such as the planar spiral (Mittra and Klock, 1966).

Several attempts to solve the cone problem itself as a source problem using spherical harmonics have not yet yielded usable results for the cone, but have proved useful for the planar spiral (Laxpati and Mittra, 1966). Nevertheless, some modes on a conical helix have been represented in the cited references to theoretical solutions of the conical helix. The approach to conical helical antennas in this report will be via the gradually changing helix.

II

LOADED SHEATH HELIX SOURCE FREE MODES

The solution of a sheath helix that has an isotropic medium inside and free space outside will be performed to compare the eigenvalues of the axial propagation constant, β_o, with those of a sheath helix in free space, with emphasis on the n = -1 mode used in endfire antennas. Other solutions to this problem for the n = 0 mode are in the literature cited. Figure 2-1 shows the geometry of the helix and defines the parameters. The helix is formed of a cylindrical sheath, with an axis along the z axis, that conducts only in the direction at the pitch angle, ψ from a normal to the z direction on the surface. Usually no periodicities in the z direction are employed in the solution, although Klock and Mittra (1963) use periodicity to put the sheath helix dispersion equation in the same general form as the tape helix solution.

2.1 Basic Equations: Full Core Loading

The basic problem of the dispersion equation for free modes on a helix is common in the literature. Following Sensiper (1951) and Watkins (1958), it is known that an arbitrary solution to the vector wave equation in cylindrical coordinates can be derived from the two scalar potentials π and π^* satisfying the same scalar wave equation; in free space,

$$(\nabla^2+k_o^2)\pi = 0 \tag{2.1}$$

$$(\nabla^2+k_o^2)\pi^* = 0 \quad , \qquad k_o^2 = \omega^2\mu_o\epsilon_o \quad , \tag{2.2}$$

for an $e^{j\omega t}$ time dependence (i.e., at one frequency). Actually, the scalars π and π^* are the magnitudes of the Hertzian vector potentials, which have only z components, i.e. $\pi=\pi_z$ and $\pi^*=\pi_z^*$.

The field components of the TE (transverse electric) and TM (transverse magnetic) modes which together can represent an arbitrary field may then be derived from the potentials in the usual way,

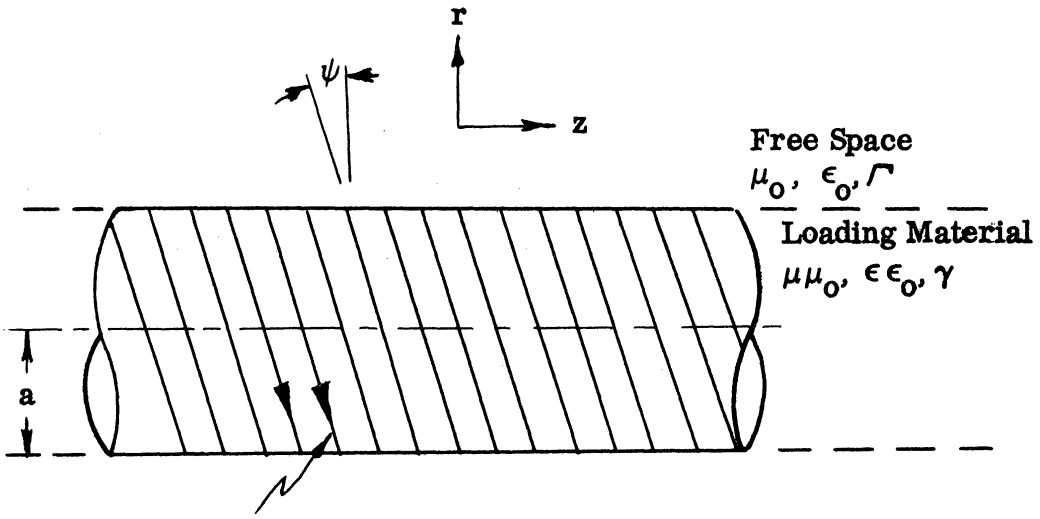

FIG. 2-1: SHEATH HELIX WITH A FULL CORE OF LOADING MATERIAL.

$$E_\phi = \frac{1}{r}\frac{\partial^2 \pi}{\partial z \partial \theta} + j\omega\mu_o \frac{\partial \pi^*}{\partial r} \tag{2.3}$$

$$E_z = \frac{\partial^2 \pi}{\partial z^2} + k_o^2 \pi \tag{2.4}$$

$$H_\phi = -j\omega\epsilon_o \frac{\partial \pi}{\partial r} + \frac{1}{r}\frac{\partial^2 \pi^*}{\partial r \partial \theta} \tag{2.5}$$

$$H_z = \frac{\partial^2 \pi^*}{\partial z^2} + k_o^2 \pi^* \tag{2.6}$$

where E_r and H_r will not be needed. Similarly, for the fields in a medium of relative permeability, μ, and relative permittivity, ϵ, the ϵ_o, μ_o and k_o are replaced by $\epsilon_o\epsilon$, $\mu_o\mu$ and $k_o\sqrt{\mu\epsilon}$, respectively. The solutions to the scalar wave equation in cylindrical coordinates are known to have the form

$$\pi^i = C^i I_n(\gamma_n r)\exp(j\omega t + jn\phi - j\beta_n z) \tag{2.7}$$

$$\pi^o = C^o K_n(\Gamma_n r)\exp(j\omega t + jn\phi - j\beta_n z) \tag{2.8}$$

$$\pi^{*i} = D^i I_n(\gamma_n r)\exp(j\omega t + jn\phi - j\beta_n z) \tag{2.9}$$

$$\pi^{*o} = D^o K_n(\Gamma_n r)\exp(j\omega t + jn\phi - j\beta_n z) \tag{2.10}$$

$n = 0, \pm 1, \pm 2, \ldots$

where

$I_n(\gamma_n r)$, $K_n(\Gamma_n r)$ are modified Bessel functions of nth order, and the primes denote derivatives with respect to argument,

β_n is the propagation constant of the nth mode in the z direction which must be the same, inside and out, for continuity

$\gamma_n = \sqrt{\beta_n^2 - k_o^2\mu\epsilon}$

$\Gamma_n = \sqrt{\beta_n^2 - k_o^2}$

$k_o = \omega\sqrt{\mu_o \epsilon_o}$

ω is the angular frequency of the wave

μ, ϵ are the relative permeability and permittivity of the medium, respectively,

n is the mode number which takes on only integral values because fields in the ϕ direction, for rotations of 2π, are identical,

i, o are subscripts referring to inside and outside fields, respectively,

$C^{o,i}$ and $D^{o,i}$ are arbitrary constants.

The fields derived from these potentials may then be written from (2.3) to (2.6) as below, where the factor $\exp(j\omega t + jn\phi - j\beta_n)$ is understood

$$E_{zn}^{i} = -\gamma_n^2 C_n^i I_n(\gamma_n r) \tag{2.11}$$

$$E_{zn}^{o} = -\Gamma_n^2 C_n^o K_n(\Gamma_n r) \tag{2.12}$$

$$H_{zn}^{i} = -\gamma_n^2 D_n^i I_n(\gamma_n r) \tag{2.13}$$

$$H_{zn}^{o} = -\Gamma_n^2 D_n^o K_n(\Gamma_n r) \tag{2.14}$$

$$E_{\phi n}^{i} = \frac{n\beta_n}{r} C_n^i I_n(\gamma_n r) + j\omega\mu_o\mu\gamma_n D_n^i I_n'(\gamma_n r) \tag{2.15}$$

$$E_{\phi n}^{o} = \frac{n\beta_n}{r} C_n^o K_n(\Gamma_n r) + j\omega\mu_o \Gamma_n D_n^o K_n'(\Gamma_n r) \tag{2.16}$$

$$H_{\phi n}^{i} = -\frac{j\omega\epsilon\epsilon_o\gamma_n}{r} C_n^i I_n'(\gamma_n r) + \frac{n\beta_n}{r} D_n^i I_n(\gamma_n r) \tag{2.17}$$

$$H_{\phi n}^{o} = -\frac{j\omega\epsilon\epsilon_o\Gamma_n}{r} C_n^o K_n'(\Gamma_n r) + \frac{n\beta_n}{r} D_n^o K_n(\Gamma_n r) \tag{2.18}$$

Such modes can be considered separately, since each is orthogonal or uncoupled because

$$\int_0^{2\pi} e^{jn\phi} e^{-jm\phi} d\phi = 0 \qquad n \neq m$$

$$= 2\pi \qquad n = m$$

and the boundary conditions for continuity of the fields are independent of both z and ϕ. Thus the boundary conditions for the continuity of a total field

$$\sum_{n=-\infty}^{\infty} F_n^i(\omega, \epsilon, \mu, a, \beta) e^{jn\phi} = \sum_{m=-\infty}^{\infty} F_m^o(\omega, \epsilon, \mu, a, \beta) e^{jm\phi}$$

may be multiplied on both sides by $e^{-jn\phi}$ and integrated over ϕ from zero to to 2π to give

$$F_n^i = F_n^o \ .$$

Since each mode can be considered separately, a shorthand notation will be employed, omitting the subscript n as well as the arguments of the Bessel functions and the exponential functions common to all fields. The arbitrary constants C and D will also be renormalized to f, g, F and G to obtain Watkin's (1958) form, with small letters used to denote inside fields and constants, capital letters for outside ones.

The fields are then written

$$e_z = f I \tag{2.19}$$

$$E_z = F K \tag{2.20}$$

$$h_z = g I \tag{2.21}$$

$$H_z = G I \tag{2.22}$$

$$e_\phi = -\frac{n\beta}{\gamma^2 r} f I - \frac{j\omega\mu_o}{\gamma} g I' \tag{2.23}$$

$$E_\phi = -\frac{n\beta}{\Gamma^2 r} F K - \frac{j\omega\mu_o}{\Gamma} G K' \tag{2.24}$$

$$h_\phi = \frac{j\omega \epsilon \epsilon_o}{\gamma} f I' - \frac{n\beta}{\gamma^2 r} g I \tag{2.25}$$

$$H_\phi = \frac{j\omega \epsilon_o}{\Gamma} F K' - \frac{n\beta}{\Gamma^2 r} G K \tag{2.26}$$

where it must always be remembered that $K = K_n(\Gamma_n r)$. The boundary conditions may then be applied; they are,

$$e_{//}\Big|_{r=a} = 0 \tag{2.27}$$

$$E_{//}\Big|_{r=a} = 0 \tag{2.28}$$

$$E_\perp = e_\perp\Big|_{r=a} \tag{2.29}$$

$$H_{//} = h_{//}\Big|_{r=a} \tag{2.30}$$

where $e_\perp$, $E_\perp$ are field components perpendicular to the current flow on the cylinder specified by r = a and $e_{//}$, $h_{//}$, $E_{//}$, $H_{//}$ are field components parallel to the current flow. Notice that in this formulation, the magnitude of the current (related to $H_\perp$) does not occur. These boundary conditions may be rewritten in terms of the field components as:

$$e_z - E_z = 0 \tag{2.31}$$

$$e_\phi - E_\phi = 0 \tag{2.32}$$

$$e_z + e_\phi \cot\psi = 0 \tag{2.33}$$

$$h_z + h_\phi \cot\psi - H_z - H_\phi \cot\psi = 0 \tag{2.34}$$

and substituting from (2.19) - (2.26),

$$fI - FK = 0 \tag{2.35}$$

$$f\left(\frac{-\beta n}{\gamma^2 a}\right) I + F\left(\frac{\beta n}{\Gamma^2 a}\right) + g\left(\frac{-j\omega\mu_o\mu}{\gamma}\right) I' + G\left(\frac{j\omega\mu_o}{\Gamma}\right) K' = 0 \tag{2.36}$$

$$fI\left[1-\frac{n\beta}{\gamma^2 a}\cot\psi\right] + g\left(\frac{-j\omega\mu_o\mu}{\gamma}\right)I' \cot\psi = 0 \qquad (2.37)$$

$$fI'\frac{j\omega\epsilon\epsilon_o}{\gamma}\cot\psi + F\left(\frac{-j\omega\epsilon_o}{\Gamma}\right)K'\cot\psi +$$

$$+gI\left[1-\frac{n\beta}{\gamma^2 a}\cot\psi\right] + GK\left[-1+\frac{n\beta}{\Gamma^2 a}\cot\psi\right] = 0 \qquad (2.38)$$

2.2 Dispersion Equation Solution

Four homogeneous equations with five unknowns must be solved. In order for a solution to exist, the determinant of these equations must be zero. The resulting determinant expresses the relation between β and k. After some algebra, the equation is

$$\frac{K'I'}{KI} = \frac{-\left[\gamma^2 a^2 - n\beta a\cot\psi\right]^2}{C^2 k^2 a^2 \gamma^2 a^2 \cot^2\psi} \qquad (2.39)$$

$$C^2 = \frac{\frac{\gamma}{\Gamma}\frac{K'}{K} - \epsilon\frac{I'}{I}}{\frac{1}{\mu}\frac{K'}{K} - \frac{\gamma^3}{\Gamma^3}\frac{I'}{I}\left[\frac{\Gamma^2 a - n\beta a\cot\psi}{\gamma^2 a - n\beta a\cot\psi}\right]} \quad . \qquad (2.40)$$

Equations (2.39) and (2.40) represent the general solution for propagation constant β vs k_o of an arbitrary mode of a sheath helix fully loaded inside the helix with an isotropic material.

2.3 Asymptotic Cases

The most simple limiting case of this rather complicated equation is when a slow wave region is encountered; that is, when $\beta = \frac{\omega}{v} >> k_o\sqrt{\mu\epsilon} \geq k_o$ where v is the velocity of propagation in the nth mode in the z direction corresponding to the propagation constant β. In this case

$$\gamma \cong \Gamma \cong \beta \qquad (2.41)$$

since

$$\gamma = \sqrt{\beta^2 - k_o^2 \mu\epsilon}$$

and

$$\Gamma = \sqrt{\beta^2 - k_o^2}$$

and the square roots are both dominated by β. In this case

$$C^2 \cong \frac{\frac{K'}{K}\frac{I}{I'} - \epsilon}{\frac{1}{\mu}\frac{K'}{K}\frac{I}{I'} - 1} \quad . \tag{2.42}$$

To further see the value of C, it is convenient to look at the asymptotic approximations to $I_n(\gamma_n a)$ and $K_n(\Gamma_n a)$. For large arguments

$$I_n(z) \sim \frac{e^z}{\sqrt{2\pi z}} \tag{2.43}$$

$$I_n'(z) \sim \frac{e^z}{\sqrt{2\pi z}} \tag{2.44}$$

$$K_n(z) \sim \sqrt{\frac{\pi}{2z}}\, e^{-z} \tag{2.45}$$

$$K_n'(z) \sim -\sqrt{\frac{\pi}{2z}}\, e^{-z} \quad . \tag{2.46}$$

Thus, if $\gamma_n a$ and $\Gamma_n a$ are large, as they are in much of the slow wave region for μ and ϵ not too large,

$$\frac{K'I}{KI'} \cong -1$$

and

$$C^2 \cong \frac{1+\epsilon}{1+\frac{1}{\mu}}$$

if

$$\beta a \cong \Gamma a \cong \gamma a \gg ka > k_o a \,, \quad ka \cong 1 \quad , \; k = k_o\sqrt{\mu\epsilon} \,.$$

The last approximation for $ka \cong 1$ follows from the fact that an antenna radiating in the endfire mode always has about this normalized radius, as will be seen later.

This large argument approximation is the only one available for the n = 0 mode and has often been applied before, as previously referenced. In the present case, however, the n = -1 mode is the important one for the endfire antenna use. Sensiper (1951), Watkins (1958), and many others have often used the large order asymptotic approximations for the calculations of a helix in free space. They are

$$I_n(nz) \sim \frac{1}{\sqrt{2\pi n}} \frac{e^{n\xi}}{u} \tag{2.47}$$

$$I_n'(nz) \sim \frac{1}{\sqrt{2\pi n}} \frac{u}{z} e^{n\xi} \tag{2.48}$$

$$K_n(nz) \sim \sqrt{\frac{\pi}{2n}} \frac{e^{-n\xi}}{u} \tag{2.49}$$

$$K_n'(nz) \sim -\sqrt{\frac{\pi}{2n}} \frac{u}{z} e^{-n\xi} \tag{2.50}$$

where

$$\xi = \sqrt{1+z^2} + \ell n \frac{z}{1+\sqrt{1+z^2}}$$

$$u = (1+z^2)^{.25}$$

$$n \gg 1, \text{angle}(z) < \frac{1}{2}\pi \quad .$$

Thus, for n large, regardless of z

$$\frac{K'I}{KI'} \cong -1$$

$$C^2 \cong \frac{1+\epsilon}{1+\frac{1}{\mu}} \quad . \tag{2.51}$$

Most important, even for $n = \pm 1$, it has been found numerically that the approximations are quite accurate even for small z (Watkins, 1958) and are far more accurate for larger arguments. Thus for the loaded sheath $|n| \geq 1$ mode, (2.51) is a good approximation for all real arguments. The author has found it much poorer for arbitrary complex argument, especially near $z \geq \pm j$. Thus, it should be recognized that near the fast wave region, particularly if $\mu\epsilon \gg 1$, γ is imaginary and the Bessel function $J_n(-j\gamma_n r)$, rather than $I_n(\gamma_n r)$, governs

the fields inside. In this region, the above asymptotic approximations do not apply. Extrapolation through this region is used herein from the slow wave region $\beta > k_o \mu\epsilon$ for the sheath solution. Later, the tape helix will be solved exactly.

An additional importance of (2.51) is that all higher order modes follow this behavior. In later tape calculations, the higher order modes will be found to be important.

The meaning of C becomes clear from comparing the dispersion equation (2.39) to that of a helix in free space, $\mu = \epsilon = C$. This equation with C = 1 is identical to Watkins' (1958) solution for a free space sheath helix, thus providing a check of (2.39). For $C \neq 1$, the slow wave assumptions (2.41) may be applied to the dispersion equation (2.39), yielding , for n = -1 and $\beta = \beta_{-1}$,

$$(ka)^2 = \frac{-K_{-1}(\beta a)I_{-1}(\beta a)}{C^2 K'_{-1}(\beta a)I'_{-1}(\beta a)} \frac{\left[\beta a + \cot\psi\right]^2}{\cot^2\psi} \tag{2.52}$$

where the solution $(\beta a) = 0$ has been ignored in dividing the top and bottom by βa. From this equation, it may be seen that for a fixed β (such as one required for endfire radiation), the size-frequency parameter, ka, is smaller when C is large due to loading. A much more simplified form of (2.51) is obtained by using the large argument asymptotic expansions (2.43) - (2.46)

$$\frac{-K_{-1}(\beta a)I_{-1}(\beta a)}{K'_{-1}I'_{-1}(\beta a)} \cong 1 \tag{2.53}$$

yielding,

$$ka \cong \frac{\beta_{-1} a \tan\psi + 1}{C} \quad . \tag{2.54}$$

This equation is a straight line on the k-β diagram shown in Fig. 2-2, whose slope is inversely proportional to C; i.e. for a given β_{-1}, fixed by the desired radiation pattern, (ka) is proportional to the reduction factor,

$$\frac{1}{C} = \sqrt{\frac{1 + 1/\mu}{1 + \epsilon}} \quad . \tag{2.55}$$

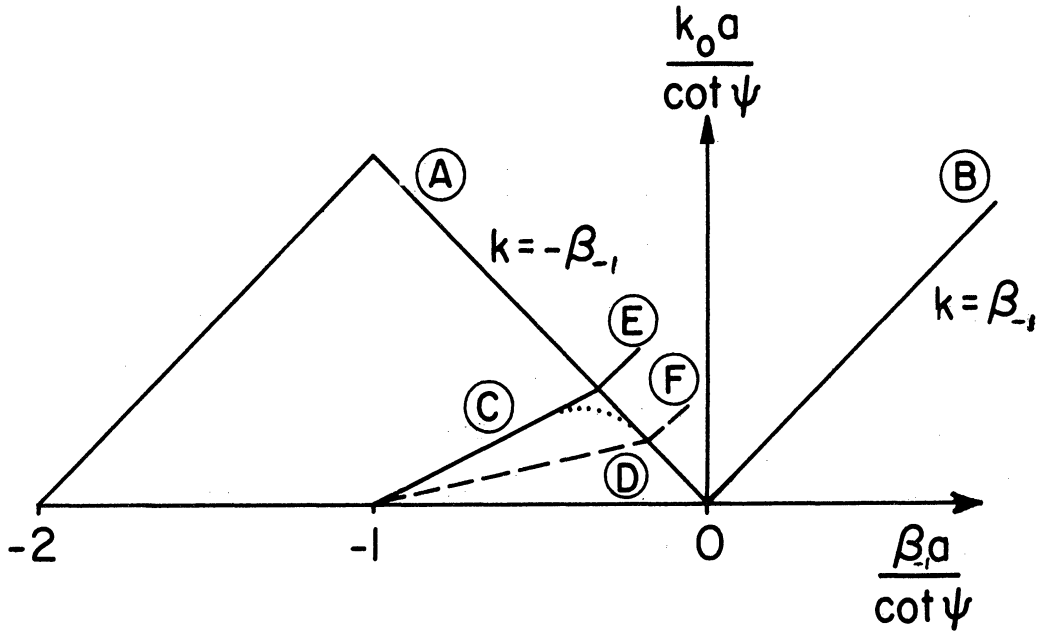

FIG. 2-2: k-β DIAGRAM FOR HELIX ANTENNA.
A = locus of backward plane wave. B = locus of forward plane wave. C = dispersion curves for typical slow-wave, unloaded helix. D = dispersion curve for typical slow-wave, loaded helix. E = radiation region for unloaded helix. F = radiation region for loaded helix.

2.4 Application to Antennas

To apply the above reduction in size to an antenna actually requires a few more assumptions that are most clearly illustrated by a k-β diagram, such as Fig. 2-2. In this typical figure, k_o is plotted vs β_{-1} from an equation similar to (2.39), and is frequently called a dispersion curve. In addition, several diagonal lines are plotted corresponding to $k_o = |\beta_{-1}|$; on these lines, the axial phase velocity of the wave is equal to the speed of light, which is known to be approximately the speed necessary for efficient radiation of the wave travelling on the helix.

In Fig. 2-2, it should be noted that the dispersion curve for the sheath helix in the slow wave (large β_{-1}) region has a smaller $k_o a$ for a given $\beta_{-1} a$ and a smaller slope when loaded than unloaded, as just discussed. However, as the dispersion curve nears the $k = -\beta_{-1}$ line (axial propagation in the negative z direction, or 'backward' at the speed of light) the curve drops down to the origin. This affect is due to the waveguide assumption that there should be no radiation; i.e., that β_{-1} must remain real.

The waveguide assumption of no radiation does not apply to this problem. The sheath helix in air with additional assumptions of periodicity has been shown to have complex solutions for the propagation constant (Klock and Mittra, 1963) corresponding to a 'leaky wave' or continuously radiating current. These complex solutions have k-β_r diagrams (where β_r is the real part of β) that continue rather close to the straight line asymptotic right into the fast wave region, as shown by the dashed lines in Fig. 2-2. The more accurate tape helix model to be discussed later has very similar solutions for complex β that come increasingly close to this straight line asymptote with decreasing tape width. The use of 'engineering solutions' of the helix as the straight asymptotic line continued from the slow wave region straight through the fast wave region (Maclean, 1962) is based on these complex solutions. Since the tape helix solution is more accurate, further discussion of these complex solutions will be postponed until the tape helix section.

If it is assumed that in the loaded helix solution, this straight line behavior from the slow to the fast wave region continues to exist, then the reduction in slope in the slow wave region actually would correspond to a reduction in the size of a loaded helix antenna that would have the necessary critical $\beta = -k$ needed for radiation. More exactly, the nominal reduction would be given by the intersection of the straight line dispersion extrapolation with the $k = -\beta$ line (Hong, 1965). The dispersion equation of the tape helix in air is known (Dyson, 1964; Klock, 1963) to be approximately

$$ka = \beta_o a \sin\psi$$

where, as will be shown in the tape helix section $\beta_n = \beta_o \pm n \cot\psi$. Thus, the dispersion equation for the loaded helix, with the assumptions above, should have the same slope except for the reduction factor (2.55), which yields

$$k_o a = \sqrt{\frac{1+1/\mu}{1+\epsilon}}\ \beta_o a \sin\psi \quad . \tag{2.56}$$

The intersection with the $k = -\beta$ line then gives

$$k_o a = \frac{\sqrt{\frac{1+1/\mu}{1+\epsilon}}\cos\psi}{1+\sqrt{\frac{1+1/\mu}{1+\epsilon}}\sin\psi} \tag{2.57}$$

which for small ψ is

$$k_o a \cong \sqrt{\frac{1+1/\mu}{1+\epsilon}} = \frac{1}{C} \tag{2.58}$$

as the relative size of the loaded helix at the nominal 'radiation point'

The behavior of the transverse propagation constants γ and Γ, is fixed for a given k-β variation and loading; however, their behavior gives a good physical insight to the mechanism of radiation. For slow wave propagation, both γ and Γ are large, causing sharp decay of the fields away from the helix surface, as seen from the asymptotic behavior (2.43 and 2.45) of $I_n(\gamma_a)$ and $K_n(\Gamma_a)$ which describe the radial behavior of the fields. This rapid decay of

the fields is a characteristic of 'tightly bound' non-radiating surface waves on all guided wave structures. On the other hand, as $\beta_n \to k$ near the radiation zone, $\Gamma_n \to 0$, which indicates that the fields decay slowly, and extend to great radial distances from the helix. This is characteristic of a 'loosely-coupled' wave that can radiate most of its power upon encountering even a small discontinuity. Since the radial variation of the fields is small and the axial phase velocity is close to the speed of light, the wave resembles a plane wave, allowing the physically intuitive picture of the helix wave 'coupling' well to a free space plane wave containing the radiated energy. For the helix in air, the fields inside the helix are also slowly varying. However, when a loading material is inserted inside the helix, the fields of the n = -1 mode near the radiation zone resemble the H_{11} hybrid mode of the dielectric rod antenna, which is described by $J_1(-j\gamma r)$ inside, and $K_1(\Gamma r)$ outside the helix for the waveguide region of operation. When $\Gamma \to 0$, as in the radiation case, γ may be large and imaginary, so that the fields inside the loading still resemble those of waveguide propagation. In particular, the energy inside the helix is concentrated close to the helix surface. It is also possible that a waveguide effect could carry some of the energy past the intended radiation zone without radiation.

2.5 Inside Layer Loading: Sheath Helix

As another workable problem, the sheath helix with a cylinder layer of isotropic loading material lends itself to calculation. The problem of layer loading is important because often the weight of a full-core loading must be decreased. Similar problems for outside layers for the n = 0 mode have been studied (Swift and Hook, 1958).

Since this problem is more complicated than the full-core problem, the slow wave assumption will be made at the outset; $\gamma_n \cong \Gamma_n \cong \beta \cong \gamma^{(3)}$, where $\gamma^{(3)}$ is the γ inside the loading cylinder in the central air core. The problem will be done with the same notation as the first, except for the new innermost region 3, Fig. 2-3, which has $\gamma^{(3)} = \gamma^{(2)} = \gamma^{(1)} = \Gamma = \beta$, $\epsilon_3 = \epsilon_0$, $\mu_3 = \mu_0$. If the notation $E^{(1)} = E$, $E^{(2)} = e$, $E^{(3)} = E^{(3)}$ is used for the E fields and similarly for the H fields,

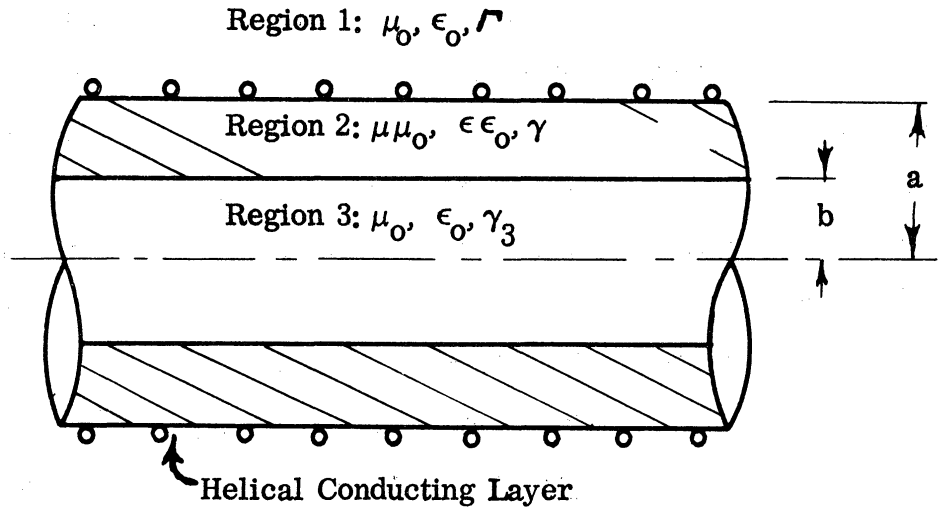

FIG. 2-3: SHEATH HELIX WITH AN INTERIOR LOADING CYLINDER.

the fields can be written in the three regions as

$$E_z = FK \qquad \text{(region 1)} \tag{2.59}$$

$$e_z = f(I+C_1K) \qquad \text{(region 2)} \tag{2.60}$$

$$E_z^{(3)} = F^{(3)}I \qquad \text{(region 3)} \tag{2.61}$$

$$H_z = GK \tag{2.62}$$

$$h_z = g(I+C_2K) \tag{2.63}$$

$$H_z^{(3)} = G^{(3)}I \tag{2.64}$$

$$E_\phi = F\left(\frac{-n\beta}{\Gamma^2_r}\right)K+G\left(\frac{-j\omega\mu_o}{\Gamma}\right)K' \tag{2.65}$$

$$e_\phi = -\frac{fn\beta}{\Gamma^2_r}(I+C_2K)-g\frac{j\omega\mu\mu_o}{\Gamma}(I'+C_2K') \tag{2.66}$$

$$E_\phi^{(3)} = F^{(3)}\left(\frac{-n\beta}{\Gamma^2_r}\right)I+G^{(3)}\left(\frac{-j\omega\mu_o}{\Gamma}\right)I' \tag{2.67}$$

$$H_\phi = F\frac{j\omega\epsilon_o}{\Gamma}K'+G\left(\frac{-n\beta}{\Gamma^2_r}\right)K \tag{2.68}$$

$$h_\phi = f\frac{j\omega\epsilon\epsilon_o}{\Gamma}(I'+C_1K')-g\frac{n\beta}{\Gamma^2_r}(I+C_2K) \tag{2.69}$$

$$H_\phi^{(3)} = F^{(3)}\frac{j\omega\epsilon_o}{\Gamma}I'+G^{(3)}\left(\frac{-n\beta}{\Gamma^2_r}\right)I \quad . \tag{2.70}$$

The constants C_1 and C_2 can first be calculated from the boundary conditions at $r = b$, the inside dielectric boundary, by employing the boundary conditions for the continuity of the tangential components of the fields

$$e_z = E_z^{(3)} \tag{2.71}$$

$$e_\phi = E_\phi^{(3)} \tag{2.72}$$

$$h_z = H_z^{(3)} \tag{2.73}$$

$$h_\phi = H_\phi^{(3)} \tag{2.74}$$

Substiting from (2.59) - (2.70), and eliminating $F^{(3)}$ and $G^{(3)}$, after some algebra, the constants C_1 and C_2 are

$$C_1 = -\frac{I(\xi)}{K(\xi)}\left[1-\frac{\epsilon\left(1-\frac{K'(\xi)I(\xi)}{K(\xi)I'(\xi)}\right)}{\left(1-\epsilon\frac{K'(\xi)I(\xi)}{K(\xi)I'(\xi)}\right)}\right] \tag{2.75}$$

$$C_2 = -\frac{I(\xi)}{K(\xi)}\left[1-\mu\frac{\left(1-\frac{K'(\xi)I(\xi)}{K(\xi)I'(\xi)}\right)}{\left(1-\mu\frac{K'(\xi)I(\xi)}{K(\xi)I'(\xi)}\right)}\right] \tag{2.76}$$

where $\xi = \gamma_n b$. Using the asymptotic approximations for large n (2.53), as well as the slow wave approximation $\beta \gg k_o\mu\epsilon$

$$C_1 \cong -\frac{I(\xi)}{K(\xi)}\frac{(1-\epsilon)}{(1+\epsilon)} \tag{2.77}$$

$$C_2 \cong -\frac{I(\xi)}{K(\xi)}\frac{(1-\mu)}{(1+\mu)} \quad . \tag{2.78}$$

The algebra for the original problem with boundary conditions at r = a (2.63) - (2.66) can be written similarly to the full-core problem, except that $(I+C_1K)$ replaces (I) 'inside' (region 2) for e_z and $(I+C_2K)$ replaces (I) inside for h_z as shown in (2.59) - (2.70). Substituting into the same sheath helix boundary conditions (2.31) - (2.34), setting the determinant of the four homogeneous equations equal to zero as before, the resulting dispersion equation is, after some algebra

$$\left.\frac{K'I'}{KI}\right|_{r=a} = \frac{-\left[\beta^2a^2-n\beta a\cot\psi\right]^2}{C_\ell^2k^2a^2\beta^2a^2\cot^2\psi} \tag{2.79}$$

where

$$C_\ell^2 = \frac{IK'}{I'K}\left\{\frac{1-\epsilon\left(\frac{I'+C_1K'}{I+C_1K}\right)\frac{K}{K'}}{\frac{1}{\mu}\frac{K'}{K}\left(\frac{I+C_2K}{I'+C_2K'}\right)-1}\right\}\Bigg|_{r=a} \qquad (2.80)$$

To verify that this constant C_ℓ approaches C as $b \to 0$, as should be the case, first note that

$$\frac{I_n(z)}{K_n(z)} \sim \frac{\left(\frac{1}{2}z\right)^{2n}}{n!\,(n-1)!} \qquad (\text{as } z \to 0) \qquad (2.81)$$

$$\frac{K_n'(z)I_n(z)}{K_n(z)I_n'(z)} \sim -1 \qquad (n \geq 1) \quad (z \to 0) \qquad (2.82)$$

thus

$$\lim_{b \to 0} C_1 = 0 \quad ; \quad \lim_{b \to 0} C_2 = 0 \qquad (2.83)$$

which gives

$$C_\ell^2 = \frac{1+\epsilon}{\frac{1}{\mu}+1} = C^2 \qquad (2.84)$$

as it should for the full core case .

For the special case $a \approx b \gg 0$, the asymptotic expansions for large argument may be employed to obtain simplifed formulas. Thus, in the numerator of (2.80)

$$C_3 \equiv \left(\frac{I'+C_1K'}{I+C_1K}\right)\frac{K}{K'} = \frac{1-\frac{I_n(\gamma_n a)K_n'(\gamma_n b)}{K_n(\gamma_n a)I_n'(\gamma_n b)}\left(\frac{1-\epsilon}{1+\epsilon}\right)}{1-\frac{I_n(\gamma_n a)K_n(\gamma_n b)}{K_n(\gamma_n a)I_n(\gamma_n b)}\left(\frac{1-\epsilon}{1+\epsilon}\right)} \qquad (2.85)$$

However, from the large argument asymptotic forms

$$\frac{I_n(\gamma_n a)K_n(\gamma_n b)}{K_n(\gamma_n a)I_n(\gamma_n b)} \sim e^{-2\gamma_n(b-a)} \tag{2.86}$$

$$\frac{I_n(\gamma_n a)K_n'(\gamma_n b)}{K_n(\gamma_n a)I_n'(\gamma_n b)} \sim e^{-2\gamma_n(b-a)} \tag{2.87}$$

Thus, (2.85) becomes

$$C_3 = \frac{1+\frac{(1-\epsilon)}{(1+\epsilon)}\, e^{-2\beta_n(b-a)}}{1-\frac{(1-\epsilon)}{(1+\epsilon)}\, e^{-2\beta_n(b-a)}} \tag{2.88}$$

Similarly,

$$C_4 \equiv \frac{K'(I+C_2K)}{K(I'+C_2K')} \cong \frac{1-\frac{(1-\mu)}{(1+\mu)}\, e^{-2\beta_n(b-a)}}{1+\frac{(1-\mu)}{(1+\mu)}\, e^{-2\beta_n(b-a)}} \quad . \tag{2.89}$$

The dispersion equation reduction constant C_ℓ then becomes approximately,

$$C_\ell^2 \cong \frac{1+\epsilon\, C_3}{1+\frac{1}{\mu}\, C_4} \tag{2.90}$$

The constants C_3 and C_4 then may be interpreted as 'effectiveness' constants of the ϵ and μ, respectively, relative to full core loading. These effectiveness constants are functions only of the ϵ or μ they multiply as well as β_n. The entire equation (2.79) could, of course, be studied numerically; however, it is illuminating to use a perturbation method for thick layers, by assuming $\beta \cong \beta_{fc}$ (full core), and to study the effectiveness constant vs thickness for β_n. Figure 2-4 plots layer effectivness of ϵ vs normalized layer thickness, $\beta_n(b-a)$, for the nth modes, with the restriction that $|n|$ must be very small compared to $\beta_n b$ and $\beta_n a$ (in our case, n = -1). The correction factor $1/C_4$ for $1/\mu$ is of

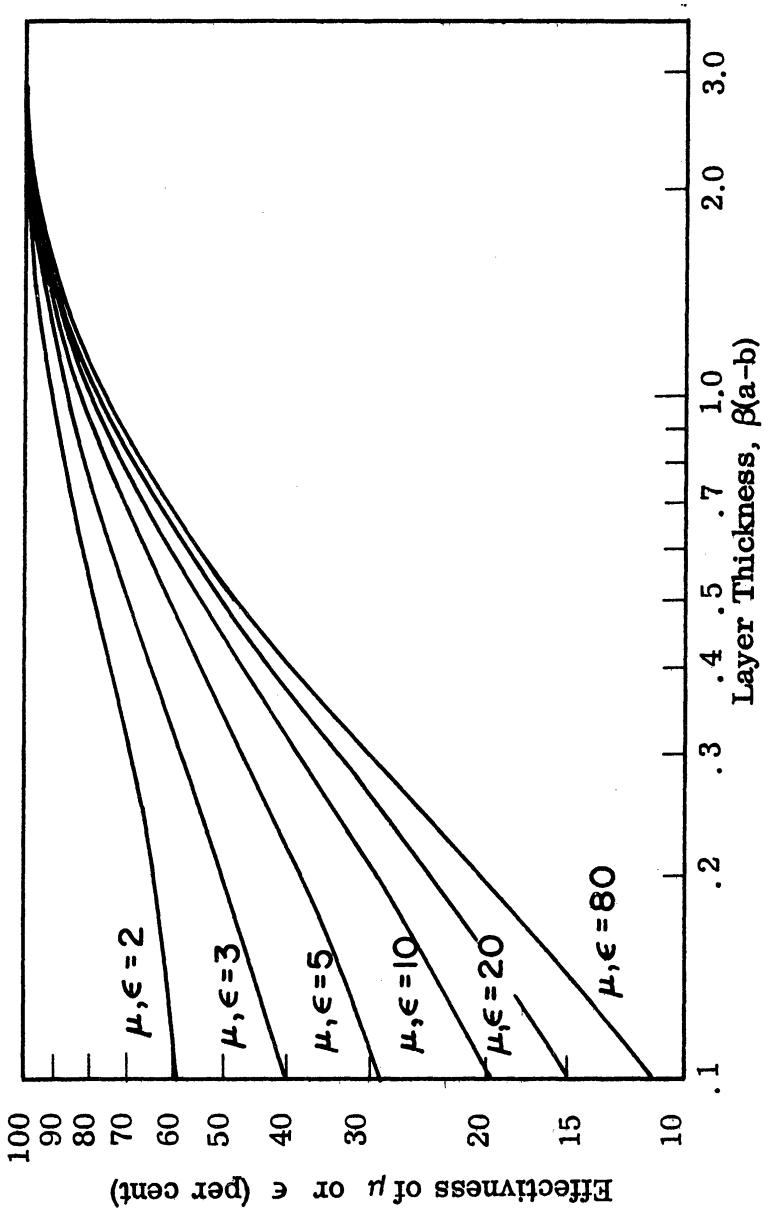

FIG. 2-4: LAYER LOADING EFFECTIVENESS.

the same form as C_3 and the same graph may be used for it.

To use Fig. 2-4, for example, note that for μ or ϵ less than 5, an effectiveness of greater than 90 per cent may be achieved with a normalized layer thickness $\beta_n(b-a) > 1.5$. To relate this to actual layer thickness for a ferrite powder on this project

$$\mu = 2.2\,; \qquad \epsilon = 3.8; \qquad C = \sqrt{\frac{1+\epsilon}{1+\frac{1}{\mu}}} \cong 1.7\,; \psi = 6^{o}\,,$$

and from the known approximate relation between β and k_o (2.56), using all of the assumptions discussed with this equation previously for the extrapolation of a sheath helix solution to a tape helix solution,

$$\beta_o = \frac{k_o C}{\sin\psi} \quad .$$

In the slow wave region at (for example) ka = .5 ,

$$\beta_{-1} = \beta_o \cong \frac{2\pi}{\lambda} \frac{C}{\sin\psi} \cong \frac{100}{\lambda}$$

Since

$$\beta_{-1}(a-b) \approx 1.5 \quad ,$$

from the graph, as stated above,

$$\frac{a-b}{\lambda} \approx \frac{1.5}{100} = 0.015$$

for 90 per cent layer effectivness. It has been verified experimentally (Chapter V) that such a layer can reduce the helix at least approximately as well as full core loading.

For additional accuracy in this perturbation method, β_n may be successfully re-estimated from the computed effectiveness, each time followed by a re-estimate of effectivness. Convergence is governed by the theory of solution of equations by iteration.

It may be verified that as b → a, that is, as the loading material thickness goes to zero,

$$\lim_{b \to a} C_3 \to 1/\epsilon \quad ; \quad \lim_{b \to a} C_4 \to \mu \quad ; \quad \lim_{b \to a} C_\ell \to 1$$

and the dispersion equation becomes that of a helix in free space.

2.6 Limitations of Sheath Solutions

The sheath solution for a 'dominant' sheath mode has several difficulties. Most important is that the assumption of a single dominant field distribution of the form exp $(-j\phi)$ for determining β_{-1} is an incorrect assumption, as will be seen later. The far field is determined by a single (near field) sheath mode on an actual helix, but an accurate near field representation requires additional modes. Another serious limitation is the assumption of a straight line extrapolation from the slow wave region $\beta > k_0 \mu \epsilon$. However, justification from the tape solution to be discussed next provides a much firmer reason for initially studying new configurations by this sheath method. The sheath helix is a very simple calculation. It could be extended to multiple layers of material, inside and out. For the n=0 mode, some cases have been solved by Swift and Hook (1958). The large (argument) asymptotes of the n=0 solutions may have behavior similar to the higher order modes. Similar calculations for multiple dielectric layers without a helix are found in Barnett (1963).

III

FULL-CORE-LOADED TAPE HELIX, FREE MODES

3.1 Solution for Constants, Approximate Boundary Conditions

The same notation will be used as for the full-core-loaded sheath helix. The fields for each spatial Fourier harmonic (sheath mode) are written the same. The major difference is in the inhomogeneous boundary conditions, different where the conductor exists and where it does not. Since the boundary conditions on ϕ are a function of z, the orthogonality argument used in the sheath helix case is not valid; i.e., the space harmonics are not orthogonal but coupled to one another in a tape helix. To satisfy one of the boundary conditions, the sum of all space harmonics must be used. Thus these harmonics cannot be called modes, or complete solutions, of propagation on a tape helix, as they were for the sheath helix.

The boundary conditions for the case of the tape helix are,

$$E_z^{(0)}\Big|_{r=a} = E^{(i)}\Big|_{r=a} \tag{3.1}$$

$$E_\phi^{(0)}\Big|_{r=a} = E_\phi^{(i)}\Big|_{r=a} \tag{3.2}$$

$$H_z^{(i)} - H_z^{(0)} = J_\phi \qquad \text{(defined as zero between conductors)} \tag{3.3}$$

$$H_\phi^{(0)} - H_\phi^{(i)} = J_z \qquad \text{(defined as zero between conductors)} \tag{3.4}$$

$$E_z^{(0)} = E_z^{(i)} = E_\phi^{(0)} = E_\phi^{(i)} = 0 \qquad \text{(on conductor)} \tag{3.5}$$

where, as before, $E_{z,\phi}$ and $H_{z,\phi}$ are components of the electric and magnetic fields, respectively, and $J_{\phi,z}$ are components of the current density on the conducting tape. In principle, the above boundary conditions completely specify a problem, which would have a unique solution for J, E and H; however, in

attempting to solve the equations exactly by expansion in terms of space harmonics, an infinite order determinant arises from equating a sum of modes to zero in (3.5). As mentioned in the Introduction, approximation methods exist for finding the β vs k dispersion equation for this problem that have had considerable success in the past for unloaded helices in both the slow and fast wave (radiation) zones, and for loaded helices in the slow wave zones; these methods will applied herein to the loaded helix in the fast wave zone, following Shestopalov's (1961) loaded slow wave solution and Klock's (1963) unloaded fast wave solution.

An approximate solution to the problem of finding the β vs k is to assume a single propagating current wave with an unknown β and an assumed distribution on the tape. With additional complexity, more than one wave could be assumed, of course. The boundary conditions (3.1) - (3.4) are then used to eliminate the unknown constants of the potentials, as in the sheath problem, having the fields expressed in terms of the assumed current, which in turn is a function of β and k. The remaining boundary condition (3.5) is replaced by an approximation to obtain β vs k; either a variational expression is used, or $E_{//}$ (the component of E parallel to the tape) is required to be zero on the center line of the tape. For an expression variational in β with respect to current distribution,

$$\int_{\substack{\text{Surface of}\\ \text{Cylinder}}} \bar{E}^* \times \bar{J} \cdot d\bar{s} = \int_S \bar{E}^* \times (\bar{H}^{(0)} - \bar{H}^{(i)}) \cdot d\bar{s} = 0 \qquad (3.6)$$

(* = complex conjugate)

is often chosen (Chodorow and Chu, 1955; Kiryushin, 1957) although more complicated and flexible expressions can also be used (Bevensee, 1964).

In applying these approximate methods, the current will be chosen in this report to be a single travelling wave on the helix tape (not a single space harmonic) which travels only in the direction of the wire, with a constant phase front in a plane z = constant, and a uniform amplitude across the tape. Defining $J_{//}$ as the current parallel to the wire centerline,

$$J_{//} = \begin{cases} Je^{-j\beta_s s} = Je^{-j\beta_o z} & \text{on the first tape} \\ -Je^{-j\beta_s s} = -Je^{-j\beta_o z} & \text{on the second tape} \\ 0 & \text{off the tapes} \end{cases} \qquad (3.7)$$

where

s = distance along the tape = $z/\sin\psi$

β_s = propagation constant along tape = $\beta_o \sin\psi$.

Here, the fact that a bifilar two-wire helix fed in 'push-pull' appears. The fields and current are expanded into spatial Fourier harmonics, as in the sheath helix,

$$E_z^{i,o} = \sum_{n,m=-\infty}^{\infty} E_{zm}^{i,o}(r)\exp(-j\beta_m z + jn\phi + j\omega t) \qquad (3.8)$$

$$H_z^{i,o} = \sum_{n,m=-\infty}^{\infty} H_{zm}^{i,o}(r)\exp(-j\beta_m z + jn\phi + j\omega t) \qquad (3.9)$$

$$J_\phi = \sum_{n,m=-\infty}^{\infty} j_{\phi m}\exp(-j\beta_m z + jn\phi + j\omega t) \qquad (3.10)$$

$$J_z = \sum_{n,m=-\infty}^{\infty} j_{zm}\exp(-j\beta_m z + jn\phi + j\omega t) \quad . \qquad (3.11)$$

An important simplification of the helix problem can be made because of its symmetries and periodicities. The helix becomes coincident with itself, if subjected to one of the following coordinate changes:

$$(r, \phi, z) \rightarrow (r, \phi, z+p) \qquad \text{(glide symmetry)} \qquad (3.12)$$

$$(r, \phi, z) \rightarrow (r, \phi + \frac{2\pi}{p}dz, z+dz) \qquad \text{(differential screw symmetry)} \qquad (3.13)$$

where p is pitch (Fig. 1-1), and

$$(r,\phi,z) \rightarrow (r,\phi,z+\tfrac{p}{2}) \qquad \text{(glide reflection symmetry)} \qquad (3.14)$$

while simultaneously

$$J \rightarrow -J \ .$$

In addition, Floquet's theorem states that if a symmetry like (3.12) exists, then the fields must be of the form

$$\bar{E}(r,\phi,z)=\bar{E}(r,\phi,z+p)\cdot C_f \qquad (3.15)$$

where C_f is some complex function (Brillouin, 1946), not necessarily with an absolute value of unity. A convenient form for C in this case is,

$$C_f=\exp(-j\beta_o z-jm\frac{2\pi}{p}z), \quad m=0,\pm1,\pm2,\ldots. \qquad (3.16)$$

In the usual helix waveguide calculations, β_o is assumed real for the lossless case, but Floquet's theorem does not require this. In our case, β_o will often be complex due to radiation. From (3.16)

$$\beta_m=\beta_o+\frac{2\pi m}{p} \ . \qquad (3.17)$$

In addition, because of the differential screw symmetry (3.13)

$$m = n \ . \qquad (3.18)$$

Also, the expansion of the currents, taking into account the glide-reflection symmetry (3.14), by ordinary Fourier analysis, yields

$$j_{\phi m}=\left| j_{\phi o}\right| \frac{\sin \pi n \delta/p}{\pi n \delta/p} (1-\cos \pi n) \qquad (3.19)$$

$$j_{zm}=\left|j_{zo}\right| \frac{\sin \pi n \delta/p}{\pi n \delta/p} (1-\cos \pi n) \qquad (3.20)$$

$$j_{\phi o} = J\frac{\delta}{p}\cos\psi \qquad (3.21)$$

$$j_{zo} = J\frac{\delta}{p}\sin\psi \qquad (3.22)$$

where

δ = tape width in z direction

and the term $e^{-j\beta_o \delta/2} \cong 1$ for the usual small δ. The first four boundary conditions (3.1) - (3.4) now may be applied; because of orthogonality of the terms in these equations of continuity after expanding the currents, these first four equations may be written for each space harmonic separately, as with the sheath modes. Again, the exponential, arguments and harmonic numbers (n) will be suppressed.

$$aI = AK \tag{3.23}$$

$$-a\frac{n\beta}{\gamma^2 a}I - b\frac{j\omega\mu_o\mu}{\gamma}I' = -A\frac{n\beta}{\Gamma^2 a}K - B\frac{j\omega\mu_o}{\Gamma}K' \tag{3.24}$$

$$a\frac{j\omega\epsilon\epsilon_o}{\gamma}I' - b\frac{n\beta}{\gamma^2 a}I - A\frac{j\omega\epsilon_o}{\Gamma}K' + B\frac{n\beta}{\Gamma^2 a}K = -j_z \tag{3.25}$$

$$BK - bI = -j_\phi \quad . \tag{3.26}$$

If k_o is assumed specified, and in addition j_ϕ and j_z are assumed functions of β_o and k_o as they are in (3.19)-(3.22), then (3.23)-(3.26) are four inhomogeneous equations in five unknowns; a, A, b, B, and β_o. They are to be solved for A, a, B and b in terms of β_o and k_o. The algebra in this problem is long, since $\Gamma \neq \gamma$, whereas $\Gamma = \gamma$ has been assumed in all other solutions in the literature. It is done in some detail in Appendix A. The results for the constants A and B as functions of β_o (via γ_n and Γ_n) are,

$$A = -j\frac{\Gamma}{k_o I' C_\epsilon}\sqrt{\frac{\mu_o}{\epsilon_o}}\left[\frac{-j_z + j_\phi C_4}{1 - C_{\mu\epsilon}}\right] \tag{3.27}$$

$$B = \frac{1}{IC_\mu}\frac{-j_\phi(C_\gamma + C_2) + j_z C_3}{1 - C_{\mu\epsilon}} \tag{3.28}$$

where

$$C_\epsilon = \left[\epsilon \frac{\Gamma}{\gamma} \frac{K}{I} - \frac{K'}{I'}\right] \tag{3.29}$$

$$C_\mu = \left[\frac{\Gamma}{\gamma} \frac{K}{I} - \frac{1}{\mu} \frac{K'}{I'}\right] \tag{3.30}$$

$$C_{\mu\epsilon} = \frac{C_\beta^2 C_{\gamma\gamma}^2 (K/I')^2}{k_o^2 \mu C_\mu C_\epsilon \Gamma^2} \tag{3.31}$$

$$C_3 = \frac{C_\beta C_{\gamma\gamma} KI}{k_o^2 \mu C_\epsilon I'^2} \tag{3.32}$$

$$C_4 = \frac{C_\beta C_\gamma^2}{\Gamma^2} \left(1 + \frac{C_{\gamma\gamma} K/I}{C_\gamma C_\mu}\right) \tag{3.33}$$

$$C_{\gamma\gamma} = \left[1 - \frac{\Gamma^2}{\gamma^2}\right] \tag{3.34}$$

$$C_\beta = \frac{n\beta}{a} \tag{3.35}$$

$$C_\gamma = \frac{\Gamma}{\gamma} \tag{3.36}$$

$$I \equiv I_n(\gamma_n a); \qquad K \equiv K_n(\Gamma_n a) \quad .$$

The constants a and b, which will not be needed, are related to A and B via (3.23) and (3.26).

At this point, the simplified methods discussed before (3.6) for handling the difficult boundary condition (3.5) must be applied. The variational technique (3.6) will be used, although the technique of setting the center line $E_{//}=0$ can be shown to give an identical dispersion equation with the exception of the squaring of the tape width factor (Watkins, 1958). This variational method for

helix dispersion calculations has been thoroughly derived and explained by Chodorow and Chu (1955) as well as others; it would suffice here to note that $\bar{E}x(\bar{H}^{(0)}-\bar{H}^{(i)})\cdot d\bar{s}$, the integrand of (3.6), should be zero everywhere. The reason for this is that on the conductor $\bar{E}x\,d\bar{s}=0$ since the tangential $\bar{E}$ field is zero on a perfect conductor. Off of the conductor, but at the same radius, r=a, $(H^{(0)}-H^{(i)})x\,d\bar{s}=0$ since the tangential component of $\bar{H}$ is continuous across any surface not containing current. The triple product integrand of (3.6) can be rearranged to contain either $\bar{E}x\,d\bar{s}$ or $(H^{(0)}-H^{(i)})\,x\,d\bar{s}$; therefore the integrand is zero everywhere. Forcing the integral of $\bar{E}x(H^{(0)}-H^{(i)})\cdot d\bar{s}$ to zero, a less strict condition, should give approximate results for β vs k. The integral (3.6) becomes

$$I=\int E_{tan}^{(0)}\cdot J_{tan}^{*}\,ds=\int\left[\sum_{n=-\infty}^{\infty}E_{zn}^{(0)}\exp(-j\beta_n z+jn\phi)\sum_{m=-\infty}^{\infty}j_{zm}^{*}\exp(j\beta_m z-jm\phi)+\right.$$

$$\left.+\sum_{n=-\infty}^{\infty}E_{\phi n}^{(0)}\exp(-j\beta_n z+jn\phi)\sum_{m=-\infty}^{\infty}j_{\phi n}\exp(j\beta_m z-jm\phi)\right]ds=0\quad.$$

With the surface taken as one periodic cell, length p, the integral of the cross product terms $m\neq n$ is zero due to orthogonality of the space harmonics, and a constant L may be defined,

$$L\triangleq\frac{I}{2\pi ap}=\sum_{n=-\infty}^{\infty}E_{zn}^{(0)}\,j_{zn}^{*}+E_{\phi n}^{(0)}\,j_{\phi n}^{*}=0\quad,\qquad(3.37)$$

$$L=\sum_{n=-\infty}^{\infty}A_n K_n j_{zn}^{*}+\left[\frac{-n\beta_n}{\Gamma_n^2 a}A_n K_n j_{\phi n}^{*}-\frac{j\omega\mu_o}{\Gamma_n}B_n K'_n j_{\phi n}^{*}\right]=0\,.\qquad(3.38)$$

An extremely important step for numerical calculations is to separate L into the 'resonant' term (that term where $\beta_n\approx k_o$) and the other berms, $\beta_n\gg k_o$, designated as the non-resonant remainder (Shestopalov, 1961).

$$L=L_R+L_{NR}\quad.\qquad(3.39)$$

In the case of backward radiation, the resonant term is n = -1. The resonant term is a very complicated one which cannot apparently be readily simplified; the non-resonant terms may be well approximated by asymptotic expressions, and these terms may be summed to get a very simple approximation for the remainder.

3.2 Resonant Term

A solution for the resonant term is really just a full solution, without further approximations, for the general nth term, L_N, of the sum L. Since only a single term, the resonant one, must be calculated from this expression, the latter name is applied.

Substituting for A_n and B_n from (3.27) and (3.28) in the general nth term of L, and omitting the nth subscript throughout,

$$L_R = L_N = -j\sqrt{\frac{\mu_o}{\epsilon_o}}\,\frac{\Gamma}{k_o}\,\frac{K/I'}{C_\epsilon(1-C_{\mu\epsilon})}\left[-j_z\cdot j_z^* + j_\phi\cdot j_z^* C_4\right] +$$

$$+\frac{jn\beta}{\Gamma_a^2}\,\frac{\Gamma}{k_o}\,\frac{K/I'}{C_\epsilon(1-C_{\mu\epsilon})}\sqrt{\frac{\mu_o}{\epsilon_o}}\left[-j_z\cdot j_\phi^* + j_\phi\cdot j_\phi^* C_4\right] -$$

$$-\frac{j\omega\mu_o}{\Gamma}\,\frac{K'/I}{C_\mu(1-C_{\mu\epsilon})}\left[-j_\phi\cdot j_\phi^*(C_\gamma+C_2)+j_z\cdot j_\phi^* C_3\right] \qquad (3.40)$$

where $j=\sqrt{-1}$, not to be confused with j_ϕ, $j_{//}$ or j_n. Substituting

$$j_{n\phi} = j_n \cos\psi \qquad (3.41)$$

$$j_{nz} = j_n \sin\psi \qquad (3.42)$$

the expression L_R becomes

$$L_R = jj_n^2\sqrt{\frac{\mu_o}{\epsilon_o}}\ \frac{k_o a}{\Gamma a}\left\{\frac{\Gamma^2 a^2\, K/I}{k_o^2 a^2 C_\epsilon(1-C_{\mu\epsilon})}(\sin^2\psi - \sin\psi\cos\psi C_4 - \frac{n\beta}{\Gamma^2 a}\sin\psi\cos\psi + \frac{n\beta}{\Gamma^2 a}\cos^2\psi C_4) + \right.$$

$$\left. + \frac{K'/I}{C_\mu(1-C_{\mu\epsilon})}\left[\cos^2\psi(C_\gamma + C_2) - \sin\psi\cos\psi C_3\right]\right\} \qquad (3.43)$$

where the constants are defined in (3.29)-(3.36). Factoring $\cos^2\psi$ and $(1-C_{\mu\epsilon})$ out, and defining $C_5 = C_4/(\Gamma a)^2$

$$L_R = jj_n^2\sqrt{\frac{\mu_o}{\epsilon_o}}\ \frac{\cos^2\psi}{(1-C_{\mu\epsilon})}\ \frac{k_o a}{\Gamma a}\left\{\frac{K/I'}{(k_o a)^2 C_\epsilon}\left[(\Gamma a)^2\tan^2\psi - n\beta a\tan\psi(1+C_5) + \right.\right.$$

$$\left.\left. + n^2\frac{(\beta a)^2}{(\Gamma a)^2}C_5\frac{K'/I}{C_\mu}(C_\gamma + C_2 - C_3)\right]\right\} \quad . \qquad (3.44)$$

Equation (3.44) is in the form used for computer analysis.

To check limiting cases of this equation against published solutions, it should be noted that if $\Gamma \to \gamma \gg 0$, and Γ and γ are essentially real, which is the degenerate slow-wave loaded tape helix case, when $C_{\gamma\gamma} \to 0$, $C_{\mu\epsilon} \to 0$, $C_\gamma \to 1$, and

$$C_\epsilon \to \left[\epsilon\frac{K}{I} - \frac{K'}{I'}\right], \quad C_\mu \to \left[\frac{K}{I} - \frac{1}{\mu}\frac{K'}{I'}\right]$$

$$L_r \to \frac{+jk_o\cos^2\psi}{\gamma} j_n^2\sqrt{\frac{\mu_o}{\epsilon_o}}\left\{\frac{\gamma^2}{k_o^2}(\tan^2\psi - \frac{n\beta}{\gamma^2 a})\frac{K/I'}{C_\epsilon} + \frac{K'/I}{C_\mu}\right\} \quad . \qquad (3.45)$$

If, also, large argument asymptotic approximations are used to the Bessel function products, as in (2.43)-(2.47)

$$\frac{K/I'}{C_\epsilon} = \frac{K/I'}{\epsilon\frac{K}{I} - \frac{K'}{I'}} \cong \frac{I/I'}{\epsilon+1} \cong \frac{1}{\epsilon+1} \tag{3.46}$$

$$\frac{K'/I}{C_\mu} \cong \frac{K'/I}{\frac{K}{I} - \frac{1}{\mu}\frac{K'}{I'}} = \frac{-I'/I}{1+\frac{1}{\mu}} \cong \frac{-1}{1+\frac{1}{\mu}} \quad . \tag{3.47}$$

Thus (3.45) becomes

$$L_R \to +j \frac{k_o}{\gamma} \cos^2\psi\, j_n^2 \sqrt{\frac{\mu_o}{\epsilon_o}} \left\{ \frac{\gamma^2}{k_o^2} (\tan^2\psi - \frac{n\beta}{\gamma^2 a}) \frac{1}{(1+\epsilon)} - \frac{1}{1+\frac{1}{\mu}} \right\} \tag{3.48}$$

which checks with Shestopalov's (1961) general term for the slow-wave loaded tape solution, after a few corrections are made to the published equations which the author found upon re-deriving Shestopalov's work. This corrected form (3.45) may be partially checked with Watkins(1958) solution (or many others which agree with Watkins) for the general term of an unloaded tape helix (the uncorrected Shestopalov formulas do not check), where $\epsilon = \mu = 1$. Upon using the Wronskian for the modified Bessel function, rearranging constants and multiplying and dividing by $\cot^2\psi$

$$L_R \to j\frac{k_o}{\gamma} \sin^2\psi\, j_n^2 \left\{ \left[(\gamma a)^2 - 2n\beta a \cot\psi + n^2\beta^2 a^2 \frac{\cot^2\psi}{\gamma^2 a^2} \right] I_n K_n + k_o^2 a^2 \cot^2\psi\, I'K' \right\} \tag{3.49}$$

which is Watkins' general form for a free-space tape helix solution. Thus, the solution to the general formula in this report (3.44) reduces to published solutions for certain limiting cases, providing a partial check of its validity. The equation (3.44), however, is believed to be new and not previously published.

Studying (3.44) for a moment, it should be noticed that no obvious simplifying assumptions can be made to this term. Since for the resonant term n is small, here n = -1, the large order asymptotic approximations to the Bessel functions are not very accurate in the general complex argument case, although

they proved acceptable in the sheath helix case for real arguments. This approximation was checked numerically by the author and found to be very poor for small complex arguments which are of interest. In particular, γ_{-1} is imaginary over much of this range; thus $I_{-1}(\gamma_{-1}a) \rightarrow -j\, J_{-1}(+j\gamma_{-1}a)$, which is an oscillatory function. No approximations to J_{-1} have yet been found useful in simplifying the resonant term. The large argument approximations are, of course, not possible since

$$\Gamma_{-1}a = \sqrt{(\beta_{-1}a)^2-(k_o a)^2} \sim 0$$

for $\beta_{-1} \sim k$. Also, the two arguments γa and Γa differ, which makes approximations of K'I/KI' and K'I'/KI, the two important products, additionally difficult, even in the regions where γ_n is real.

To calculate the term (3.44) by brute force on a computer is not especially easy either, although that procedure was followed herein. The major difficulty is that programs for modified Bessel functions of complex argument are not readily available for the computer as subroutines, and those programs that were later found and might have been changed for the present use were usually for a limited range of argument and order, as well as requiring the slow double precision calculations. Appendix B discusses the Bessel function subroutines written by the author for use in this problem and other known work in this area.

3.3 Non-Resonant Remainder

For the rest of the terms of the infinite series representing L, a brute force calculation could be used. The costs of computer time would be very large, additional time for study of programming for the computer for accurate Bessel functions of complex argument and higher order would be required, and no simple well-known function for the total non-resonant remainder would be obtained. The method to follow shows this total non-resonant term clearly and simply.

Since for the non-resonant terms, $\beta_n \gg k_o$,

$$\Gamma_n a = \sqrt{\beta_n^2 a^2 - k_o^2 a^2} \cong \beta_n a \gg 0 \quad . \tag{3.50}$$

Also, except at isolated regions in the slow wave zone where $\beta_n \sim k\sqrt{\mu\epsilon}$ for small n, $\beta_n \gg k\sqrt{\mu\epsilon}$, and

$$\gamma_n a = \sqrt{(\beta_n a)^2 - (k_o a)^2 \mu\epsilon} \cong \beta_n a \gg 0 \quad . \tag{3.51}$$

In addition, both $\Gamma_n a$ and $\gamma_n a$ are almost purely real, and $\Gamma \sim \gamma$ for $|n| > 1$, $\cot\psi$ large, and $\mu\epsilon$ not too large .

This combination of fairly large, nearly real arguments assures the accuracy of a large order asymptotic approximation for the Bessel function products. The large argument approximations are not applicable because the series is of increasing order, n . In other words, all the usual slow wave approximations apply to the non-resonant terms, except that large order, rather than large argument, expansions are used.

For the non-resonant term, start with the slow wave ($\Gamma_n \approx \gamma_n$) expression for a loaded helix (3.45) and rewrite the first factor inside the brackets (using $\Gamma_n \sim \gamma_n$)

$$T = \frac{\Gamma_n^2 a^2}{k_o^2 a^2}\left(\tan^2\psi - \frac{n\beta_n}{\Gamma_n^2 a}\right) = \frac{1}{(k_o a)^2}\left\{(\Gamma_n a)^2 \tan^2\psi - 2n\beta_n a \tan\psi + \frac{n^2\beta_n^2 a^2}{\Gamma_n^2 a^2}\right\} . \tag{3.53}$$

Using the relations

$$\beta_n a = \left(\beta_o + \frac{2\pi n}{p}\right)a = \beta_o a + n\cot\psi \tag{3.54}$$

$$\Gamma_n^2 a^2 = \beta_n^2 a^2 - k_o^2 a^2 \tag{3.55}$$

the factor T becomes

$$T = \left[(\beta_o a)^2 - (k_o a)^2 \tan^2\psi + \frac{n^2 k_o^2 a^2}{\Gamma_n^2 a^2} \right] \quad . \tag{3.56}$$

This simplified factor is essentially the one used by Tien (1953) and Sensiper (1951, p. 59) for the tape helix in air. The effect of loading comes in the other terms. A further simplification results for large n, since

$$\Gamma_n^2 a^2 = \left[(\beta_o a + n\cot\psi)^2 - k_o^2 a^2 \right] \tag{3.57}$$

$$\cong n^2 \cot^2\psi \qquad \text{(n large)}$$

$$T \cong \beta_o^2 a^2 \tan^2\psi \quad . \tag{3.58}$$

This simplification will be used to approximate all non-resonant terms, since usually

$$\beta_o a \ll n\cot\psi \quad \text{and} \quad k_o a \mu^2 \epsilon^2 \ll n\cot\psi \quad . \tag{3.59}$$

For μ and ϵ very large, the second approximation may not hold for small n and for large ψ, and additional terms would have to be calculated using the exact expression (3.44), which was used for the resonant term.

The sum of the non-resonant terms may then be written, where rn = resonant n, as

$$L_{NR} = +j \sum_{\substack{n=-\infty \\ n \neq rn}}^{\infty} j_n^2 \cos^2\psi \left(\frac{k_o a}{\Gamma_n a}\right) \left\{ \frac{\beta_o^2 a^2 \tan^2\psi}{k_o^2 a^2} \; \frac{K/I'}{C_\epsilon} + \frac{K'/I}{C_\mu} \right\} \quad . \tag{3.60}$$

Simplifying still further using the large order asymptotic expansions as in (2.48) through (2.53), similarly to (3.46) and (3.47)

$$\frac{K/I'}{C_\epsilon} \cong \frac{I/I'}{\epsilon+1} \cong \frac{\cos\psi}{\epsilon+1} \tag{3.61}$$

$$\frac{K'/I}{C_\mu} \cong \frac{-I'/I}{1+\frac{1}{\mu}} \cong \frac{-1/\cos\psi}{1+\frac{1}{\mu}} \quad . \tag{3.62}$$

The cos ψ appears above, although it does not in (3.46) and (3.47) since from (2.49) - (2.53)

$$\frac{I_n(\Gamma_n a)}{I_n'(\Gamma_n a)} \cong \frac{\Gamma_n a}{n\sqrt{1+\frac{\Gamma_n^2 a^2}{n^2}}} = \frac{\Gamma_n a}{\sqrt{n^2+\Gamma_n^2 a^2}} \tag{3.63}$$

Using (3.57) for large n

$$\frac{I}{I'} \cong \frac{n\cot\psi}{\sqrt{n^2+n^2\cot^2\psi}} = \frac{\cot\psi}{\csc\psi} = \cos\psi \quad . \tag{3.64}$$

Substituting (3.61) and (3.62) into (3.60), and multiplying and dividing by cos ψ,

$$L_{NR} = +j \sum_{\substack{n=-\infty \\ n\neq r\,n}}^{\infty} j_n^2 \cos\psi \, \frac{k_o a}{\Gamma_n a} \left\{ \frac{\beta_o^2 a^2}{k_o^2 a^2} \, \frac{\sin^2\psi}{\epsilon+1} - \frac{1}{1+\frac{1}{\mu}} \right\}. \tag{3.65}$$

This non-resonant expression is close to Shestopalov's (1961), except that he uses somewhat different slow wave approximations with large argument expansions, resulting in an expression with γ_o instead of β_o, and tan ψ rather than sin ψ. The expression (3.65) is felt to be more exact and useful.

At this point, it is seen that the entire bracket is independent of n. In addition, the n-dependent terms outside the bracket vary as

$$S_n = 2\left[\frac{\sin\frac{\pi\delta}{p}n}{\frac{\pi\delta}{p}n}\right]^2 \frac{\cos\psi}{n\cot\psi} = 2\sin\psi\,\frac{1}{n}\left[\frac{\sin n\Delta}{n\Delta}\right]^2 \qquad \text{(n odd)} \qquad (3.66)$$

$$S_n = 0 \qquad \text{(n even)}$$

where $\Delta = \pi\delta/p$ and where (3.57) and (3.19) - (3.20) have been used for j_n and Γ_n respectively. For small Δ (thin wires), the term varies as $1/n$ until n is quite large; i.e., the convergence is very slow. It is felt that even modern computers cannot handle convergence as slow as this in the original Bessel function form, and indeed there is no necessity to have the series in such a slowly converging form. Although it is not mentioned in many non-Russian articles on the tape helix, the series L_{NR} can be well approximated by a single term. To be more exact, the series can be changed into a much more rapidly convergent series, which is so good that the first term approximates the series very well. The general problem of increasing the convergence of such series has often been studied (Collin, 1960; Morse and Feshbach, 1953; Marcuvitz, 1964) and has also been applied to helices and dipole arrays (Sensiper, 1951; Chodorow and Chu, 1954; Serracchioli and Levis, 1959), but the importance of only the first term used to get an excellent picture of the effect of all the higher modes is mainly emphasized by the Russians (Shestopalov, 1961; Kogan, 1949, 1959). Indeed, a very commonly used method in Russian literature for any problem involving a narrow conductor or narrow gap in any geometry is the so-called 'averaged boundary condition', originally developed in the untranslated literature but discussed by Moizhes (1958) and Smirnov (1958). In this method, the boundary conditions contain a term logarithmic in $1/\Delta$ essentially the same as the first term of the sum of the series L_{NR}. Except for this term in the boundary condition, the problem is handled like a sheath analysis. However, it appears that for air gaps between the material and the helix, or for layers of material, this method is inaccurate and gives little insight to the problem.

The importance of this asymptotic approximation is that it will usually appear in thin conductor or gap problems and gives some physical insight to the solution, whereas the associated original Fourier series will always be very slowly converging and difficult to apply numerically, while giving no simple insight into the problem. Rearranging the series for increased convergence, while not stating the importance of the first term, fails to give the physical insight To summarize, the series written for increased convergence is simply

$$L = L_R + L_{NR}$$

$$= L_R + j \sum_{\substack{n=-\infty \\ n \neq rn}}^{\infty} S_n \cdot F_{k\beta} + \sum_{\substack{n=-\infty \\ n \neq rn}}^{\infty} L_N - (jS_n \cdot F_{k\beta}) \qquad (3.67)$$

where

S_n is given by (3.66)

$$F_{k\beta} = \left\{ \frac{\beta_o^2 a^2}{k_o^2 a^2} \quad \frac{\sin^2 \psi}{\epsilon + 1} - \frac{1}{1 + \frac{1}{\mu}} \right\} . \qquad (3.68)$$

This last summation term is simply the error between the exact term L_n and the asymptotic approximation for large n. This correction series could be used on the computer since it converges rapidly. However, it will be assumed negligible, since it has already been seen that the asymptotic approximations for the Bessel function for large n are very accurate, if the argument is fairly large and essentially real.

Series similar to (3.65) have been summed by Collin(1960), Chodorow and Chu (1954), Kogan (1959) and others; however the sum for n odd has not been found in the literature by the author. Appendix C indicates the method which gives

$$\frac{1}{\sin\psi}\sum_{\substack{n=-\infty\\ n\neq rn}}^{\infty} S_n \cong \ell n\,\frac{1}{\Delta}+\frac{1}{2} \equiv F_c \quad . \tag{3.69}$$

Thus, the final approximate dispersion equation for the loaded tape helix is

$$L=L_R+L_{NR} \cong L_R+j\,F_{k\beta}\,F_c \sin\psi \tag{3.70}$$

where L_R is calculated from (3.44), $F_{k\beta}$ from (3.68) and F_c from (3.69). The equation (3.70) was solved on a digital computer for k_o vs β as will be described in the next section. Just by inspection, however, considerable insight into the solution can be gained. As $\Delta \to 0$, that is, as the tape width becomes small, the log term increases in importance until it completely dominates the solution, i.e., $F_c \to \infty$. Thus, for the limiting case $\Delta \to 0$, the dispersion equation becomes

$$F_{k\beta} \cong 0$$

$$\frac{\beta_o^2 a^2}{k_o^2 a^2}\,\frac{\sin^2\psi}{\epsilon+1} - \frac{1}{1+\frac{1}{\mu}} = 0 \tag{3.71}$$

$$k_o a = \pm\ \beta_o a \sin\psi \sqrt{\frac{1+1/\mu}{1+\epsilon}} \quad . \tag{3.72}$$

This equation will be recognized as the same as (2.56), which was derived in the sheath helix case using the well known narrow conductor asymptote in free space,

$$k_o a=\beta_o a \sin\psi \tag{3.73}$$

from the tape helix theory and applying the slow wave reduction factor

$$\frac{1}{C} = \sqrt{\frac{1+1/\mu}{1+\epsilon}}$$

found from slow-wave sheath theory. Actually, (3.73) for the helix in air, although well known in the slow-wave region, has been shown valid in the leaky-wave radiation region only recently by Klock (1963) using arguments based on

the whole series. It has been extended to the loaded case above, using a summation term which shows not only the behavior at $\Delta \rightarrow 0$, but the quantitative behavior for small Δ. Numerically, it happens that the dominance of L_{NR} occurs even at moderately small tape widths.

The logarithmic variation shows the dispersion equation is insensitive to the exact tape width used. This is fortunate because the tape model itself is not met in practice. If a more exact L_{NR} was desired, which does not seem very important for the present case, the actual conductor shape would also have to be considered, using perhaps the developed tape model for the higher order terms.

Equations (3.70), (3.72) and (3.73) also give another very important approximate physical interpretation to the solution. Equation (3.73) indicates that for very small conductors on a helix in free space, the phase velocity along the wire is approximately the speed of light, that of a TEM wave. This suggests that, as a good first approximation, the helix may be treated as an isolated, straight, infinitely long wire propagating a TEM wave when calculations of conductor phase velocity, fields and effect of conductor shape and loading are considered. The $\log(1/\Delta)$ term, which occurs also in calculations of self inductance of a straight wire, also supports this model. In other words, the self inductance of the thin wire helix dominates over any cross coupling of fields between different loops. The above conclusion actually need not be restricted to the helix but probably occurs with most narrow-conductor structures. The Fletcher (1952) method for dealing with the interdigital slow wave structure assumes this TEM wave with considerable success. Also, the 'developed' or 'plane' helix model uses this assumption, which depends on a very close binding of the fields to the vicinity of the wires in at least the higher space harmonics, so that changes in geometry (such as bending the plane into a cylinder) do not affect the propagation constant.

The reduction factors in (3.72) for the effect of material loading has in fact been obtained and used by this 'developed helix' model with Fletcher's TEM approximation (Ash, et al, 1964; Hair, 1964) and greatly facilitates the interpretation of the loading effects of an anisotropic ferrite upon a helix slow wave in the latter reference. The loading effect for an isotropic material, on the inside of a developed helix only, can be seen to be essentially the effect of ϵ_0 and $\epsilon_0\epsilon$ in parallel and the μ_0 and $\mu_0\mu$ in parallel. The effect of the permittivity may be thought of as a lumped capacitance, and since capacitors in parallel add like

$$C_T = C_1 + C_2$$

the effective dielectric constant, ϵ_{eff}, of the two different dielectrics may be written as

$$e_{eff} = (\epsilon_1 + \epsilon_2)/2 \quad .$$

Similarly, if the effect of the two μ's is thought of as lumped inductance, which add in parallel as

$$\frac{1}{L_T} = \frac{1}{L_1} + \frac{1}{L_2} \tag{3.74}$$

The phase velocity reciprocal is

$$\frac{1}{v_p} \sim \sqrt{L_1 C_1} = \sqrt{\mu_{eff}\epsilon_{eff}} = \sqrt{\frac{\epsilon_1+\epsilon_2}{\frac{1}{\mu_1}+\frac{1}{\mu_2}}} \quad .$$

From a physical picture of the fields, the two routes of the electric field between two helix wires (capacity), one route inside and one outside the loading, appear in parallel. The route of the magnetic field around the wire is half in the material, half outside. The reluctance (magnetic impedance) to the magnetic flux around the wire which is added up around the magnetic path, is inversely proportional to inductance, thus causing the 'inductances' of the two parts of the path to add as inverses, as shown in (3.74) .

Finally, in the interpretation of (3.70), it is noted that L_R must still be considered in the fast wave region, since the argument of the Bessel function $K_n(\Gamma_n a)$ gets small there, causing the outside fields, such as (2.12) and (2.14), to get very large. Physically, this means that the strong surface wave approximated by the resonant space harmonic couples of the current wave to the radiation fields. It is not obvious, however, in what manner μ and ϵ affect this radiation. Numerical calculations appear necessary here.

3.4 Numerical Calculation of Tape Dispersion Equation

The numerical calculation of (3.70) required three large areas to be investigated. First, subroutines for modified Bessel functions of complex argument had to be written that permitted a large range of arguments from very small to very large, at any argument angle. Higher orders of Bessel Functions were also considered, for the problem of error estimate of the L_{NR} approximation. Appendix B discusses these subroutines. The second problem area is the general method solution of an equation like (3.70) in the complex plane. The Newton-Raphson method was chosen in this study. Mittra and Laxpati (1964) also chose this method for finding the complex zeros of a similar simpler dispersion equation. The final problem area was to implement this method in a program that would find a solution for a given initial guess of β_0 and given values of k_0, μ, ϵ, ψ etc., and track this solution as k_0 was varied in small steps. The tracking of the solution improves the speed of investigating the solutions as well saving much computer time. Without a method of tracking in the complex plane, the instability of the Newton-Raphson method makes it almost impossible to obtain results. A three-point extrapolation was used to obtain each new point on the k-β diagram, with a starter subroutine that searched for the first three points, beginning in regions where the solution was approximately known.

The Newton-Raphson method is a common technique for the numerical solution for an implicit equation G(x)=0 for real variable (Hildebrand , 1956). The technique begins with a guess x_1, of the correct solution , x_o . A derivative $dG(x_1)/dx$ is then calculated, and the next approximation to x_o is x_2 ,

$$x_2 = \frac{G(x_1)}{G'(x_1)} \quad .$$

If the first guess x_1 is 'sufficiently'close to x_o , the solution will converge; in fact, the convergence is very rapid, called 'quadratic', since the error ϵ_i of x_i is of the order $(\epsilon_{i-1})^2$ where ϵ_{i-1} is the error in the x_{i-1} approximation. This method can be extended to the complex plane although very little appears to have been written on such solutions. In the complex domain, restricting G(z) to an analytic function in the region of interest,

$$Z_i = \frac{G(z_{i-1})}{G'(z_{i-1})}$$

where G' is well-defined for an analytic function, and is the same regardless of direction of approach to x_{i-1} . In the computer program, the approximation used was

$$G'(z_{i-1}) \cong \frac{G(z_{i-1}) - G(z_{i-1} - \Delta z)}{\Delta z} \qquad (3.75)$$

where Δz was taken rather small, and could be changed to investigate stability and validity of the solution .

Equation (3.75) was programmed directly as written, where $G(z)=L(\beta)$ from equation (3.70). Complex arithmetical subroutines were used to perform the complex arithmetical operations, since the MAD interpretive language used at The University of Michigan had no defined complex numbers at the time. All other subroutines (such as sin, cos) had to be revised. There is now a MAD definition package for complex arithmetic that makes such programming much

easier. FORTRAN could also be used, which has defined complex arithmetic.

A problem with the Newton-Raphson technique is that (3.75) may give a relatively inaccurate G' for small Δz since there is a difference of two nearly equal functions. In addition, this function $G(z) = L(\beta)$, with only eight digits of accuracy available for single precision computer work, is a complicated combination of Bessel functions which are themselves difficult to compute accurately because of subtraction of nearly equal quantities in the formation of the defining series. Attention to 'accuracy' was necessary throughout, although actually 'resolution' (the number of significant figures before the occurence of random numbers) was found more important than accuracy (the number of significant figures that are identical with the correct $L(\beta_o)$)in obtaining accurate derivatives.

The initial guesses for $\beta_o = \beta_{or} + j\beta_{oi}$ were made in the two regions where experience has shown the answers are approximately known; a) the slow wave region, and b) the 'radiation' point at the intersection of the asymptotic $k-\beta$ solution (3.72) with the backward plane wave TEM line $k_o = 1-\beta_o$. In (a), the asymptotic line (3.72) is an excellent approximation, with $\beta_{oi} \cong 0$ (a real variable solution), since little radiation takes place. For (b), the radiation point determined β_{or} and β_{oi} was taken nominally at -.01 and varied if instability occurred. The second point in (b) was initially guessed by a small shift from the first points. The third point was initially guessed by a linear extrapolation of both β_{or} and β_{oi} . The variation of β_{oi} was extremely rapid near the slow wave region, causing instabilities in the solution, so that initially in (b) the $k-\beta$ diagram was extended to the right, then to the left from the initial point.

Note that the Newton-Raphson technique automatically gives the quantity $dL/d\beta$ which is related to the residue of the leaky wave pole associated with this complex wave. In cases where numerical methods are used, it would seem that the contribution of any pole in the complex plane to a contour integral is more easily taken into account by numerically finding the residue than by numerically integrating over the contour.

It is important to note that the complex poles appear in pairs $\beta_{or} \pm j\,\beta_{oi}$, so that the particular sign of β_{oi} found in a root is not crucial to the solution; only one root is physically acceptable. The proof of this property follows from the property for Bessel functions,

$$I_n(z^*) = I_n^*(z) \qquad K_n(z^*) = K_n^*(z)$$
$$I_n'(z^*) = I_n'^*(z) \qquad K_n'(z^*) = K_n'^*(z)$$

and of the transverse propagation constants,

$$\gamma_n(\beta^*) = \gamma_n^*(\beta) \qquad \Gamma_n(\beta^*) = \Gamma_n^*(\beta)$$

where * indicates complex conjugate. Since L is formed from real constants, including k_o, and arithmetic operations upon the γ, β, and the Bessel functions, the function $L(\beta)$ must also have the property $L(\beta^*) = L^*(\beta)$.

3.5 Results of the Computer Computation

The results of the computation are shown in Figs. 3-1 to 3-13, in the form of k-β diagrams. In each diagram

$$\begin{aligned} \overline{k}_o &\triangleq k_o a/\cot\psi = k_o p/2\pi \\ \overline{\beta}_r &\triangleq \beta_{or} a/\cot\psi = \beta_{or} p/2\pi \\ \overline{\beta}_i &\triangleq \beta_{oi} a/\cot\psi = \beta_{oi} p/2\pi \\ \Delta &= \pi\,\delta/p \end{aligned} \qquad (3.76)$$

where, as usual, the subscripts r and i refer to real and imaginary components of a complex variable. The figures are grouped by the three pitch angles ($\psi = 2.6^o$, 5^o, 25^o) and the two normalized tape widths used ($\Delta = .1,\ .01$). with separate figures for dielectric loading, and combined magnetic ($\mu > 1$) and dielectric loading. The particular sets of values (μ=6. 6, ϵ=12. 6; ϵ = 3.77, μ = 2.2) correspond to two ferrites in use on this project.

Figure 3-1, for $\epsilon = 1$, shows a typical behavior of an unloaded backward-fire helical current wave T_o (the notation will be discussed later). The k-β_r diagram is similar to the extrapolated k-β diagram shown in Fig. 2-2 for the sheath helix, but jutting upward away from the line, $\bar{k} = \bar{\beta}_r \sin\psi$, shown in Fig. 3-1. The imaginary part of $\bar{\beta}$, $\bar{\beta}_i$, is plotted to the right hand side of the figure, using the same ordinate, $\bar{k}$, but a different abscissa scale. For the unloaded helix ($\epsilon=1$), the $\bar{\beta}_i$ is seen to be very small for all values of $\bar{k}$ such that the $\bar{k}$-$\bar{\beta}_r$ line is in the non-radiating region, i. e. to the left of the $\bar{k}=1-\bar{\beta}$ line, where the n=-1 space harmonic has an axial plane velocity less than the speed of light. As the $\bar{k}$-$\bar{\beta}_r$ line for $\epsilon = 1$ approaches $\bar{k} = 1-\bar{\beta}$ line; i. e. as the axial phase velocity of the n=-1 space harmonic approaches the speed of light, the value of $\bar{\beta}_i$ suddenly increases greatly. Based upon experimental evidence, β_i is the rate of radiation attenuation. It can be expected to fall off after the $\bar{k} - \bar{\beta}_r$ line is deep in the radiation region, often rising afterward. Only the behavior close to the sudden rise, where radiation is backward fire and the T_o current wave dominates, is of interest at present.

Figure 3-1 shows the typical behavior of the dielectric loading. As ϵ is increased, the radiation zone moves to lower values of the frequency-size parameter, $\bar{k}$. The radiation zone can clearly be seen from the increase in the attenuation ($\bar{\beta}_i$) due to radiation, and is seen to occur near the nominal 'radiation point' at the intersection of the lines

$$\bar{k}_o = 1-\bar{\beta} = -\bar{\beta}_{-1} \tag{3.77}$$

$$\bar{k}_o = \bar{\beta} \sin\psi \sqrt{\frac{1/\mu+1}{\epsilon+1}} \quad . \tag{3.78}$$

However, the radiation attenuation, $\bar{\beta}_i$, also decreases with each increase in the loading ϵ. If the factor of reduction in $\bar{\beta}_i$ is greater than that of $\bar{k}_o$, then the active zone length will be unchanged with loading since both radiation rate per unit of pitch distance, β_i, and the pitch distance (proportional to k_o) are decreased equally. Notice in Fig. 3-1 that the solutions are quite close to the asymptotic line given by (3.78),

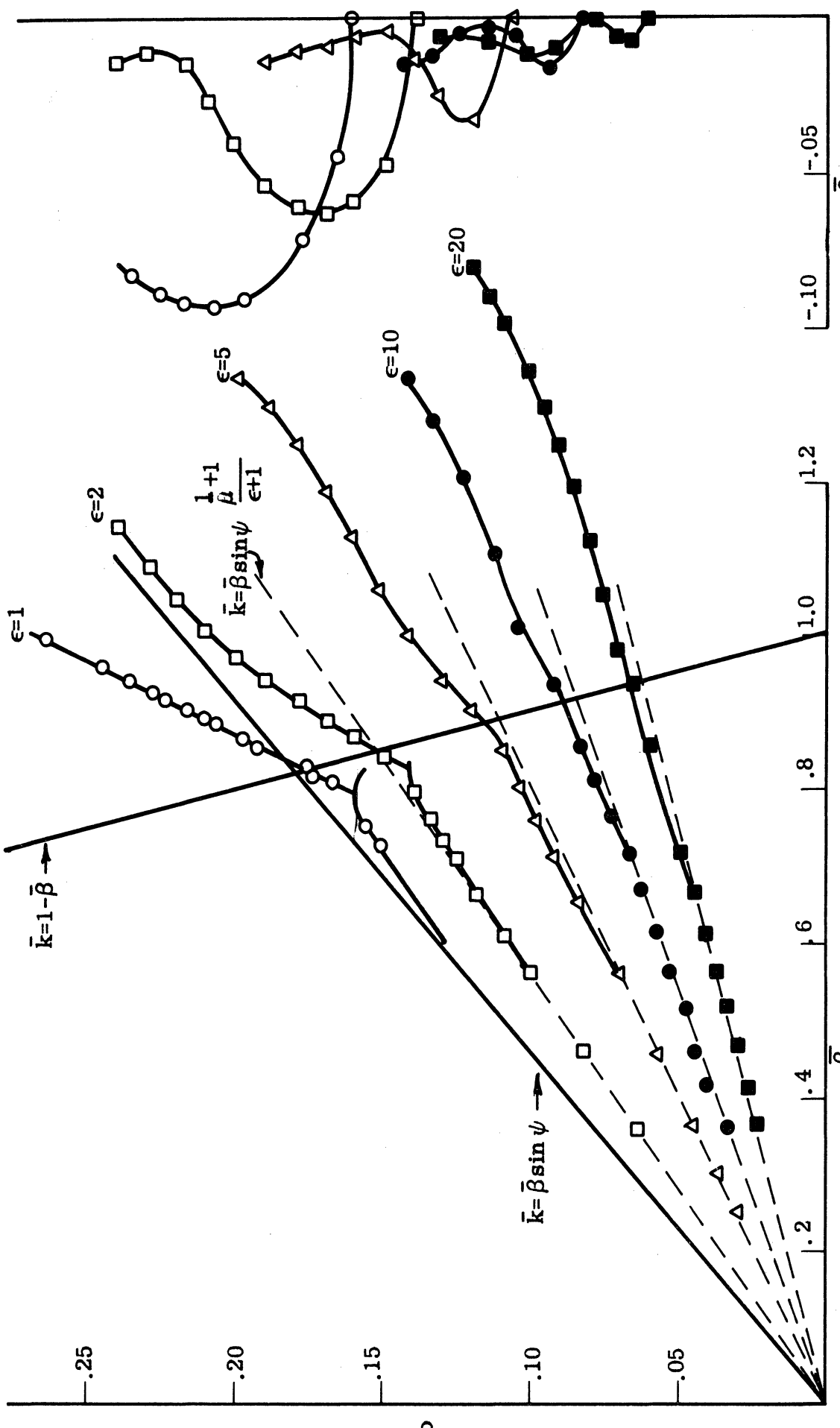

FIG. 3-1: EFFECT OF DIELECTRIC LOADING ON DISPERSION.
ψ = 12.6°, Δ = .1, μ = 1; see Fig. 6-2 for ψ and Δ.

especially in the slow wave region and for the larger loadings in the fast wave region.

In Fig. 3-2, the effect of raising μ rather than ϵ in the loadings is shown. The solutions are again quite close to the asymptotic, and give only small reductions even for large μ. Nevertheless, the effect on $\bar{\beta}_i$ is very interesting; it does not decrease as much as for high ϵ, but on the contrary, even increases for some values of μ.

Figure 3-3 shows that a smaller tape width, $\Delta = .01$, decreases $\bar{\beta}_i$ somewhat, but not drastically, in all cases. Figure 3-4 shows a similar effect for loading with μ. In addition, several materials with both μ and ϵ greater than air are shown. The compound (μ=2.2, ϵ=3.77) has the characteristics of a ferrite powder used in the experimental program (Chapter V). The high $\bar{\beta}_i$ with the compound ($\epsilon = 5$, $\mu = 10$) is notable, with the reservations noted later about the rather large $\bar{\beta}_i$. The other two compounds, while showing a diameter reduction in $\bar{k}a$, also show a considerable reduction in $\bar{\beta}_i$.

Figures 3-5 through 3-8 show the effect of loading on a helix of greatly reduced pitch angle, only 5°. Again, as in the previous figures, ϵ reduces the diameter of the active zone more than μ, but also reduces the $\bar{\beta}_i$. The combination ($\mu = 2.2$, $\epsilon = 3.77$) again appears to be a poor combination in yielding a lower $\bar{\beta}_i$ than even ($\epsilon = 5$, $\mu = 1$), even though both have approximately the same diameter reduction capability. The curve for ($\mu = 10$, $\epsilon = 1$) has a $\bar{\beta}_i$ even higher than free space, as in the previous figures, but the same behavior of $\bar{\beta}_r$ departing strongly from the asymptotic line.

Figures 3-9 through 3-12 show the effects of loading upon a helix of rather large pitch angle, 25°. Some of the curves are somewhat incomplete in their range of $\bar{k}_o$, due to a computational choice rather than any inherent difficulty. The change of scale on the ordinate should be noticed. The curves on Fig. 3-9 are quite comparable with those for the other pitch angles. Apparently $\bar{\beta}_i$ (attenuation per unit of normalized pitch $p/2\pi$) is insensitive to changes in

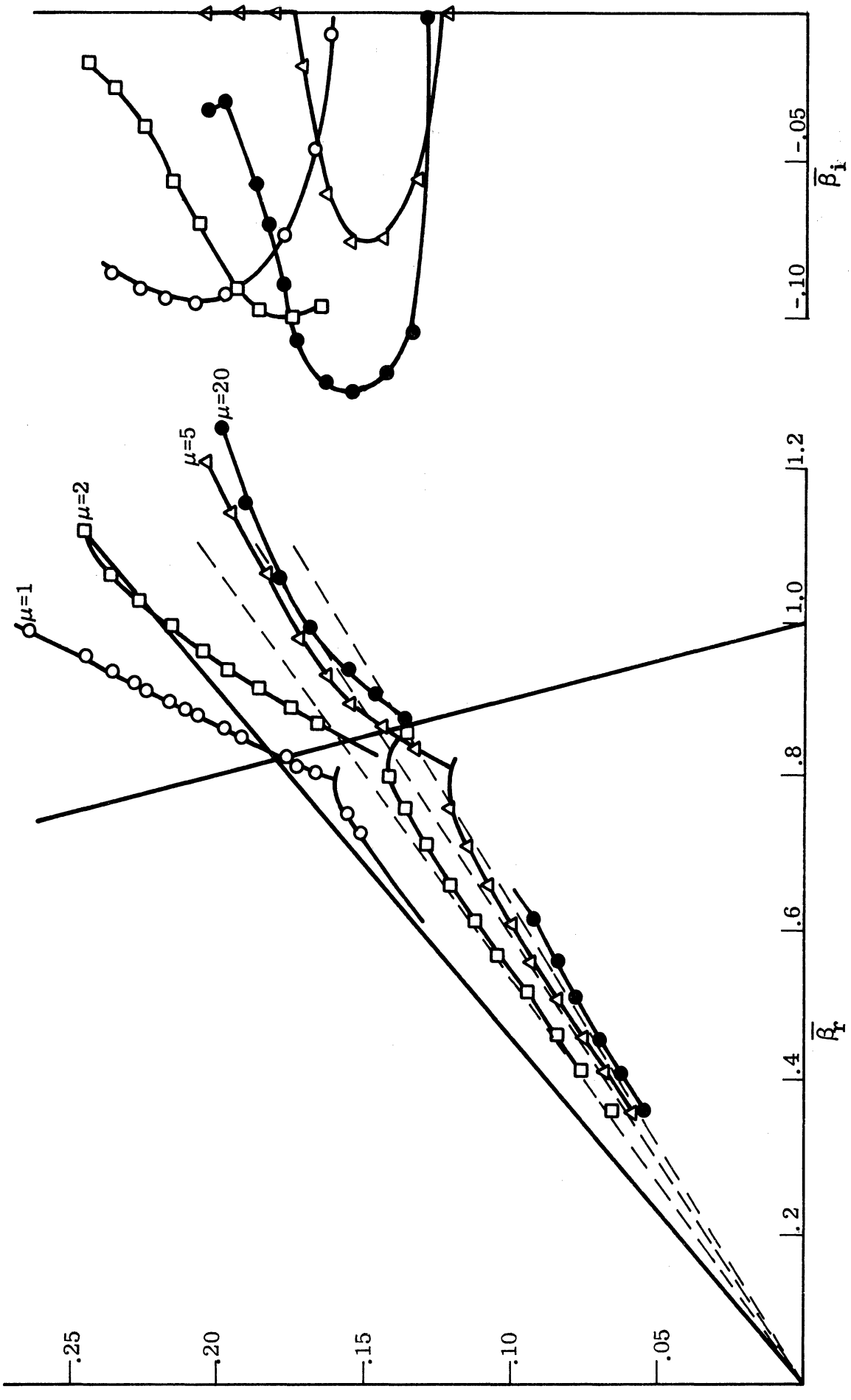

FIG. 3-2: THE EFFECT OF MAGNETIC LOADING ON DISPERSION.
ψ = 12.6°, Δ = .1, ϵ = 1; see Fig. 6-2 for ψ and Δ.

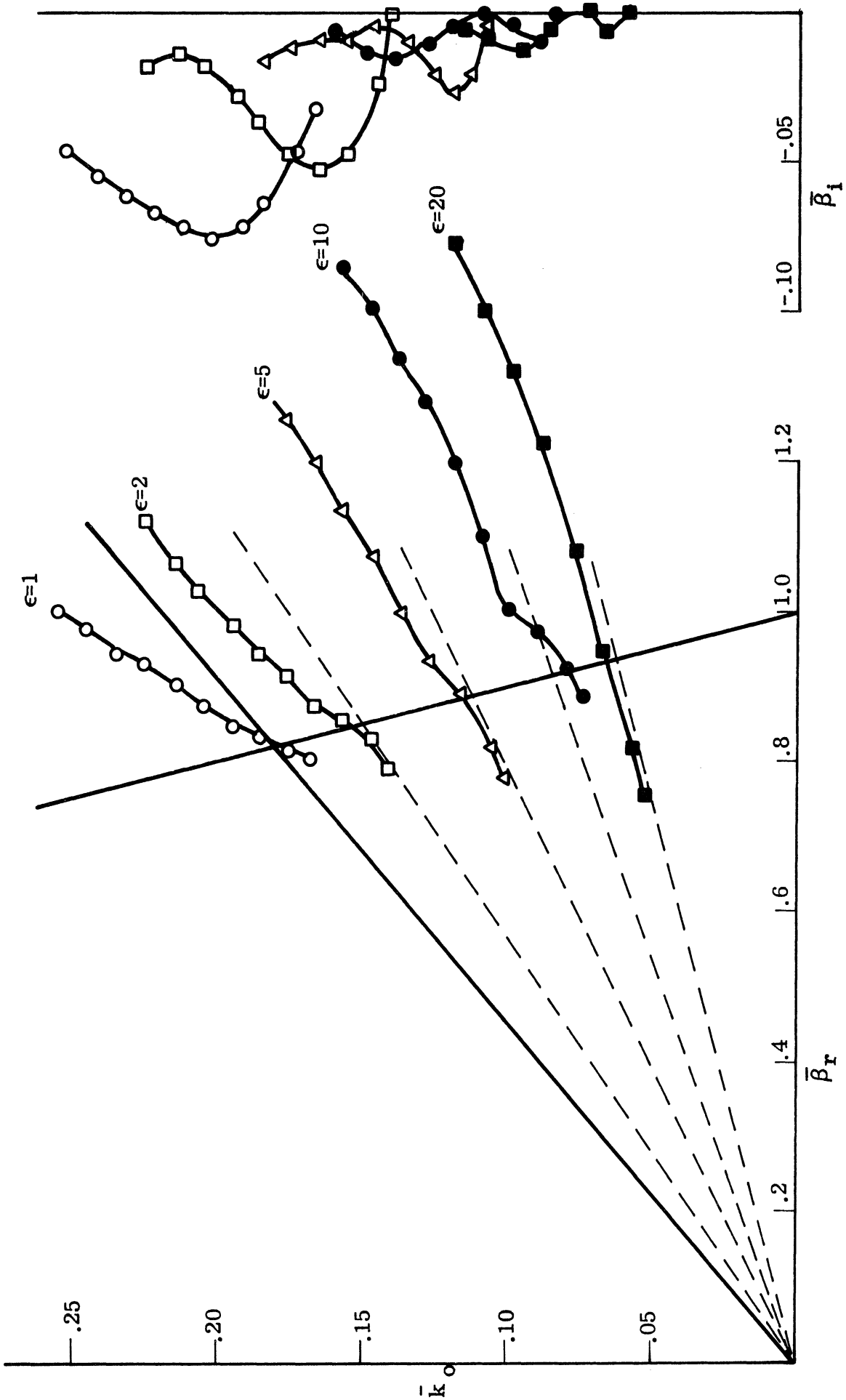

FIG. 3-3: EFFECT OF DIELECTRIC ON DISPERSION.
$\psi = 12.6^o$, $\Delta = .01$, $\mu = 1$; see Fig. 6-2 for ψ and Δ.

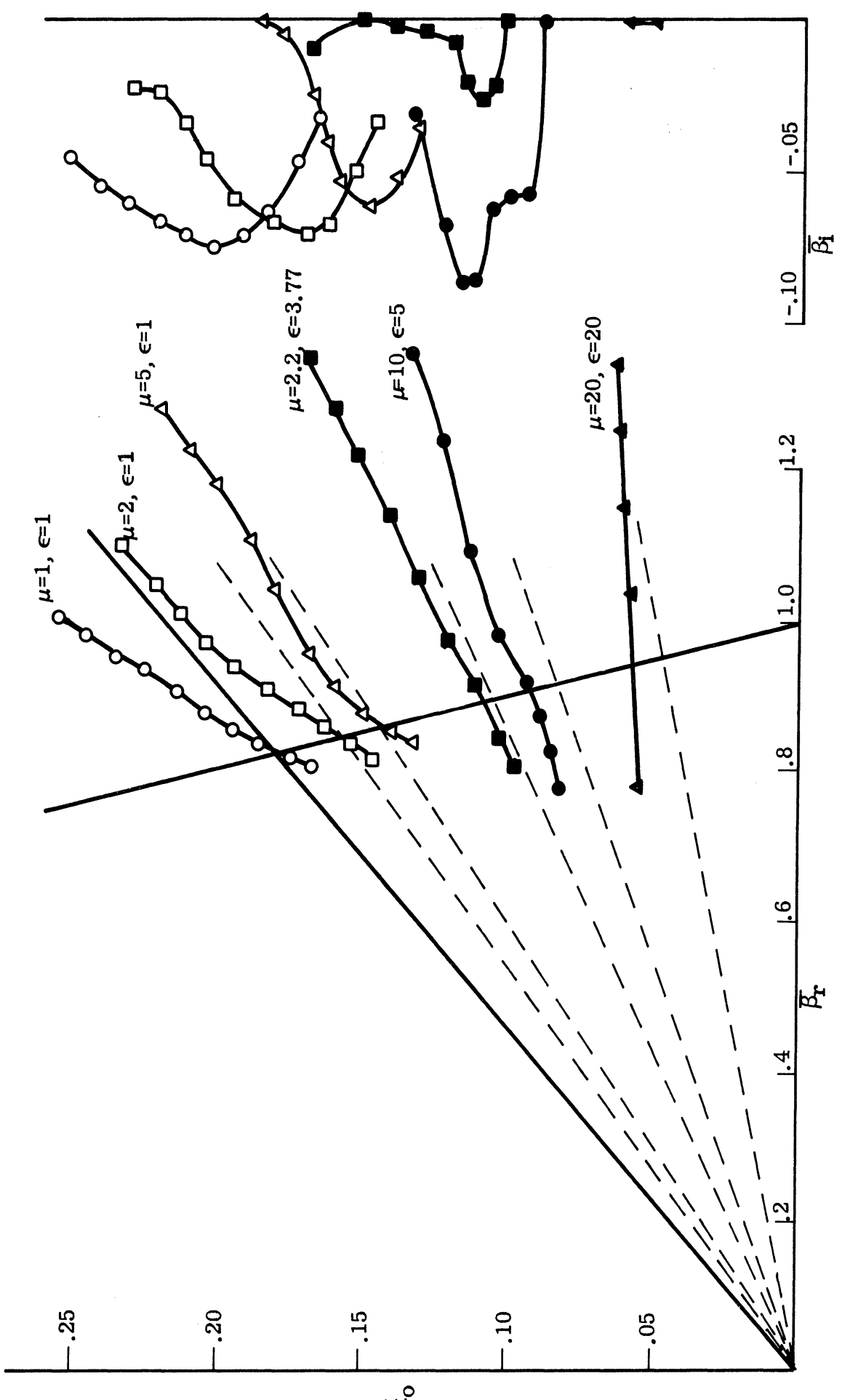

FIG. 3-4: EFFECT OF MAGNETIC AND DIELECTRIC LOADING.
$\psi = 12.6^{o}$, $\Delta = .01$; see Fig. 6-2 for ψ and Δ.

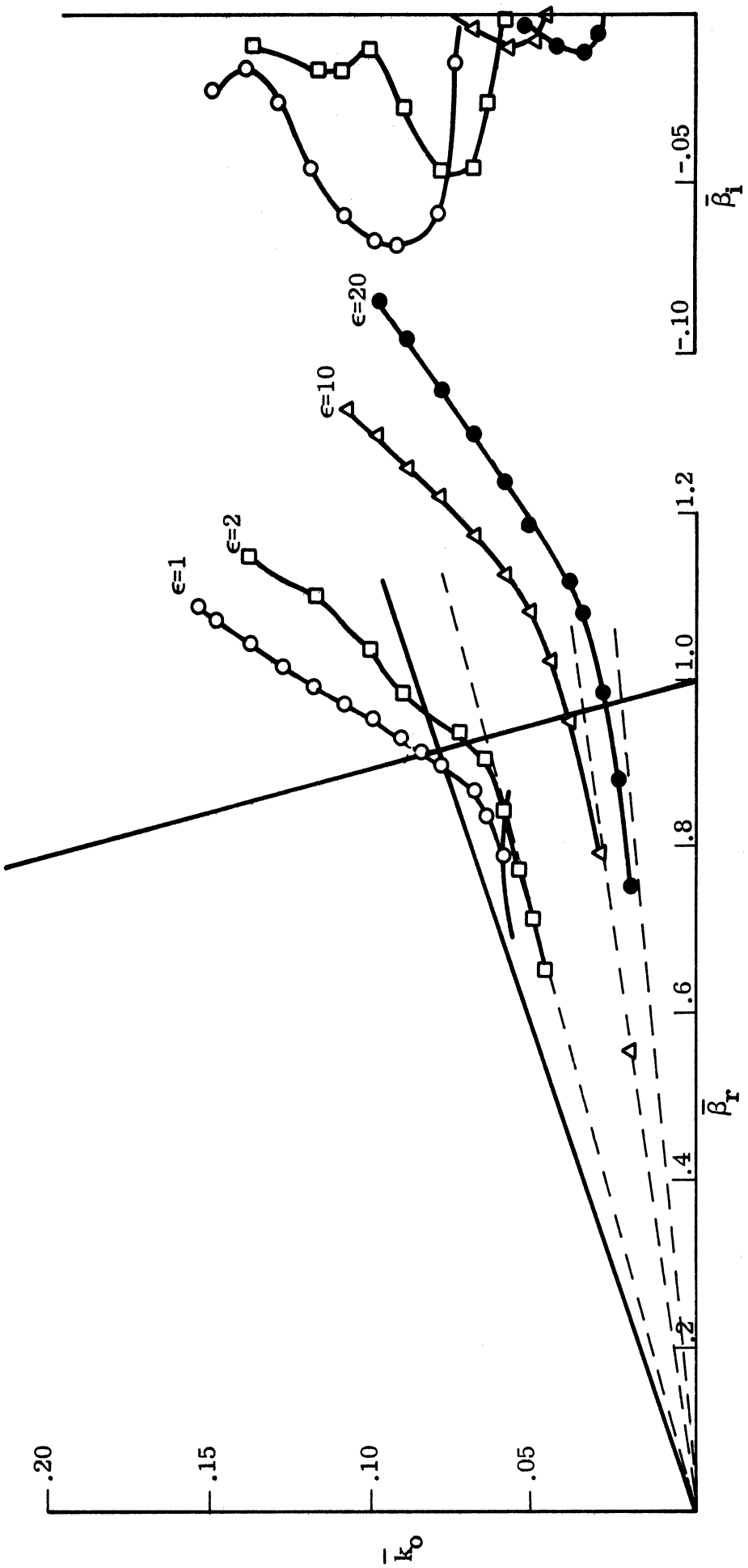

FIG. 3-5; EFFECT OF DIELECTRIC LOADING.
$\psi = 5^o$, $\Delta = .1$, $\mu = 1$; see Fig. 6-2 for ψ and Δ.

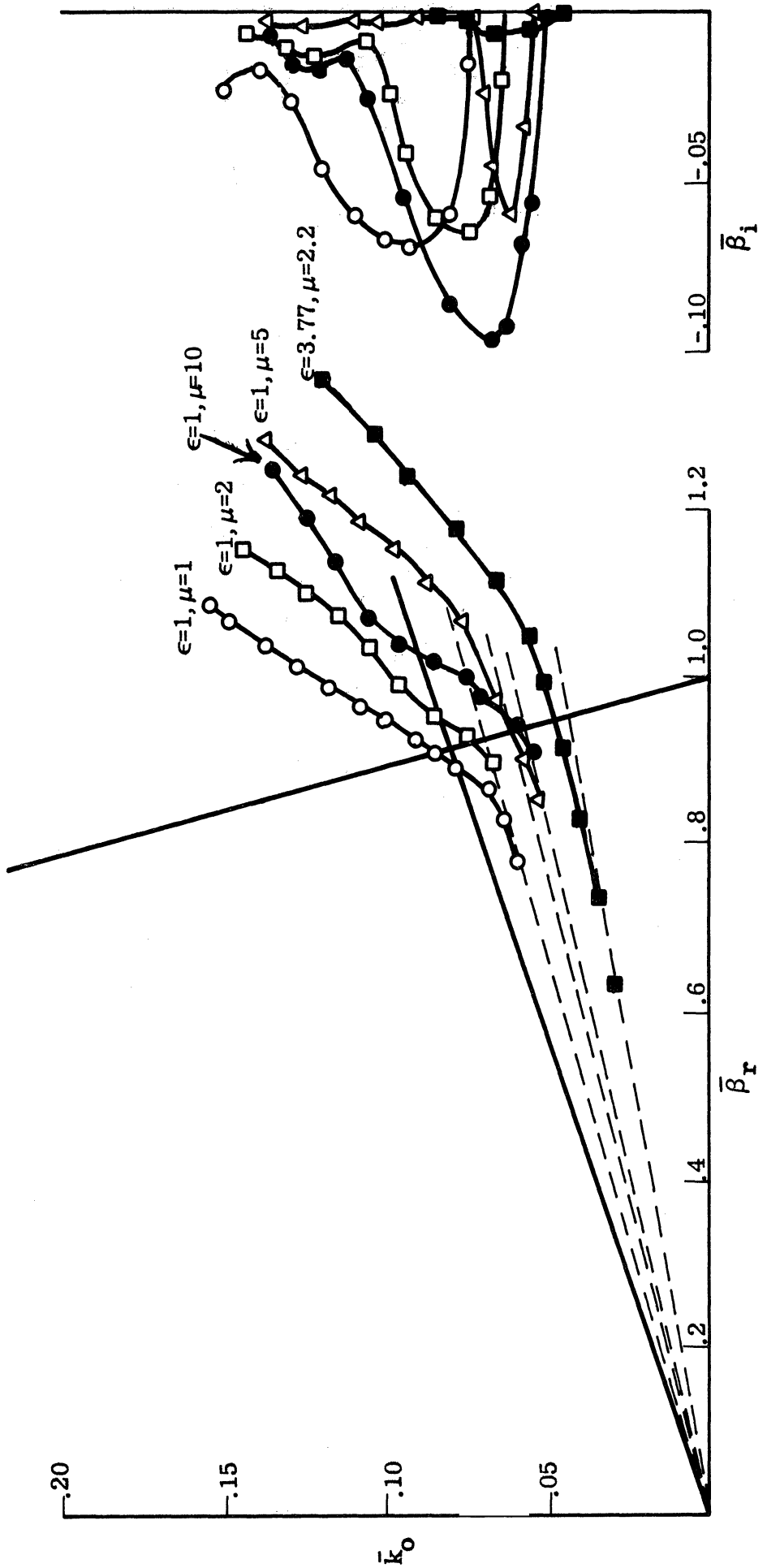

FIG. 3-6: EFFECT OF MAGNETIC AND DIELECTRIC LOADING. $\psi = 5^o$, $\Delta = .1$; see Fig. 6-2 for ψ and Δ.

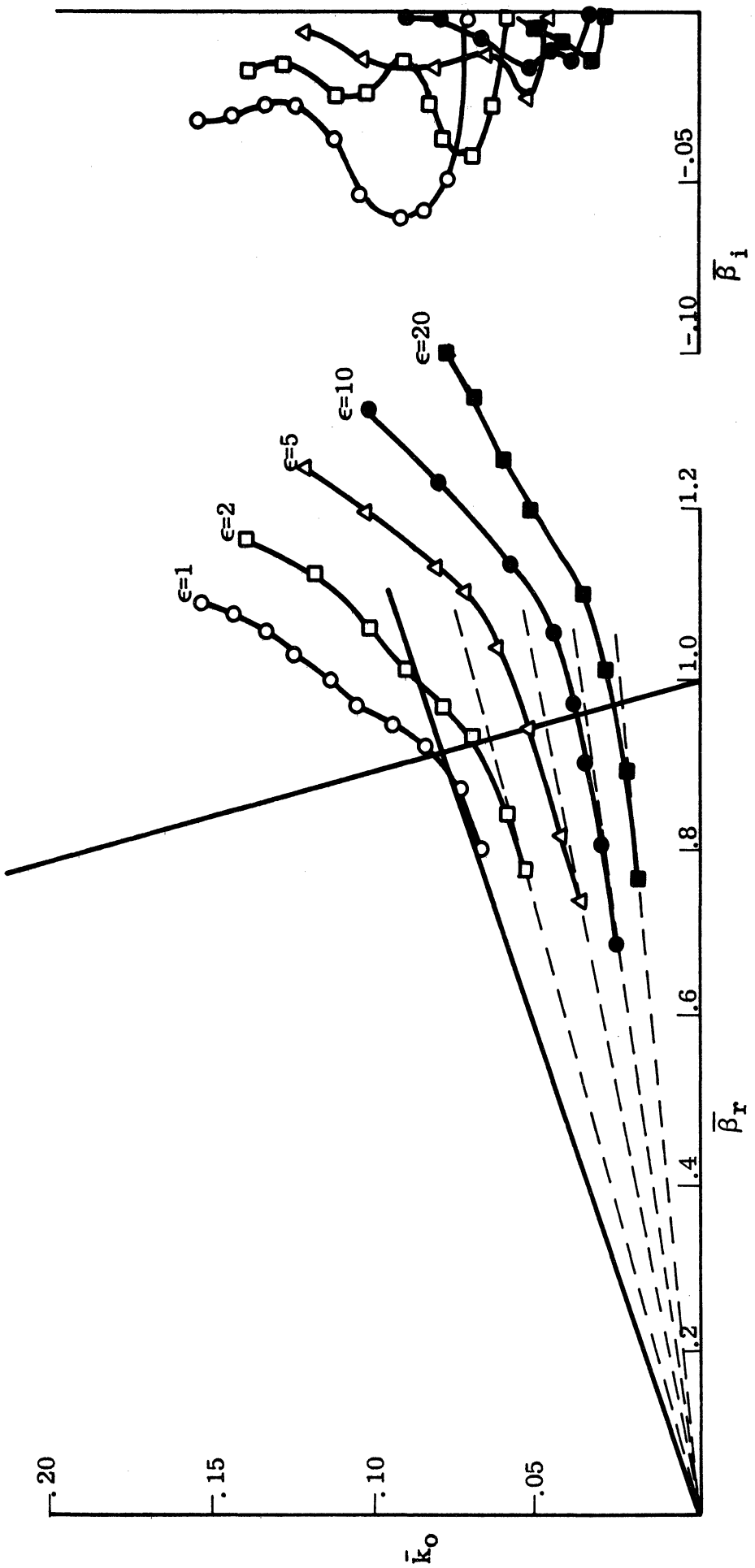

FIG. 3-7: EFFECT OF DIELCTRIC LOADING.
$\psi = 5^o$, $\Delta = .01$, $\mu = 1$; see Fig. 6-2 for ψ and Δ.

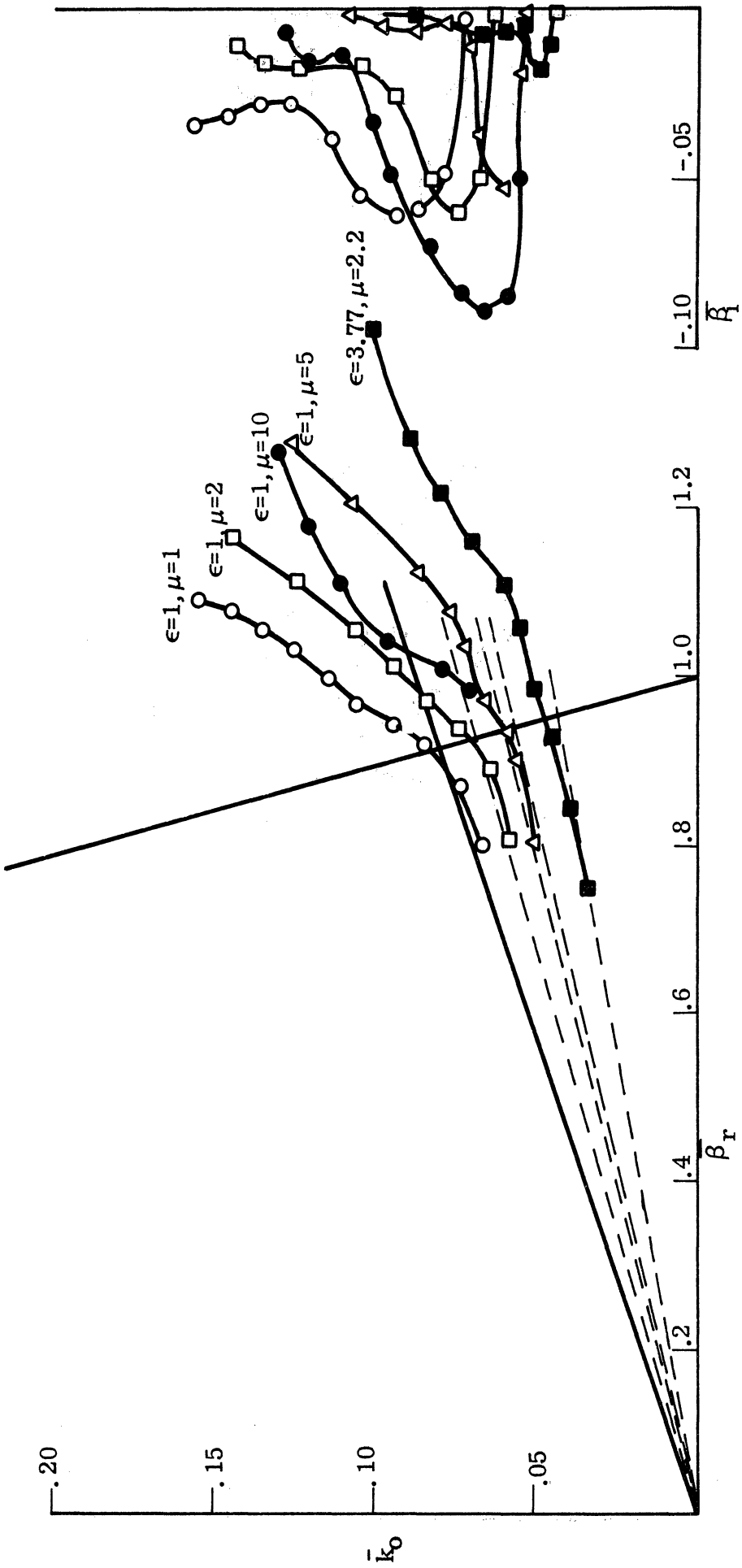

FIG. 3-8: EFFECT OF MAGNETIC AND DIELECTRIC LOADING. $\psi = 5^{\circ}$, $\Delta = .01$; see Fig. 6-2 for ψ and Δ.

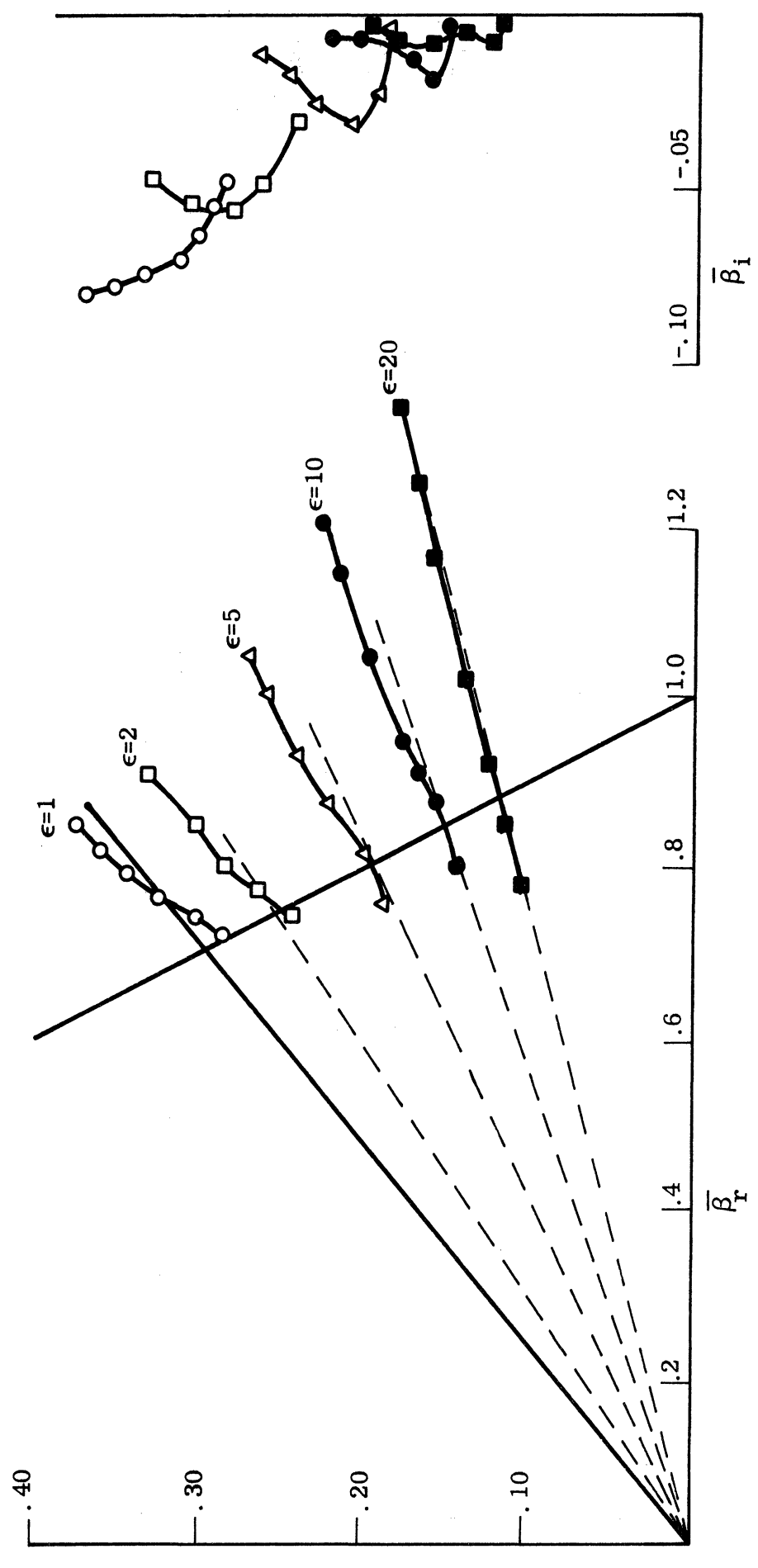

FIG. 3-9: EFFECT OF DIELECTRIC LOADING.
$\psi = 25^o$, $\Delta = .1$, $\mu = 1$; see Fig. 6-2 for ψ and Δ.

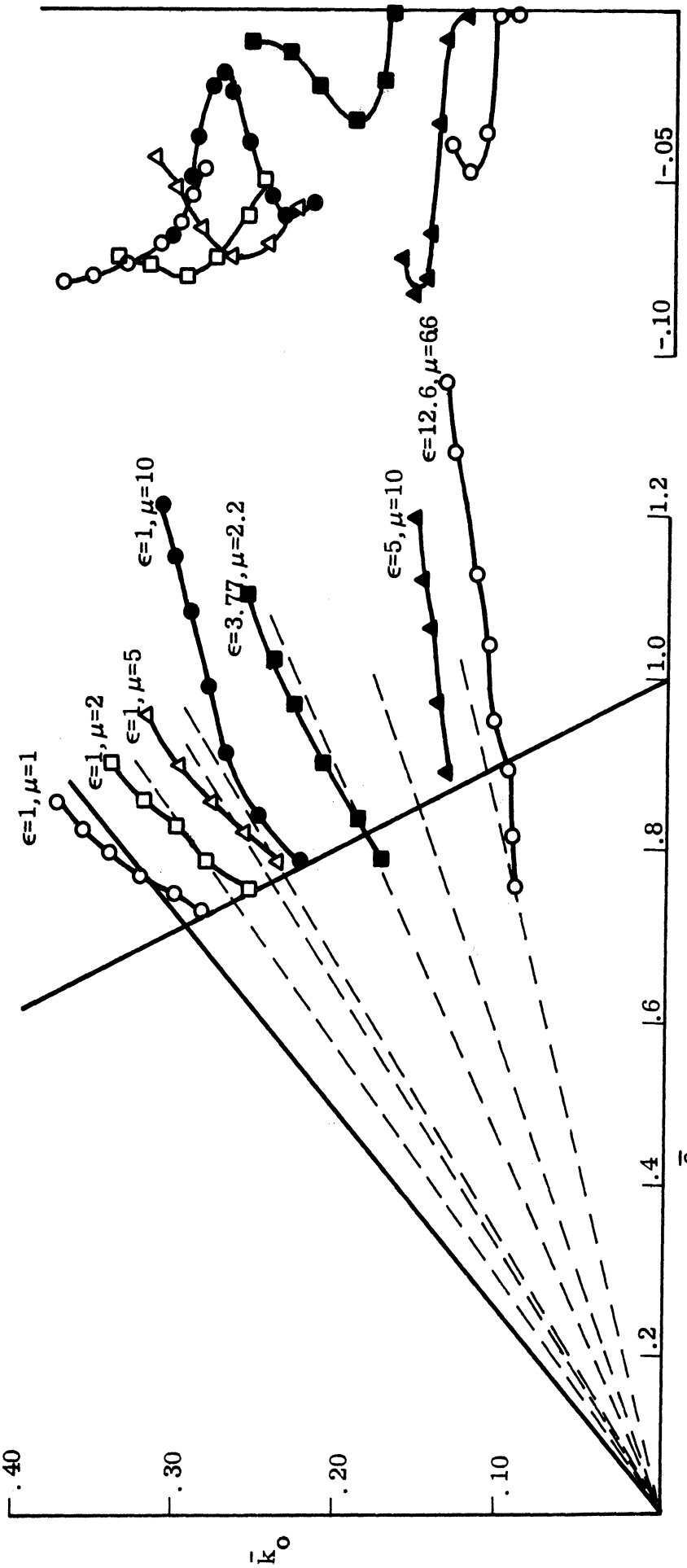

FIG. 3-10: EFFECT OF MAGNETIC AND DIELECTRIC LOADING. $\psi = 25^{\circ}$, $\Delta = .1$; see Fig. 6-2 for ψ and Δ.

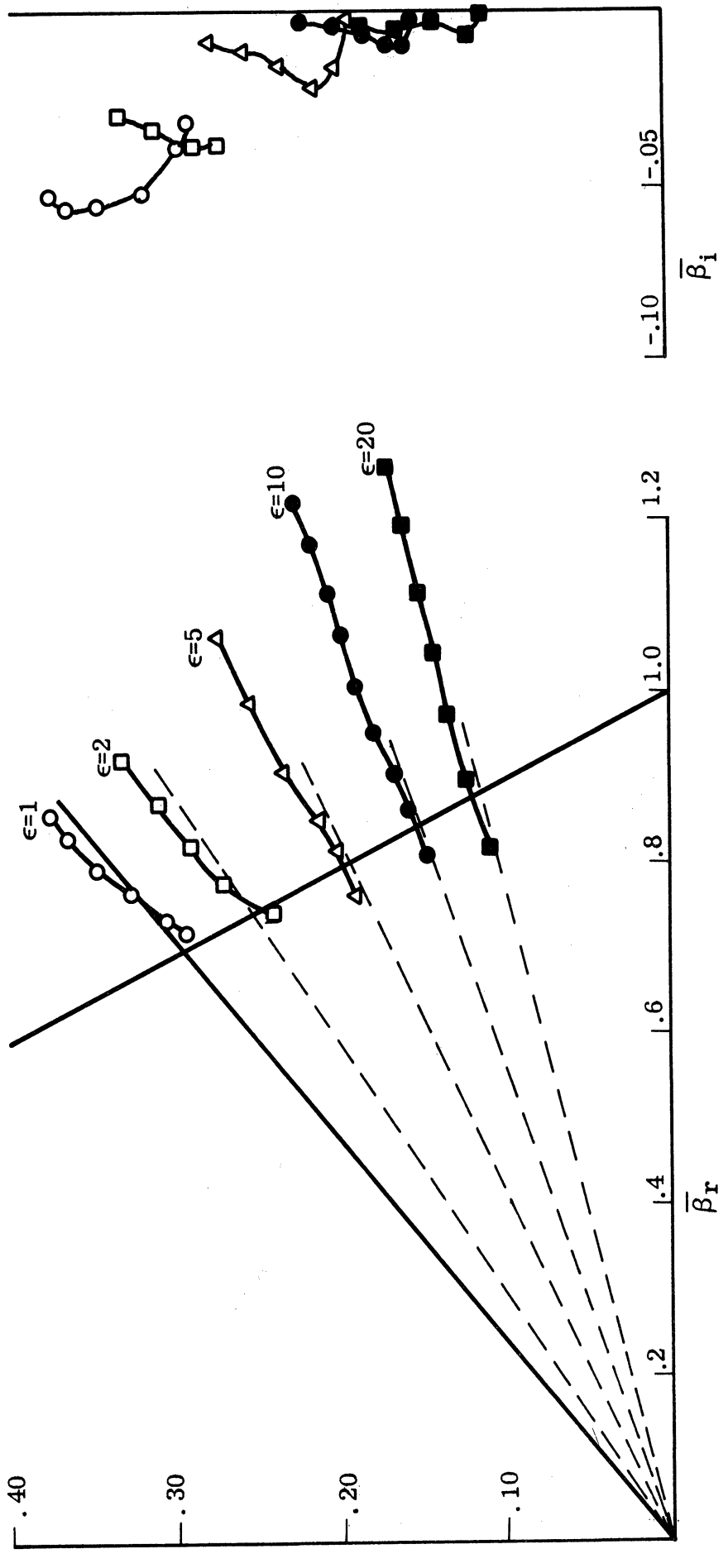

FIG. 3-11: EFFECT OF DIELECTRIC LOADING.
$\psi = 25^o$, $\Delta = .01$, $\mu = 1$; see Fig. 6-2 for ψ and Δ.

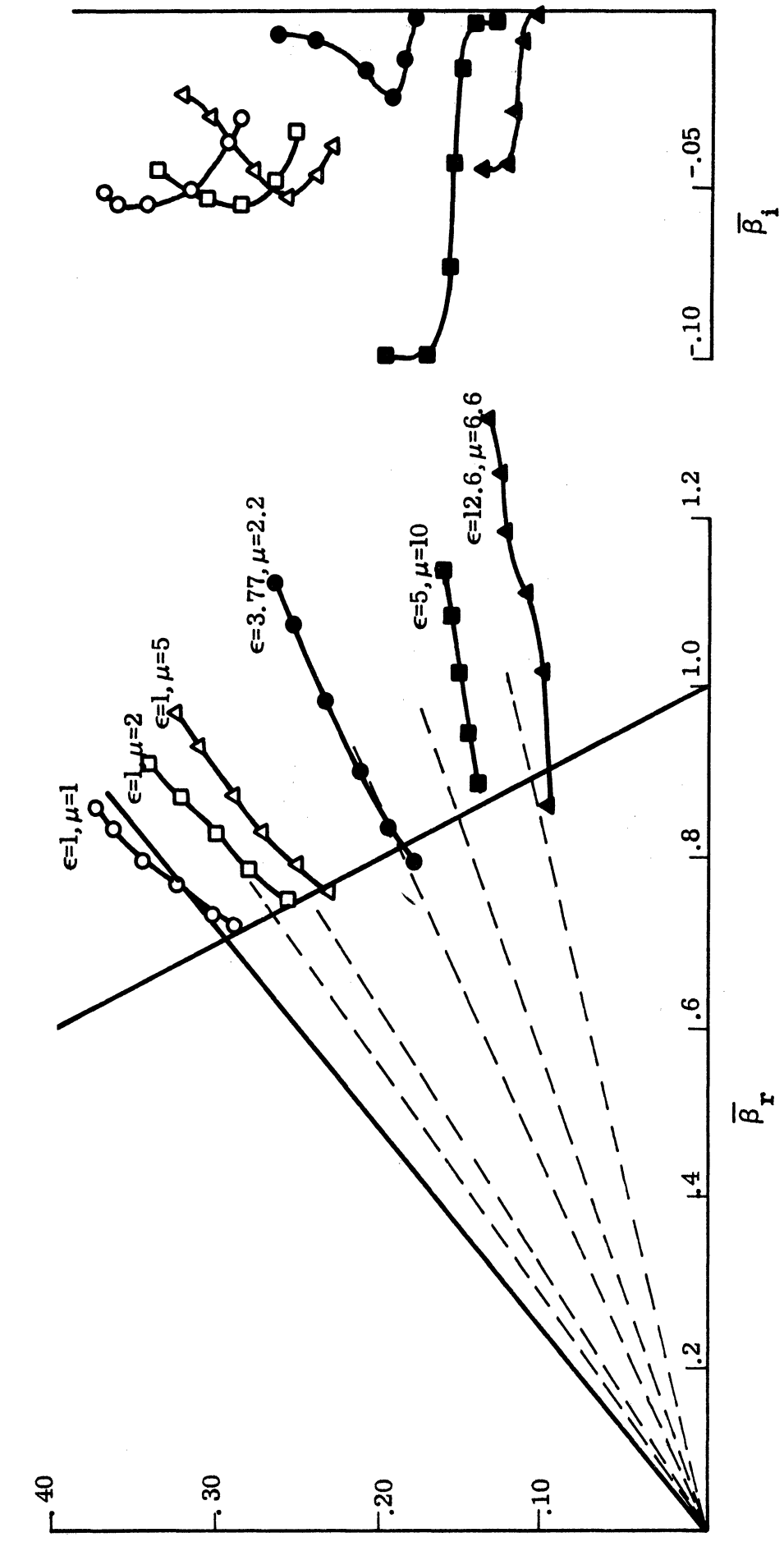

FIG. 3-12: EFFECT OF MAGNETIC AND DIELECTRIC LOADING. $\psi = 25^o$, $\Delta = .01$; see Fig. 6-2 for ψ and Δ.

pitch angle, although slightly less for $\psi = 5^{o}$. Figure 3-10 shows that at $\psi = 25^{o}$, the combination (ϵ=3.77, μ=2.2) is considerably better in terms of $\bar{\beta}_i$. The material (ϵ=5, μ=10) is still uniquely high in β_i, apparently due to the large content of μ. The material (ϵ=12.6, μ=6.6), corresponding to a solid ferrite used by this Laboratory, has a very good $\bar{\beta}_i$ considering the great diameter reduction accomplished. The performance is maintained at the smaller tape width as well.

The solutions of the dispersion equation shown in Figs. 3-1 through 3-12 clearly correspond to a current wave with velocity along the wire approximately the speed of light times the reduction factor of the loading material. This current wave can exist alone; i.e. it is a complete solution or 'mode' which satisfies all the boundary conditions; each spatial harmonic does not. This 'mode' has variously been called the T_0 mode by Kraus (1950) or the Mode 1 by Klock (1963). There is a Mode 2 or T_1 mode which has been ignored throughout this paper, but which is important to forward fire ($\bar{\beta} > 1$) helices. Also, at least in the loaded helix case, solutions have been found to the dispersion equation with rather large β_i, such as the examples shown in Fig. 3-13. With the exception of the $\psi = 25^{o}$ curve, all these solutions were for $\bar{\beta} > 1$, but no concerted search for all possible solutions have been made. The residue for these waves were considerably smaller than for the T_0 solutions, indicating they are harder to excite. Since they decay more rapidly than the T_0 wave, the T_0 wave will predominate on the antenna for most of its length for values of $\bar{\beta} < 1$, for which Mode 2 is not strong. It would appear that a more thorough investigation of these other waves should be made. In this study, it is assumed that means exist to selectively excite only the T_0 mode; the log-conical taper has been experimentally found to be an excellent method, while the truncated helix is not quite as good a method.

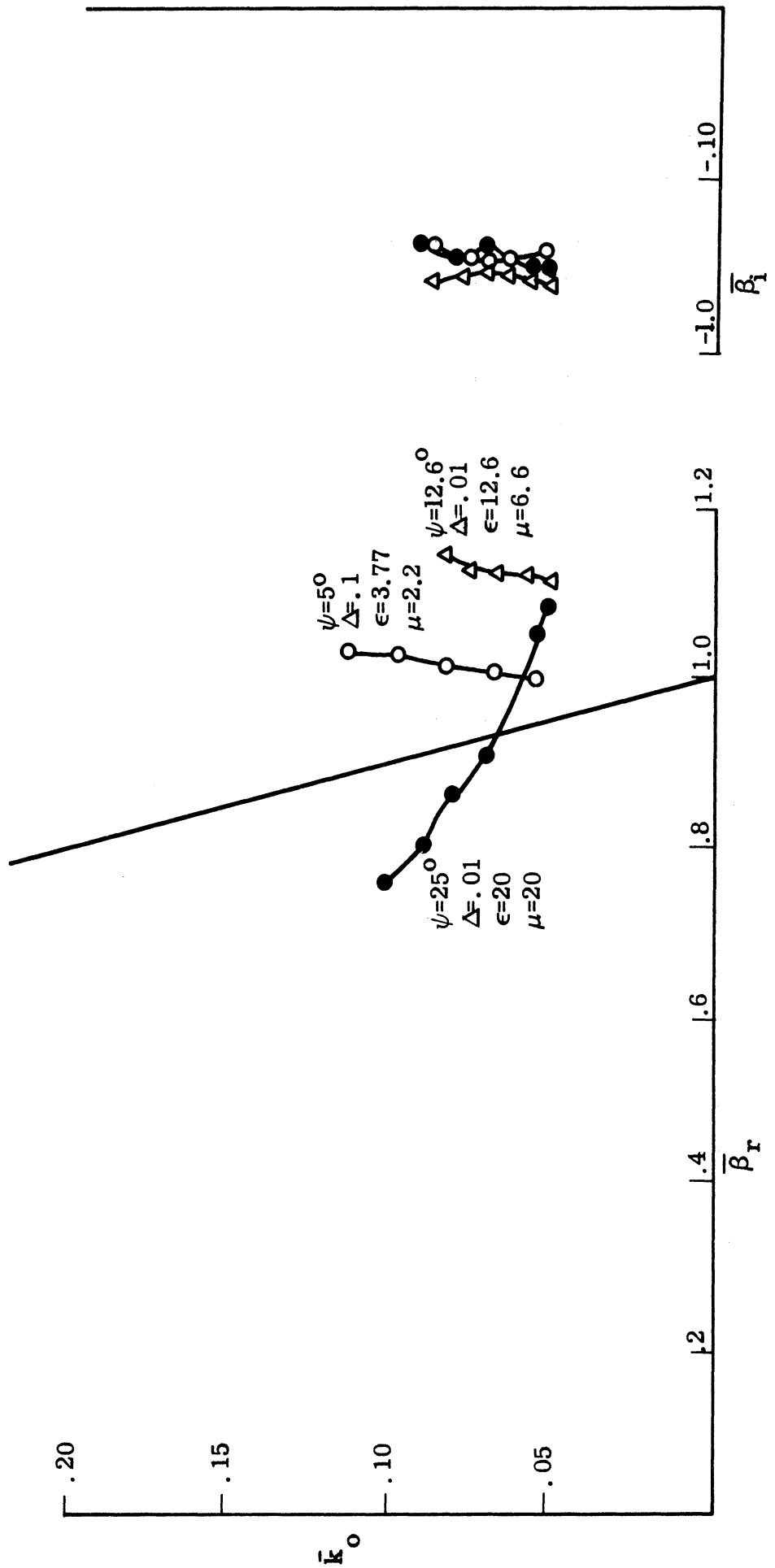

FIG. 3-13: EXAMPLES OF HIGH ATTENUATION LEAKY WAVES FOUND; see Fig. 6-2 for ψ and Δ.

The computer solutions for large μ ($\geq$ 10) show some unexpected behavior, with the attenuation increasing drastically, above even that of the helix in free space; in addition, diameter reduction with loading decreased from that with smaller μ . The physical reason for these solutions is not known. Checks of the solution include considerable care in numerical checking, and the closeness of the solutions to the known asymptotic solutions.

It may be concluded that from the computer solutions shown in Figs. 3-1 through 3-12, that loading of a helix antenna with a full core of material can provide considerable diameter (or frequency) reduction, but that the active length of the helix that takes part in radiation is not correspondingly reduced when only dielectric loading is used. These conclusions can be seen from the fact that the $\bar{k}_0$ of the radiation point is reduced when loading is applied (showing size-frequency reduction); however, $\overline{\beta}_i$ is also reduced. The attenuation per normalized cell, $\overline{\beta_i}$, would have to remain fixed for a scaling of the active zone with diameter reduction. The use of materials having both high permittivity and permeability (e.g. ferrites) appears to offer better hope of reducing this active length, since $\overline{\beta_i}$ is still high for at least some combinations.

A final conclusion is that although the effect of pitch angle is rather strong for some ferrites, otherwise neither ψ nor the tape width Δ seem to have a large effect on the radiation.

IV

FORMULATION OF A TAPE HELIX WITH A SOURCE

One of the simplest source problems for a helix is an infinite helix with a very small voltage discontinuity source in the middle. The major object of discussing this source problem in this report is to clarify the role of the complex (leaky) wave solved for in Chapter III. This wave is shown to be a part of the solution of a source problem in certain regions close to the antenna. In fact, the point in solving for the leaky wave propagation constants has been to use the complex T_0 (leaky) wave alone as a good representation of the current on the helix. Once the current on the helix has been obtained, the far fields may be obtained by the usual integration. This method was used successfully by Tamir and Oliner (1963) on another problem as an alternative to the usual saddle point integration for the far field. The actual evaluation of all the integrals involved for the present function in the region of the antenna (near field) proved too complicated for this report.

This problem of a small source for an infinite helix in air has been previously formulated by Sensiper (1951), under the assumption that no complex solution to the determinental equation existed, and by Klock (1963), who used the numerically found residues of the complex poles, but did not cover the problem of the branch cut integrals involved. A solution for a simpler related problem having periodic boundary conditions has been performed by Sigelmann and Ishimaru (1965) for an infinite plane slab of dielectric covered on one side by solid metal and on the other by periodic uniformly wide strips of metal with narrow air gaps, and excited by a magnetic current source. This reference covers the complete solution to the problem including the effect of the branch points and leaky wave poles by the saddle point method, but only for the far field. The location of the poles were not solved for. Karjala and Mittra (1965) have solved a source problem with periodic corrugated surface.

4.1 Formulation of the Inversion Integral

Much of the calculation is simplified by the results of Chapter III. The source requires that the E-field parallel to the wire ($E_{//}$) to be

$$E_{//} = \begin{cases} E & \text{in the gap (source)} \quad |z| < \ell/2 \\ 0 & \text{on the conductor} \quad |z| > \ell/2 \end{cases} , \tag{4.1}$$

assuming that $\ell << \Delta$; i.e., no fringe affects in the gap. Admittedly, for a very small Δ, such a gap becomes physically impossible.

The Fourier transform $E_{//}$ of the E-field can then be written as

$$\tilde{E}_{//}(\beta) = \frac{1}{2\pi} \int_{-\infty}^{\infty} E_{//}(z) e^{+j\beta z} \, dz$$

$$= \frac{E}{\pi\beta} \sin \beta \, \ell/2 \quad . \tag{4.2}$$

However $\tilde{E}_{//}(\beta)$ can be written as the product

$$\tilde{E}_{//}(\beta) = \tilde{I}(\beta) \, \tilde{G}(\beta) \tag{4.3}$$

where $\tilde{I}(\beta)$ and $\tilde{G}(\beta)$ are the Fourier transforms of the current in the helix with the source and the Green's function for this problem, respectively. In this form, however, the transform of the Green's function can be recognized immediately, without re-calculation since it was essentially obtained in Chapter III.

In Sensiper's original method for finding the dispersion equation mentioned in Chapter III, the equation

$$E_{//}^{NS}(z) \Big|_{\substack{\text{centerline} \\ \text{of tape}}} = 0 \tag{4.4}$$

where NS refers to the no source or free mode case, was used rather than the variational formulation (3.37) used in this report,

$$L(\beta)= \sum_{n=-\infty}^{\infty} E^{NS}_{zn\alpha} j^{*}_{zn} + E^{NS}_{\phi n}\, j^{*}_{\phi n} = \sum_{n=-\infty}^{\infty} E^{NS}_{//n}\, j^{*}_{n} = 0 \quad . \tag{4.5}$$

From (4.4) and (4.5),

$$E^{NS}_{//}(z)= \exp\,(j\omega t - j\beta_o z + jn\phi) \sum_{n=-\infty}^{\infty} \frac{L_n(\beta)}{j^{*}_{n}} \quad . \tag{4.6}$$

Actually, the presence of the exponential factor is simply a way of avoiding the general Fourier transform, by assuming a single frequency and a single β_o propagation constant for the current wave in the free mode case. The current is assumed in the form

$$I^{NS}_{//}(z)= J \exp(j\omega t - j\beta_o z + jn\phi) \quad . \tag{4.7}$$

The Fourier transforms of the electric field and the assumed current 'causing' the field obviously contain a delta function, indicating only one current wave was considered in the source free case,

$$\tilde{E}^{NS}_{//}(\beta_o) = \frac{\delta(\beta-\beta_o)}{2\pi} \sum \frac{L_n(\beta)}{j^{*}_{n}}$$

$$\tilde{I}^{NS}_{//}(\beta_o) = \frac{J}{2\pi}\,\delta(\beta-\beta_o)$$

where the δ is the usual delta function. The Green's function relating this particular assumed current to the field is

$$\tilde{G}(\beta) = \frac{\tilde{E}^{NS}_{//}(\beta_o)}{\tilde{I}^{NS}_{//}(\beta)} = \frac{1}{J} \sum \frac{L_n(\beta)}{j^{*}_{n}} \tag{4.8}$$

where the Green's function is valid for any k and β, not just for the particular ones assumed in the source free problem.

Using this Green's function, derived from the source-free problem, the current in a general source problem can be obtained as follows.

From (4. 3)

$$\tilde{I}(\beta) = \frac{\tilde{E}_{//}(\beta)}{\tilde{G}(\beta)} \quad . \tag{4.9}$$

The inverse Fourier transform gives

$$I(z) = \int_{-\infty}^{\infty} \frac{\tilde{E}_{//}(\beta)}{\tilde{G}(\beta)} e^{-j\beta z} dz \quad . \tag{4. 10}$$

Substituting from (4.8) and (4.2) ,

$$I(z) = \frac{E}{\pi} \int_{-\infty}^{\infty} \frac{\sin \beta \ell/z}{\beta \tilde{G}(\beta)} e^{-j\beta z} dz = \frac{E\ell}{2\pi} \int_{-\infty}^{\infty} \frac{\frac{\sin \beta \ell/z}{\beta \ell/z}}{\tilde{G}(\beta)} e^{-j\beta z} dz \quad . \tag{4. 11}$$

An almost identical integral, for the case of the unloaded infinite helix, has been obtained by Klock (1963), Sensiper (1951) and Kogan (1949) by the method of setting up the fundamental integral equation for the problem, and then solving it approximately using expansions in terms of space harmonics. Sensiper (1951) and Klock (1963) also used the method in Chapter III (mode-matching by boundary conditions) for the unloaded source-free helix, and showed how the solutions compared.

4. 2 Contribution of Leaky Wave Poles; Relation to Free Mode Solutions

Notice that the solution for I(z) is now presented as an inversion integral in which the zeros of $G(\beta)$, which are also the zeros of the $L(\beta)$ obtained in Chapter III, are now the poles of the inversion integral. The complex β plane,

with the poles and branch cuts of (4.11), is shown in Fig. 4-1. Only the odd modes are excited; thus, only the odd 'cells' of ($\frac{2\pi}{p}$ n) have branch cuts and poles. The poles corresponding to the complex (leaky) waves are also shown in Fig. 4-1, along with the surface wave poles corresponding to the higher modes.

The path of integration for the inversion integral (4.11) is along the real β axis as shown. This integral is very involved due to the complexity of $L(\beta)$, but it could be performed numerically. A more common procedure in this integral is to deform the contour of the integral in the β plane to the infinite semicircle in the third and fourth quadrants of the β plane ($\beta=\beta_r+j\beta_i$), as shown in Fig. 4-1. Because of the exponential factor in the integrand, the integral is zero over this semicircle. However, since the deformation of the path sweeps across the poles shown in the upper half of the β plane, residues of the poles appear in the inversion integral in those regions of space where the fields satisfy the radiation condition, such as on the surface of the antenna. The actual problems of where the residues of complex waves contribute to the inversion integral is best discussed via saddlepoint (steepest descent) methods (Tamir and Oliner, 1963; Bernard and Ishimaru, 1963).

4.3 Contribution of the Branch Cut Integrals to the Inversion Integral

The residues of the poles enclosed in the semicircle are not the only contributions to the integral. The path around the semicircle must be brought in around the branch cuts, as shown, causing contributions due to these branch cuts. These contributions form the radiation fields and decay at least as rapidly as $(kz)^{-3/2}$ along the antenna (Tamir and Oliner, 1963).

The usual method of evaluating such integrals, including the effect of the poles, is by the saddle point integration. However, this method depends upon integrals of the form

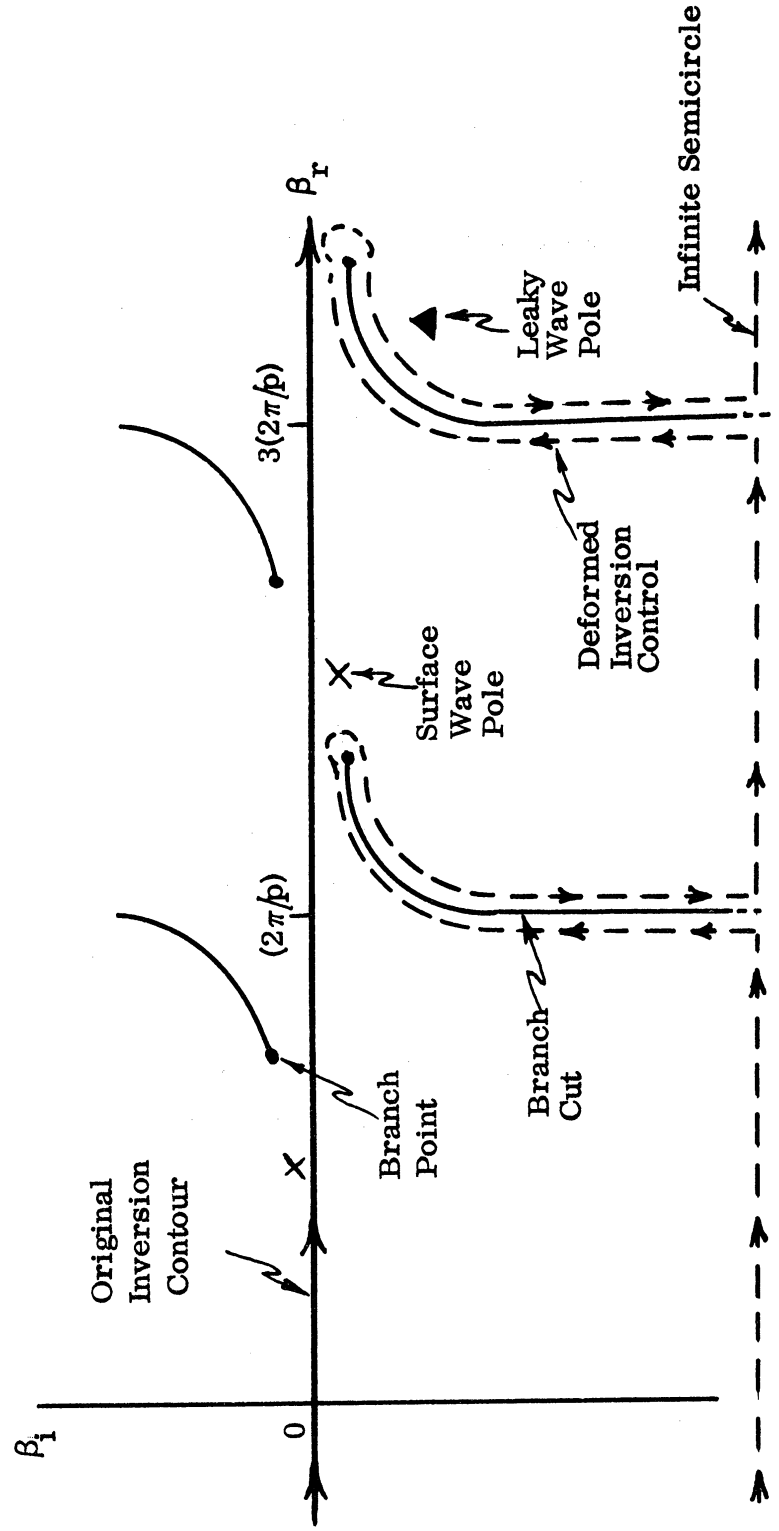

FIG. 4-1: COMPLEX β PLANE WITH ORIGINAL AND DEFORMED INVERSION CONTOURS.

$$I = \int F(\gamma) e^{-j\Gamma x} e^{-j\beta z} d\beta$$

$$= \int F(\phi) e^{-jk\cos(\theta-\phi)} d\phi$$

where the dependence of the fields in both dimensions of the two-dimensional problem is exponential. The inversion integral (4.11) is more difficult because of the Bessel function dependence for (Γr). An asymptotic approximation to the Bessel functions could be made to get an approximate exponential dependence for the fields as a function of radius, such as was done by Patton (1962).

The saddle point method must be modified in the case that only small distances are considered, as for the near fields of antennas, or when the steepest descent contour passes close to a pole of the integrand. These modified methods are mathematically presented in Van Der Waerden (1951) and very clearly in Bernard and Ishimaru (1963). Both modifications appear in the present problem.

Because of the difficulty involved in performing the branch cut integrals, particularly at the small distances on the surface of the antenna, an explicit integration is not given here. Nevertheless, there are many cases when one can say that the residue contributions from the poles are larger than the branch cut integrals along a surface wave device. Briefly, if the exponential decay factor of a surface wave pole is very small, then at moderate distances from the source, the surface wave field corresponding to that pole will dominate over the corresponding branch cut integral in the near field because of the greater decay $(kR)^{-3/2}$, of the radiation field of the branch cut integral. In addition, Tamir and Oliner (1963) have shown that the fields of a leaky wave with a small imaginary part may also be dominant over the corresponding branch cut fields on the surface of an antenna. A modified expression including an error function and the pole

residue is said to be (Bernard and Ishimaru, 1963) an excellent near field approximation in the general direction of travel of a leaky wave.

The magnitude of the residue as well as the relative excitation of the leaky wave versus the radiation field are both important additional factors. The residue of the leaky wave in the helix case is quite large, which would indicate a dominance of this leaky wave. Nevertheless, its attenuation coefficient is fairly large.

Another recent report by Laxpati and Mittra (1966) on the source problem for a planar spiral antenna shows more clearly that the integrals not associated with the residue of the surface wave are very small if the gap across which the source feds power is very small at the center of the spiral. Although attempts to extend this work to a conical spiral antenna have so far been unsuccessful, the principle is probably the same.

The main evidence for the dominance of the leaky wave contribution over the other fields on the surface of the antenna, in the case of loaded helical antennas, must at present come from the experimental measurements, due to the complexity of the branch cut integrals. Experiments in Chapter V definitely show an exponential decay of the currents for the helix. In addition, phase measurements on the loaded conical helix (Chapter V) and amplitude and phase measurements on the unloaded conical helix (Dyson, 1964) show a propagation constant, including decay, such as predicted by the leaky wave pole corresponding to the T_o current wave calculated in Chapter III.

4.4 Relative Magnitude of Pole Contributions

If the residues are dominant in (4.11), then the current on the conductor may be represented by the residue theorem

$$I(z) \cong \frac{E\ell}{2\pi} \sum_{m} \begin{matrix}\text{Residues} \\ \text{of the poles}\end{matrix} \left(\frac{\sin \beta_o^{(m)} \ell/2}{\beta_o^{(m)} G(\beta)} \right) e^{-j\beta_o^{(m)} z} \qquad (4.12)$$

assuming that the integral on the infinite semicircle vanishes.

$$\cong \frac{E\ell}{2\pi} \sum_{m} \frac{e^{-j\beta_o^{(m)} z}}{\frac{d\, G(\beta)}{d\beta}} \quad , \tag{4.13}$$

where

$\frac{\sin \beta \ell/2}{\beta \ell/2} \cong 1$ for m small, assuming only a few current waves are large,

$\beta_o^{(m)}$ is the current wave propagation constant for the mth current wave (not β_n, the propagation constant for the nth spatial harmonic) .

Although the residue versus the branch cut (space wave) contributions have been discussed, no mention has been made of the relative amounts of the residues from the various current waves (zeros of $G(\beta)$) that can propagate. Indeed, only the T_0 current wave has been discussed. However, numerical calculations of residues for the free space monofilar helix (Klock, 1963) have shown that near $ka \leq 1$, the residue of the T_0 current mode is dominant over the T_1 current mode.

Experimentally, the phase velocity measurements of a narrow wire bifilar conical helix in air for $ka \leq 1$ always give velocities of current propagation near the speed of light, corresponding to (4.14) and the T_0 current mode.

A possible explanation of the dominance of the T_0 wave residues is the following; it is seen from (3.72) that the T_0 current wave corresponding to the propagation constant β_0 used in this report, is given for narrow conductors by the non-resonant sum equal to approximately zero,

$$k_o a \cong \beta_o a \sin \psi \sqrt{\frac{1+1/\mu}{1+\epsilon}} \quad . \tag{4.14}$$

For a zero to occur in $L(\beta)$ at any other β_o, say $\beta_o^{(n)}$, the resonant term would have to be very large to cancel the large non-resonant term. This could cause large derivatives which could cause the residues of these other modes to be very small compared to the T_o wave solution β_o.

Rather than numerically computing the dispersion equation using Bessel functions, a complete numerical solution to the integral equation problem for unloaded thin wire antennas may be performed . Mei (1965) has some such computations, yielding similar results for the current distributions of a planar spiral antenna, but with a standing wave in addition. A comparison of such calculations to model calculations is given in Laxpati and Mittra (1966). The problem of extending such calculations to material loaded antennas lies in the resulting three-dimensional integrals compared to the one-dimension integrals in the unloaded wire case.

V

EXTENSION TO THE CONICAL HELIX

5.1 Basic Step-wise Approximation; WKB Improvement

As has been discussed in the introduction there have been successful studies of unloaded conical helix antennas as a helix with gradually varying parameters (Mittra and Klock, 1966; Dyson, 1964) since an isolated 'active' zone on the conical helix antenna is the main contributor to radiation. One simple way to analyze the conical helix, then, is to use the k-β diagram for a cylindrical helix of the same pitch and tape width as the conical helix has near its active zone. The region smaller than the active zone is merely a good tapered feed for the active zone; it does not contribute to radiation. The region larger than the active zone does not possess any currents or fields, if the active zone is well-designed to radiate all the energy fed to the antenna. Since the k-β diagram is usually normalized as $k_o a$ versus $\beta_o a$ or $k_o a/\cot\psi$ versus $\beta_o a/\cot\psi$, one can consider that either frequency k_o or the radius a changes. For the conical helix case, then, one only needs to gradually move up the k-β diagram as the cone-radius increases to find the appropriate complex β_o for each part of the cone. The real part of β_o gives the phase constant at each point; the imaginary part gives the attenuation rate per unit distance. By integrating these effects along the wire, phase and amplitude of the current can be obtained at each point. Far field patterns can then be calculated. Actually, the phase velocity (from β_r) gives immediate knowledge of the general direction of radiation, while inspection of attenuation rate (β_i) indicates the active zone extent; together, they indicate fairly well the performance of the conical helix as an antenna. A fast attenuation rate is necessary for complete radiation in a conical helix that has a wide cone angle. A slower attenuation rate indicates a longer active zone, and a necessarily small cone angle so that the phasing of

all parts of the active zone will be for backfire radiation.

Instead of a stepwise approximation, some improvement may be obtained by using the WKB method, often used in optics for ray tracing in inhomogeneous media that have only slow spatial variations (Morse and Feshbach, 1953). Using this method, Mittra and Klock (1966) report that instead of the form for the current $J(n')$ at a postion n' ,

$$J(n') = J(0)e^{-j\int_0^{n'}\beta(\xi)d\xi}$$

obtained for the stepwise approximation by integrating of the phase effects, one obtains a formula characteristic of the WKB method,

$$J(n')=J(0)\sqrt{\frac{\beta(0)}{\beta(n')}}\exp\left[-j\int_0^{n'}\beta(\xi)\,d\xi\right] \quad .$$

The analysis does assume a single T_o current wave predominant along the conical helix tape. This is true for a well-designed slowly-tapered conical helix, but has not always been the case for the loaded conical helix or the cylindrical helix , probably due to inadequate tapering.

5.2 Effect of Antenna Loading on Active Region: Example

To discuss a specific example, from the results in Chapter III, Fig. 3-1 shows that an unloaded helix ($\psi=12.6^{o}$, $\Delta = .1$) has a maximum attenuation constant of approximately $\overline{\beta}_i = .1$, which means an exponential attenuation of the form

$$I(z) \sim e^{-\overline{\beta}_i \cdot 2\pi z/p} \quad .$$

Thus for the current to be down by e^{-2},

$$W \cong \frac{2p}{2\pi\overline{\beta}_i} \cong \frac{2p}{.6} \cong 3.3\,p \quad ,$$

i. e. one must have somewhat more than three cells, or pitch distances, in the active region, defined by the diametrical range $.17 < ka/\cot\psi < .25$, approximately . If the helix is loaded with a dielectric of $\epsilon = 5$, the $\bar{\beta}_i$ is reduced to .03 - .04 maximum over a region $.11 < ka < .13$ as seen in Fig. 3-1. In this region $W = 10p'$, or ten loaded pitch distances, p', must be within the much narrower diametrical range. On the other hand, the pitch distances (twice the wire to wire spacing) are less when the diameter D is smaller; in the above case, if the ratio

$$p/p' \cong D/D' \cong .11/.17 \cong .65$$
$$W = 10p' \cong 6.5\ p$$

where W is the required axial length for the active region and has a value about twice the original active zone length. Since this distance must be achieved in a much narrower diametrical range, the maximum permissible cone angle (i. e., taper) will have to be drastically reduced over the maximum permissible cone angle in the unloaded case. Note that regardless of the shape of the $\bar{\beta}_i$ curve, the upper limits of $\bar{k}$ must be considerably less than the value at the intersection of the $\bar{k}$-$\bar{\beta}_r$ diagram with $\beta = 1$ line of broadside radiation, if backfire radiation is to be achieved.

For cases where μ and ϵ are both used, or μ alone, β_i remains high in many cases, permitting larger maximum permissible cone angles than in the dielectrically loaded case, and opening the possibility of having a decrease in the active region size.

VI

EXPERIMENTAL RESULTS

A large part of the present study was an experimental investigation of the effect of material loading of helix and conical-helix antennas. Interior loading was emphasized, but due to a lack of loading material and a desire to keep the weight down, inside layers were emphasized rather than full-core loading, which makes direct comparison with theory additionally difficult.

6.1 Facilities.

The measurements were performed both in the far field and near field of the antennas. Far field measurements are very standard. Linear power was recorded from the test antenna with a linearly polarized zig-zag transmitting antenna, as the test antenna was rotated through 360^{o}. A serious problem with far field measurements in the frequency range used (200 - 1000 MHz) is the reflection from objects, particularly the ground plane. An outdoor range was necessary. Careful attention to the reflection problem was paid, but still many irregularities appear in the patterns. Absolute field measurements, particularly for the antenna efficiency, are very difficult.

The near fields were measured on a range described by Knott (1965), used mainly for surface field measurements of currents on metallic bodies that are scattering incident S-band (3000 MHz) power. The probe available on the near field range is a shielded loop probe designed to measure magnetic fields at metallic surfaces due to surface currents. It is not fully balanced, but has a single, very small, gap in the center of the loop. Whiteside (1962) shows that such a loop measures H fields accurately when its diameter is very small compared to a wavelength, as in the present case in which the loop diameter is .131" diameter, or when the gap of the probe is against a metallic surface as in the case of surface current measurements. The loop

must also be very small compared to a wavelength and to the wire spacing in order to sample fields without significant variation of the fields across the loop. The particular set-ups used in these experiments are described in Lyon et al (1966). The near field measurements used a Scientific-Atlanta receiver in order to pick up the very low signal levels. The phase measurements were made using a standard amplitude-phase cancellation set-up with a reference signal from the transmitter.

An interesting aspect of the near field measurements that that an anechoic chamber was used that was designed for frequencies well above those used. In fact, the room was only several wavelengths across at most points, although long and tapered in the other dimension, the one in which the antennas were pointed. In order to investigate the validity of such measurements, some crude experiments were run in which metal plates and other objects were brought in the vicinity of the antennas being measured. The effects upon the near field measurements indicated that for measurements very close to the antennas, the patterns were not disturbed, although the absolute amplitude was changed somewhat. These experiments also indicated that the effects of the probe upon the current distribution were small.

Only when the metal plate was directly in the path of the radiation pattern were there any significant effects. Thus, the absorbing room, although not good enough for far field measurements, allowed near field measurements to be taken indoors. Since the advantages of indoor measurements over outdoor measurements are very great, this indoor near field measurement technique appears very valuable. Nevertheless, when complicated near field patterns occurred, the prediction of far field patterns was too difficult. Both measurements appear necessary.

6.2 Helix Experiments

In Chapter V, the close relation between the cylindrical helix and the log-conical helix was explained. An experimental study of the cylindrical helix was made, mainly in order to extrapolate the experimental data to a conical helix case.

The construction of a cylindrical helix is shown in Figs. 6-1 and 6-2. It is wound over a fiberglass shell with RG-58U coaxial wire in an infinite balun arrangement, i. e., the helix is bifilar, fed 180° out of phase at the tip (lower left of Fig. 6-2), but the feed wire from the tip is actually the inside of the coaxial wire of one of the arms. As long as the antenna currents decay to zero before they reach the base, the feed is a balanced one (Dyson, 1964) in that no currents flow down the feed wire. The loading is depicted in Fig. 6-3. The loading effects of the fiberglass shell and balsa wood have been found to be very small in the frequency range 200 - 900 MHz (Lyon et al 1966).

The two loading powders used were an isotropic, low loss ferrite powder with $\epsilon = 3.8$, $\mu = 2.2$ and a dielectric powder of $\epsilon = 10$ (Emerson and Cuming, Eccoflo, HiK-10). This admittedly gives only two check points for the theoretical formula. Several other experiments have been reported with different dielectric constants. Shestopalov's (1961) reported data are very sketchy far field patterns and near field amplitudes for the forward-radiation case. Wong and Thomas (1959) used ϵ quite small, giving little reduction. In the slow waveguide region, the dielectric data is better (Shestopalov, 1960) and verifies the theory of the slow wave loaded tape helix in that reference, but is of less use in this study of antennas than data in the radiation region.

6.2.1: Far Field Measurements of the Loaded Helix

Figures 6-4 through 6-7 show the effects on the far field patterns of helix No. 217 loaded with a full core or .25" layer of ferrite or dielectric. The parameters of the helix are shown in Table IV-1. In Figs. 6-3 and 6-4, the solid lines representing the unloaded antenna patterns, show unsatisfactory

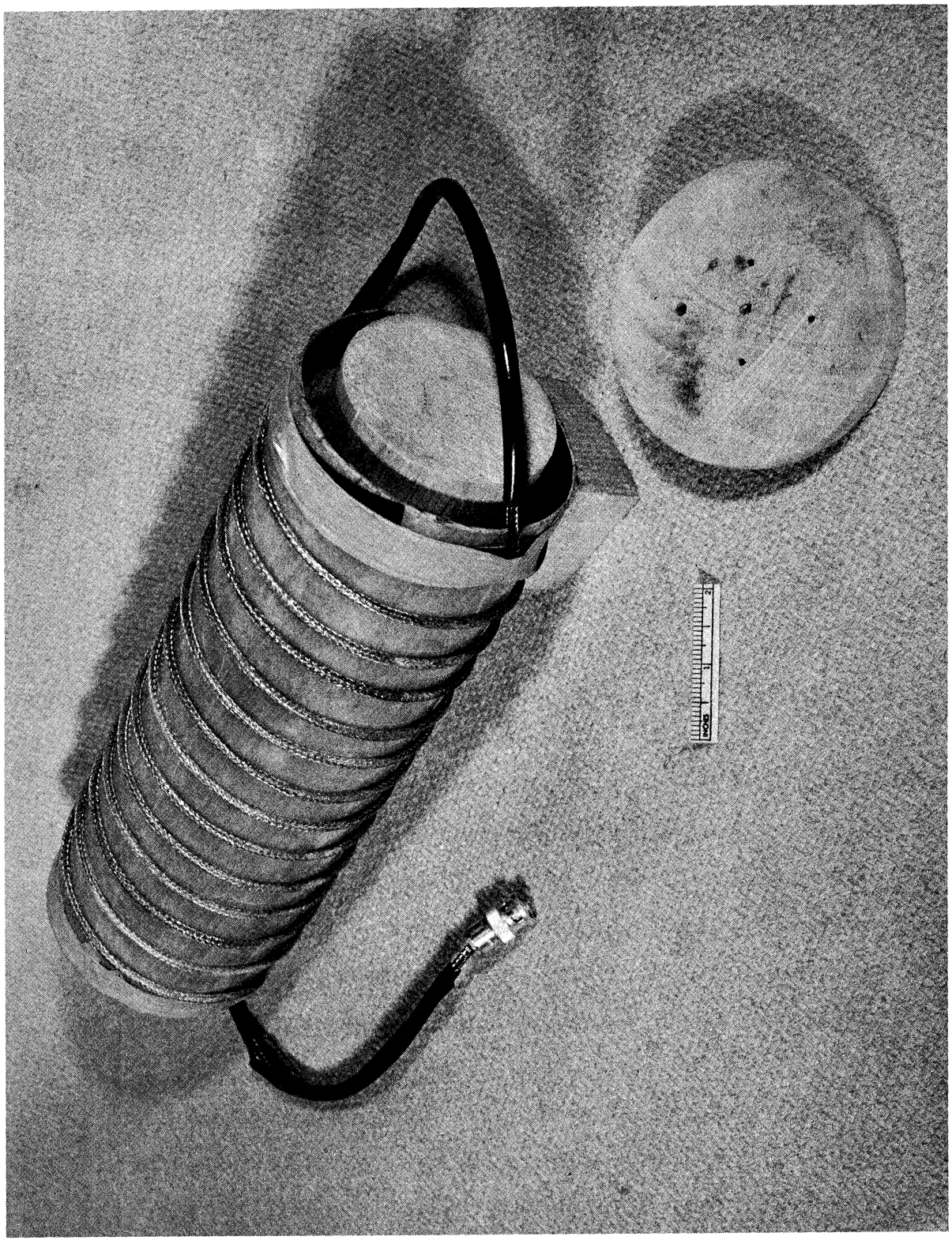

FIG. 6-1: BIFILAR 4" DIA. HELIX WITH BALSA WOOD CORE AND CAP.

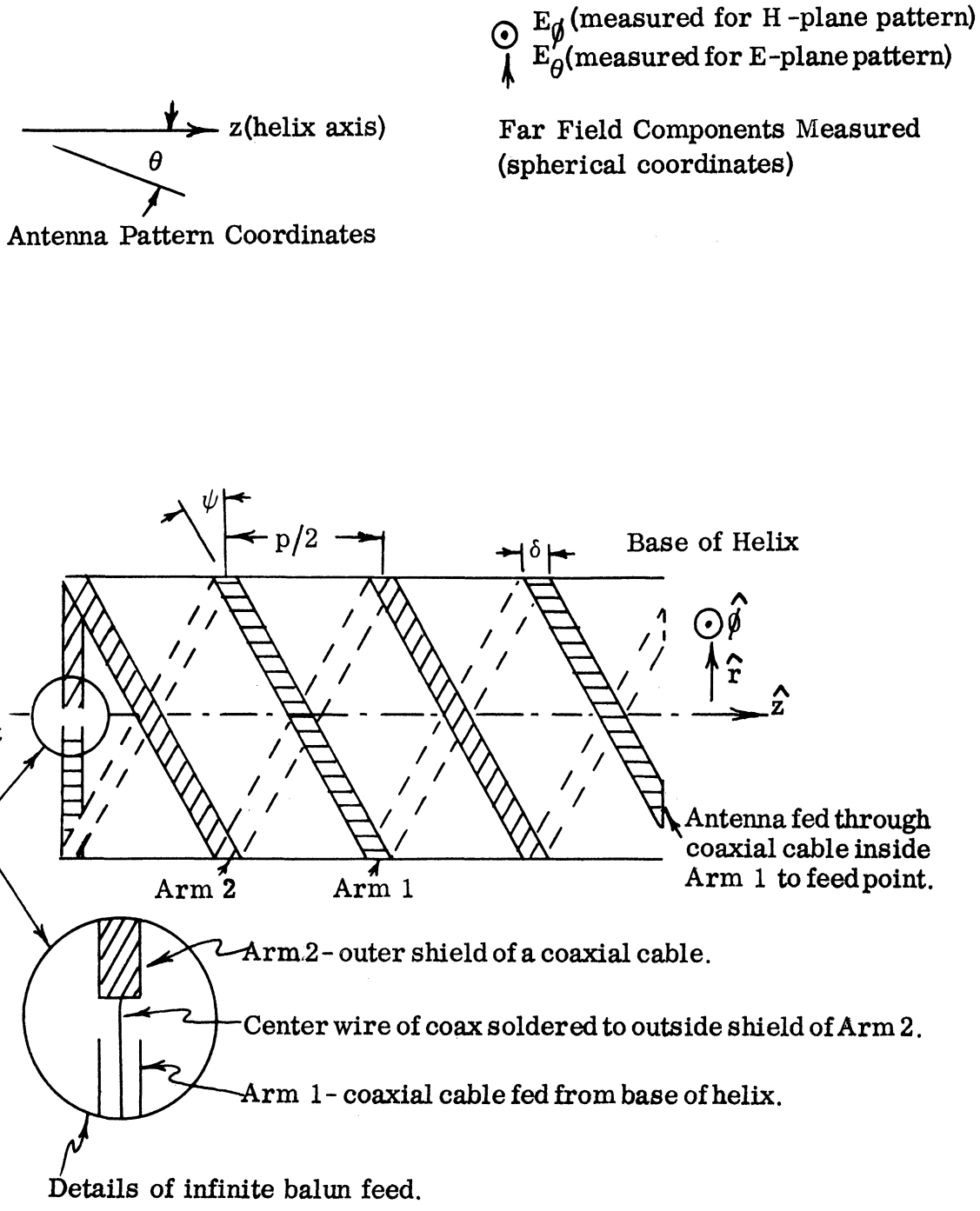

FIG. 6-2: THE BIFILAR CYLINDRICAL HELIX.
Normalized Tape Width, $\Delta = \pi \delta / p$.

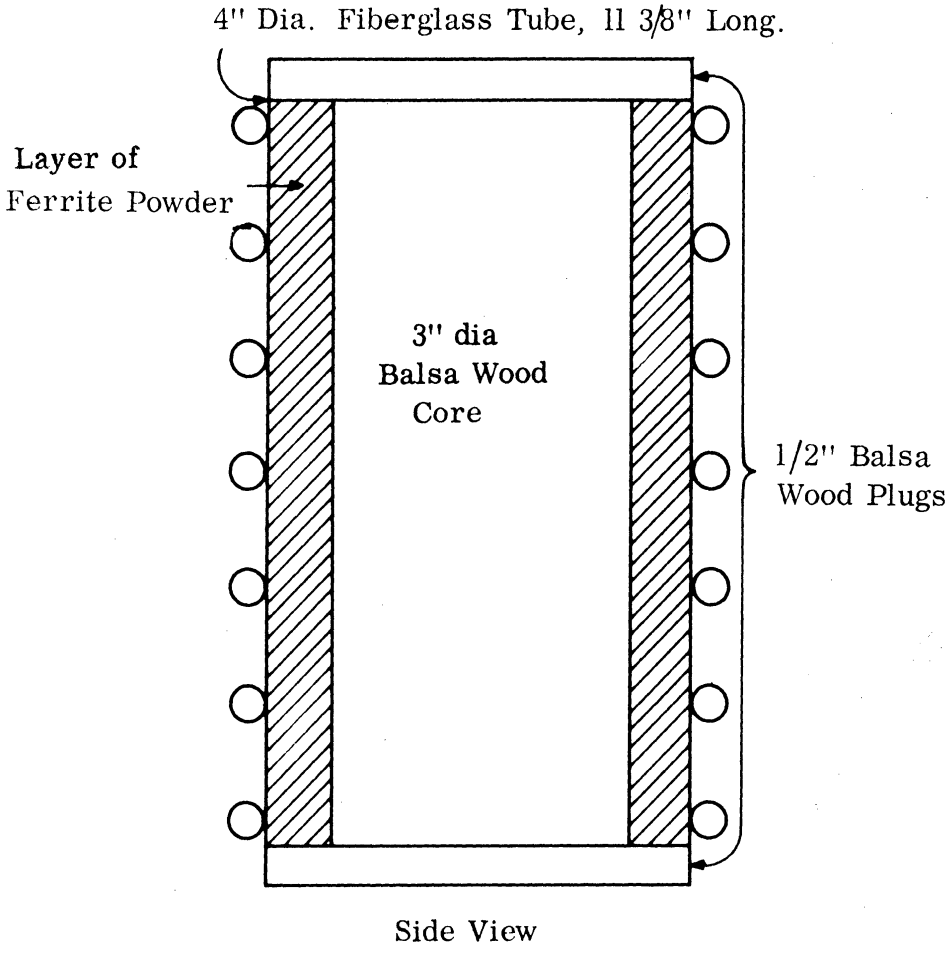

FIG. 6-3: LOADING DIAGRAM: BIFILAR HELIX (No. 213) LAYER LOADING.

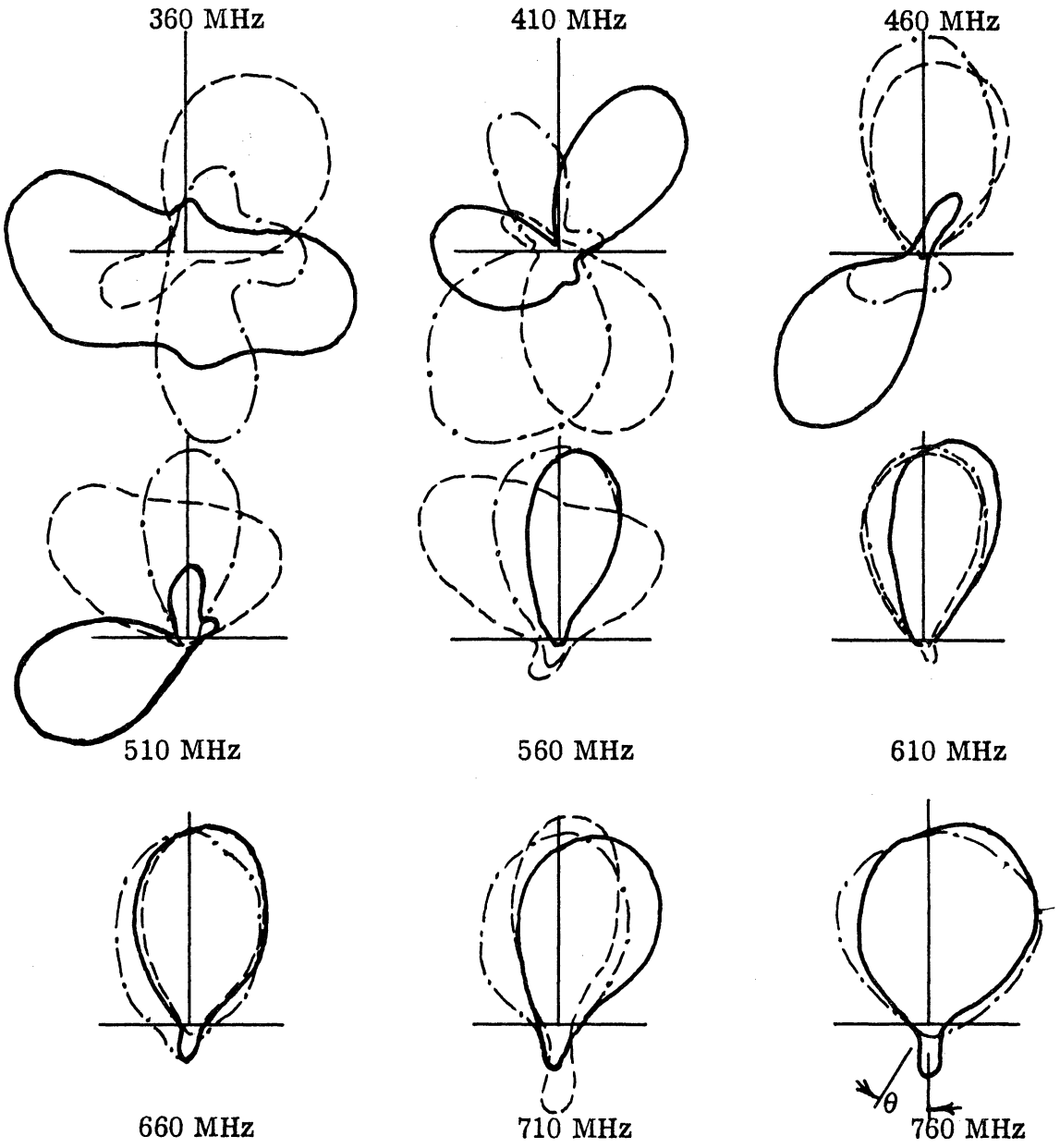

—— Unloaded —· —· .25" interior layer ----- full core load.

FIG. 6-4: HELIX WITH DIELECTRIC LOADING. PLOTS OF $|E_\phi|^2$. Dielectric ϵ=10, Antenna No. 217 (4.7 " dia.), coordinates from Fig. 6-2, $\theta = 180^o$ is "backward",

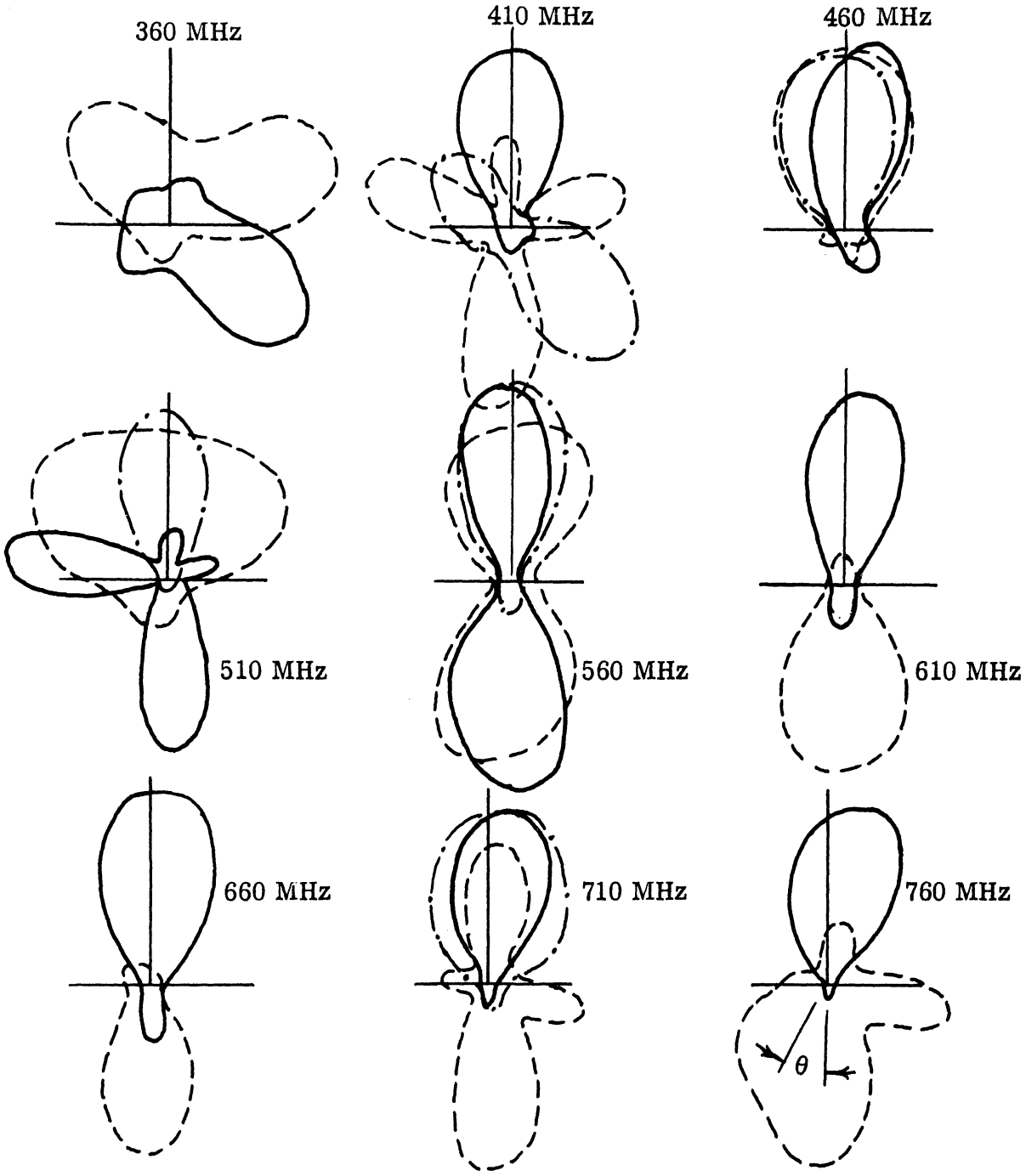

— Unloaded — · — . 25" interior layer ----- Full core load.

FIG. 6-5: HELIX WITH DIELECTRIC LOADING. PLOTS OF $|E_\theta|^2$. Dielectric ϵ=10, Antenna No. 217(4.7" dia), coordinates from Fig. 6-2, θ=180^o.is "backward".

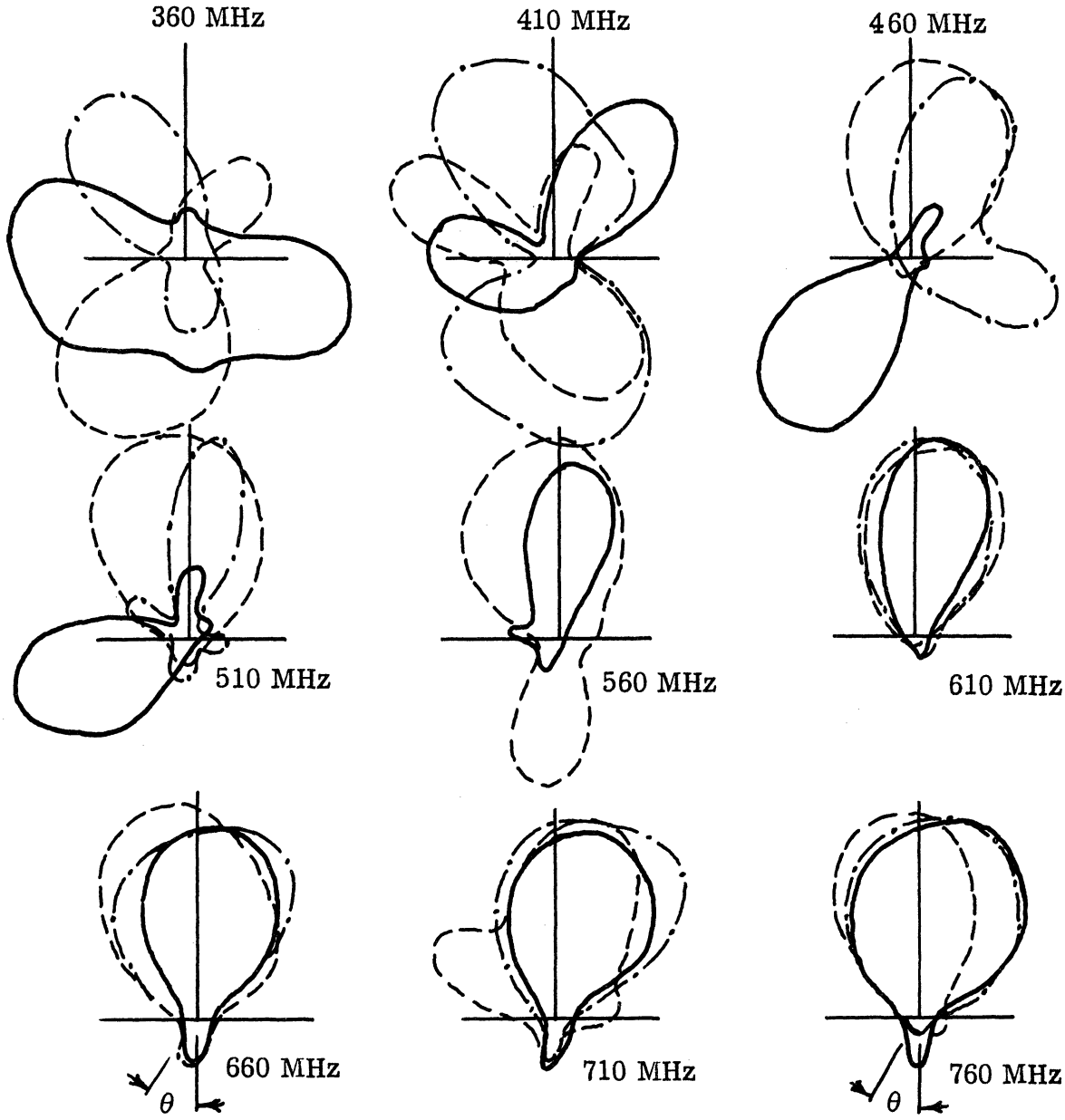

— Unloaded — · — .25" interior layer ----- Full core load.

FIG. 6-6: HELIX WITH FERRITE LOADING. PLOTS OF $|E_\phi|^2$. Ferrite powder ϵ=3.77, μ=2.2, Antenna No. 217 (4.7" dia.), coordinates from Fig. 6-2, $\theta = 180^o$ is "backward".

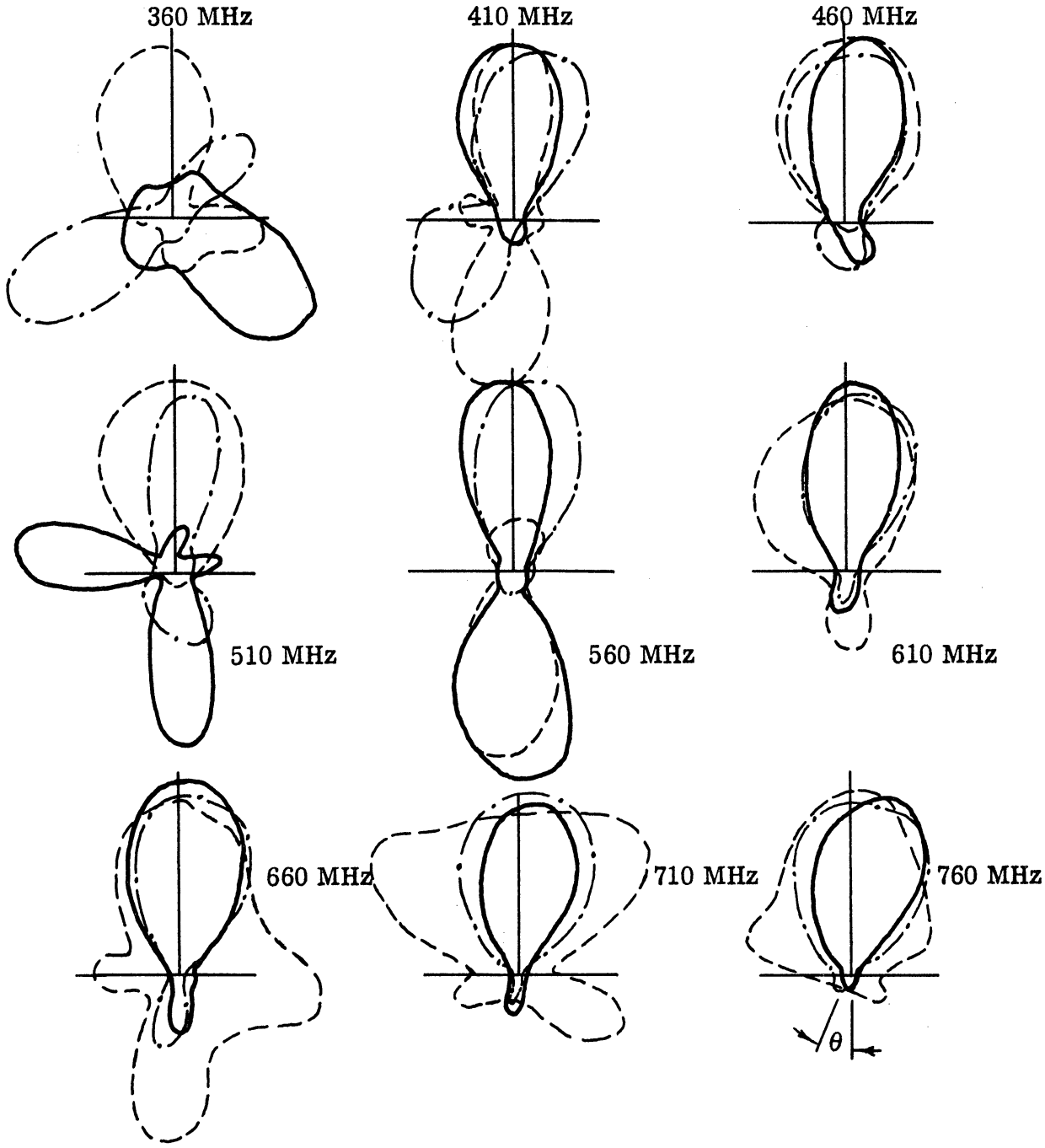

— Unloaded —·—. 25" interior layer ---- Full core load.

FIG. 6-6: HELIX WITH FERRITE LOADING. PLOTS OF $|E_\theta|^2$.
Ferrite ϵ=3.77 μ=2.2, Antenna No. 217 (4.5"dia).
$\theta = 180^o$. is "backward".

TABLE VI-1: SPECIFICATIONS OF HELIX TEST ANTENNAS

Dimension	I. D. No. 213	I. D. No. 217
Type	Bifilar	Bifilar
Diameter	4. 15"	4. 65"
Length	10"	16"
Conductor	RG58U	RG58U
Turns	6. 5	9. 5
Pitch	6. 6^{o}	7^{o}
	(1. 5")	(1. 8")

patterns below 610 MHz in either $|E_{\phi}|$ or $|E_{\theta}|$. The notation for the fields is shown in Fig. 6-2. With either a full core or a . 25" layer of dielectric powder (ϵ=10), however, the antenna patterns have a single lobe near θ=180^{o} down to 460 MHz, a reduction of 150 MHz in the lowest operating frequency for backward radiation, or a reduction factor of 460/610=0. 75. Actually, the full core dielectric loading produces pattern degradation above 500 MHz, especially in $|E_{\theta}|$, so that a . 25" layer loading of dielectric is much superior to full core loading in bandwidth. Many other loadings, whose patterns are not shown in this report are summarized in the tables to follow. A thick layer, such as . 75" produces some high frequency pattern degradation similar to the full core loading.

In Figs. 6-5 and 6-6, for $|E_{\phi}|$ and $|E_{\theta}|$ with ferrite loading, the antenna patterns of the full core loading are good down to 460 MHz, and are much more narrow-band than the unloaded helix, because the antenna patterns above 510 MHz are degraded. Above this frequency, the antenna radiates in the forward (θ=0^{o}) direction. Also, similar to the case of dielectric loading, the . 25" layer loading has a much wider bandwidth than the full core loading. Antenna patterns are improved over the unloaded case, although not as good as the dielectric case, down to 460-510 MHz, a reduction of 100 - 150 MHz.

The frequencies of best backward radiation correspond to $k \approx -\beta_{-1}$, which is sometimes called the 'resonant' frequency of the helix, corresponding to the large resonant term discussed in Section 3.2.

The patterns show that the bandwidths of this antenna are very broad, so that shifts of a resonant frequency are hard to measure accurately. With the much broader band conical-helix, the problem is much worse. Another problem with the far field antenna pattern of the helix is that, for extrapolation to conical-helix operation, an 'efficiency of radiation' in the backward direction (θ=180°) is desired to predict active zone characteristics in the conical helix. Table VI-2 shows the frequencies at which a maximum power was received at θ=180° by a helix relative to a half-wave dipole. Data from another helix, No. 213(Table VI-1) is also shown. Table VI-3 shows reduction factors computed using the lowest frequencies for a good antenna pattern from Figs. 6-4 through 6-7, and also reduction factors computed using the frequency for maximum received power at θ=180° from Table VI-2. In both cases, the reduction factor was computed by dividing the critical frequency with loading by the critical frequency without loading, as was done in the dielectric loading reduction example above. The reduction factors are seen to be less in every case than the theoretical reduction formula for full core loading. The theoretical reduction is obtained from (2.57) by dividing the loaded ($k_0 a$) by the unloaded ($k_0 a$), which is slightly more accurate than the simplified formula $\sqrt{(1+1/\mu)/(\epsilon+1)}$. Near field measurements and measurements on conical helices produce better checks with the theory. The more exact theoretical values obtained from Figs. 3-5 and 3-6 agree within several per cent with the simplified reduction formula used above.

6.2.2: Near Field Measurements of the Loaded Helix

A more direct and sensitive measure of the loading effects of the materials can be seen from near field measurements. In fact, the near field phase measurements should give approximately the parameter β_{or}

TABLE VI-2: FREQUENCIES OF PEAK RECEIVED POWER AT $\theta = 180^{o}$ FOR LOADED BIFILAR HELICES

Antenna	Loading Thickness, t (inches)	(t/λ)	Loading Material	Freq. for Max. Radiated Power, MHz
No. 217	0		Air	730
No. 217	1/16	.0033	Ferrite	625
No. 217	1/8	.0064	Ferrite	600
No. 217	1/4	.0116	Ferrite	560
No. 217	Full Core		Ferrite	460
No. 213	0		Air	820
No. 213	1/2	.0238	Ferrite	560
No. 213	1/2 (outside)	.0216	Ferrite	510
No. 213	Full Core		Ferrite	530
No. 217	0		Air	730
No. 217	1/8	.0064	Dielectric	610
No. 217	1/4	.012	Dielectric	610
No. 217	Full Core		Dielectric	445

NOTES

1. Thickness relative to λ is taken at the frequencies listed in the last column.
2. Layers are inside and within .04" of the conductor, unless specified otherwise.
3. Frequencies for best circular polarization were usually lower, e.g., for 1/8" dielectric, 550 MHz was the best frequency.

Antenna	Loading Material	Inside Loading Thickness (t/λ)	Experimental Reduction Factor		
			Lowest Freq. for Good Pattern.	Freq. of Max. Rec'd Power ($\theta=180^{o}$)	Simplified Theoretical Reduction Factor from (2.57)
No. 217	Ferrite	Full Core	.75 - .84	.63	.58
No. 213	Ferrite	.022 (outside)	.7	.62	
No. 213	Ferrite	.024	.78	.68	
No. 217	Ferrite	.012	.75	.77	
No. 217	Ferrite	.006	.82 - .9	.82	
No. 217	Ferrite	.003	.85 - .9	.85	
No. 217	Dielectric	Full Core	.75	.61	.45
No. 217	Dielectric	.012	.75	.78	
No. 217	Dielectric	.006	.9	.83	

TABLE VI-3: REDUCTION FACTORS FOR LOADED HELICES

calculated by theory. The actual near field measurements in this section were largely performed by Pei-Rin Wu of the Radiation Laboratory (Wu, 1966; Lyon, 1966). Figures 6-8 and 6-9 show the near field amplitude of the helix antenna No. 217 when loaded and unloaded with a ferrite powder layer 3/8" thick (. 02 λ thick, helix dia. 4.7"). From the figures, the best (resonant) frequency of operation may be seen as the one that decays quickly along the helix away from the feed point without rising to other high maxima. Without loading, this best frequency is between 700 - 800 MHz; with loading it is between 550 - 700 MHz, a reduction factor of approximately 0.8. Note that the measurement is more sensitive to changes in frequency than either the far field patterns or the maximum-radiated-power measurement. The corresponding frequencies from Table VI-2 are 720 MHz, unloaded and 535 MHz, loaded; a reasonable, but not excellent check.

The near field phase measurement of the loaded case was so difficult and time consuming that only a few were made. Since signal power was very low in the resonant frequency region, two frequencies somewhat off center were chosen, 500 and 900 MHz. The measurements showed a reduction factor of . 6 (Lyon, et al 1966) which is the closest yet to the . 58 from crude full core loading theory. This is the most sensitive measurement for finding the phase velocity for checks with theoretical calculated phase velocity; however, the far field and near field amplitude patterns show that more than phase velocity information is needed to predict far field effects.

The variations in near-field amplitude of the helices off resonant frequency cannot be completely explained by reflections from the end of the helix, because of the amplitudes involved. Therefore, other waves must be present off resonance, probably a current wave travelling up the helix toward the feed. This effect is not seen (at least as strongly) in the unloaded conical helix, indicating that it is a consequence of the abrupt feeding discontinuity at the tip of the helix that does not occur with a well-tapered feed such as the forward tip of a conical helix, and may make predictions of the conical helix

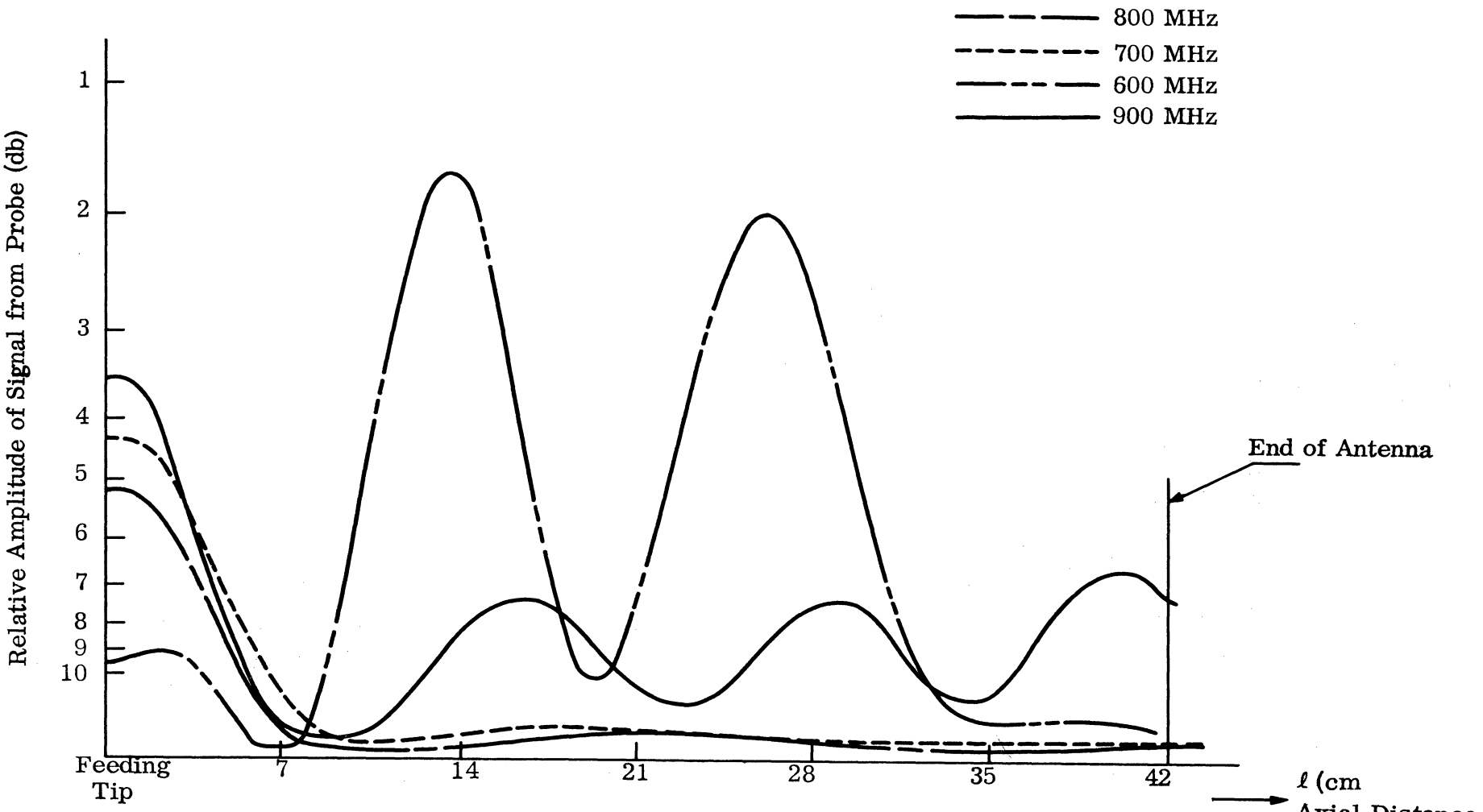

FIG. 6-8: NEAR FIELD AMPLITUDE OF $|H_\phi|$ ON ANTENNA NO. 217. PROBE POSITION $\lambda/6$ ABOVE ANTENNA SURFACE.

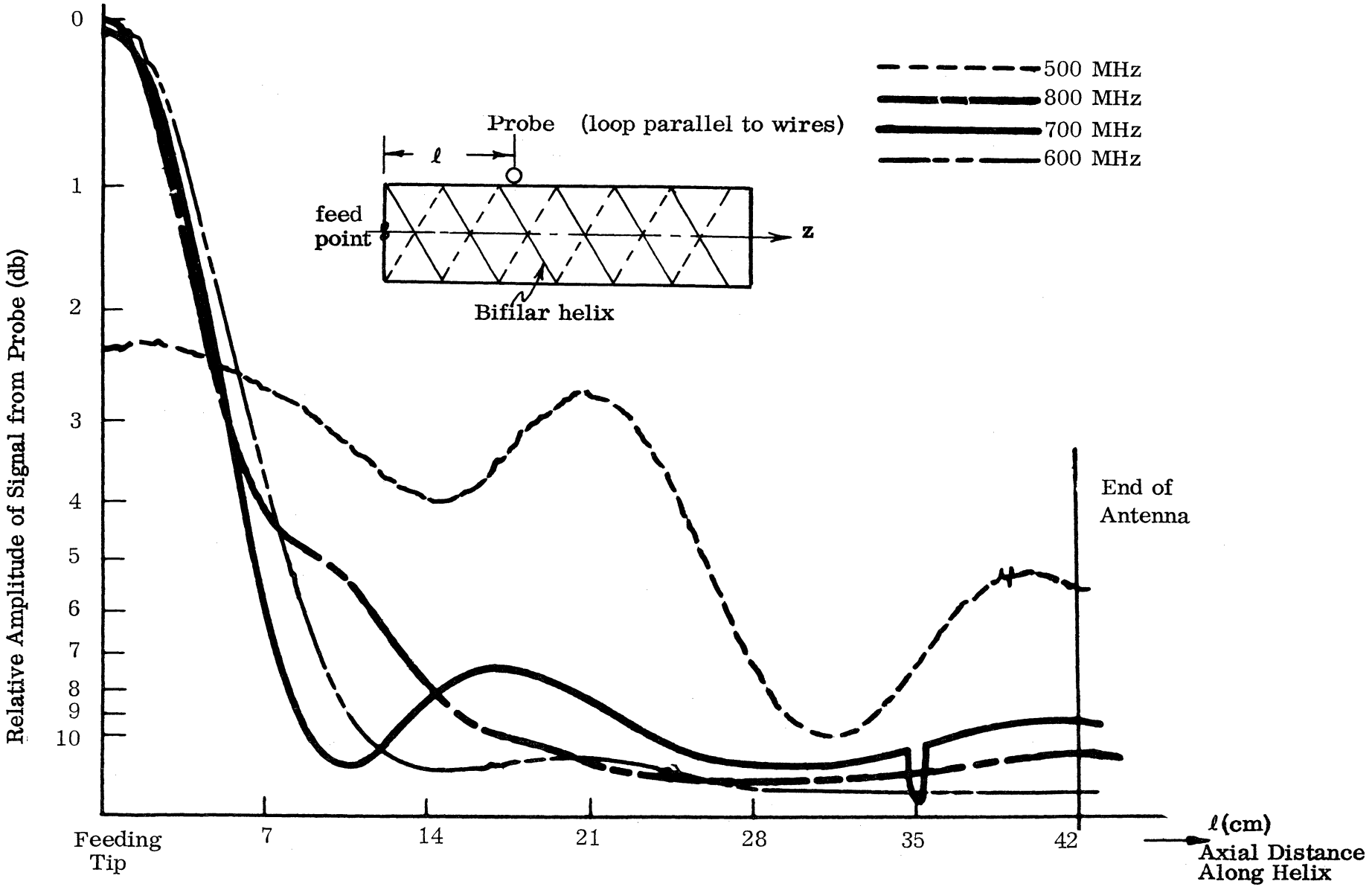

FIG. 6-9: NEAR FIELD AMPLITUDE OF $|H_\phi|$ ON ANTENNA NO. 217 WITH FERRITE LAYER 3/8" THICK. PROBE POSITION $\lambda/5$ ABOVE ANTENNA SURFACE.

from cylindrical helix operation more difficult. The infinite helix theory also does not account for a feed discontinuity, making comparisons with theory more difficult. A possibly similar effect has recently been reported for the Yagi antenna (Ingerson and Mayes, 1966).

6.3 Log-Pyramidal Helix Experiments

The two pyramidal helices used in these experiments, which have almost identical parameters, are described in Table VI-4. They are logarithmic in the sense that the distance from the vertex to the wire varies exponentially with the azimuthal angle about the axis z. This assures a wideband frequency of operation; however, the conductors used were constant-size wire and did not scale with the distance from the vertex. The effect of constant wire size is small for tightly wrapped (small pitch angle) helices (Dyson, 1964) as is the effect of using four-sided pyramidal approximations to right circular cones. Again, layer loadings were usually used. Some far field plots were made, but since the active region moves with frequency, the antennas are very broadband and only the lower cutoff frequency can show any loading reduction.

6.3.1: Far Field Measurements of Log-Pyramidal Helices

Figures 6-10 and 6-11 show the far field patterns for two different loadings on the two different pyramidal helices. In both, the loaded patterns at the very low frequencies are seen to be better than their unloaded counterparts. Using a lowest frequency criteria, a 0.7 reduction factor may be obtained, roughly similar to the loaded helices. The loading shown in Fig. 6-11 is a tapered loading, with the object being to load the low frequency (large) end of the conical helix in order to reduce the large part of the cone while keeping the relatively small tip of the cone unloaded. If the beamwidth, or some other pattern factor is plotted versus frequency for Fig. 6-11, it can be seen that the conical helix in air has relatively constant parameters down to 600 MHz; with loading, this first-pattern-disturbance criteria gives 300 - 350 MHz, for a considerably greater reduction (reduction factors, .5 - .6) than was computed above or in the case of the loaded cylindrical helices.

TABLE VI-4: SPECIFICATIONS OF LOG-PYRAMIDAL HELIX ANTENNAS

Dimension	I. D. Number 221	223
Base, Side	9.47"	9.47"
Apex, Side	1.56"	.47"
Height	13.44"	15.38"
Apex, Cone Angle	45°	45°
Pitch Angle	85°	85°
Turns	8.5	14.75
Outer Conductor	RG58U	No.20 Enamel Coated Wire
Feed	Infinite Balun	Wideband Hybrid
Nominal Freq. Range Unloaded	500-900 MHz	500-3000MHz

NOTE

Both antennas were pyramidal with a square cross section. Construction of No. 221 consisted of two-layer fiberglass epoxy layers forming the inside supporting pyramid upon which the coax was wound. Antenna No. 223 was made of 1" thick styrofoam layers forming the outside supporting pyramid, with the antenna conductor cemented inside with epoxy.

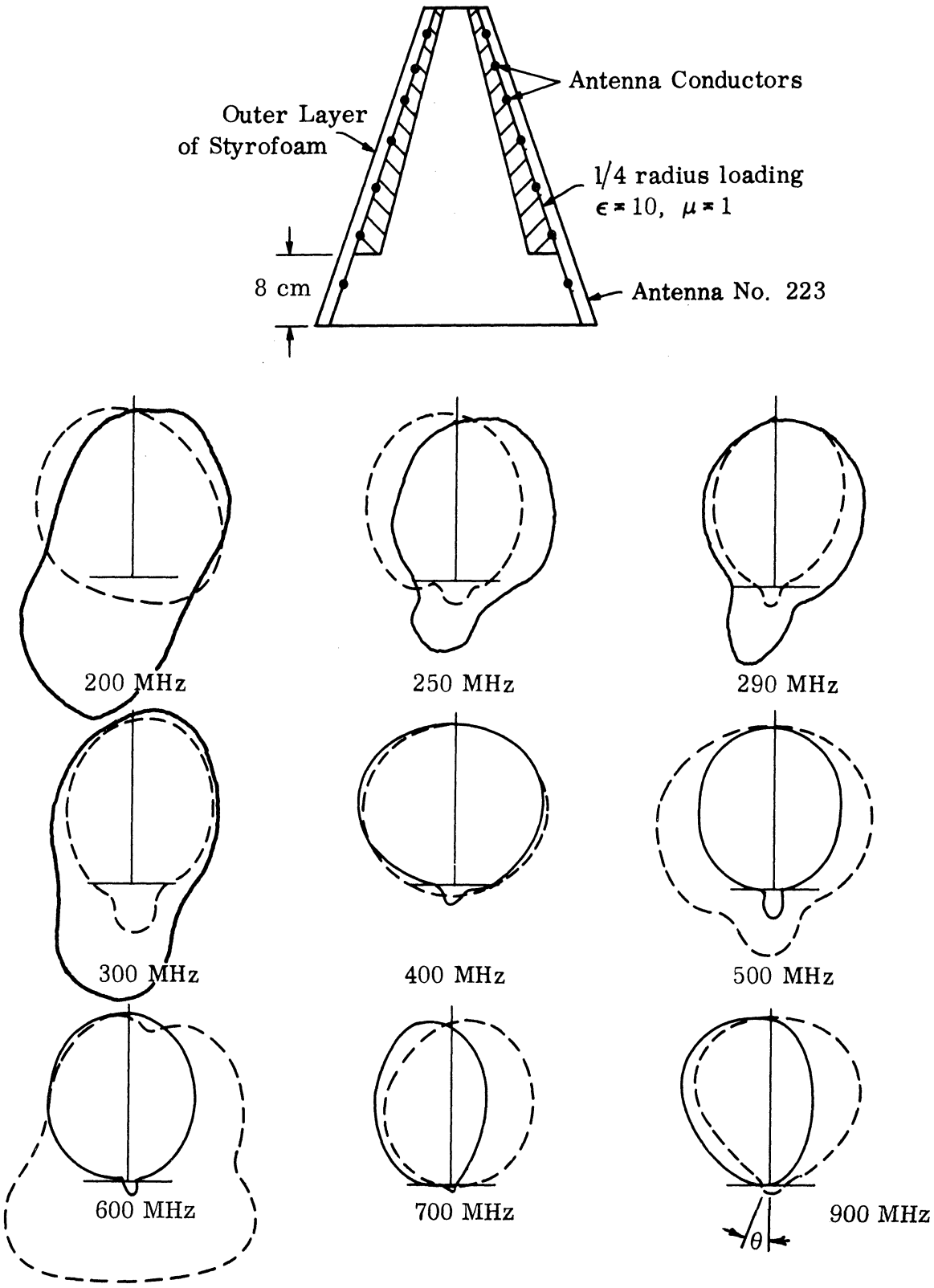

FIG. 6-10: TAPERED LOADING OF LOG-PYRAMIDAL HELIX NO. 223.
— Unloaded, – – – Loaded, Plots of $|E_\phi|^2$.

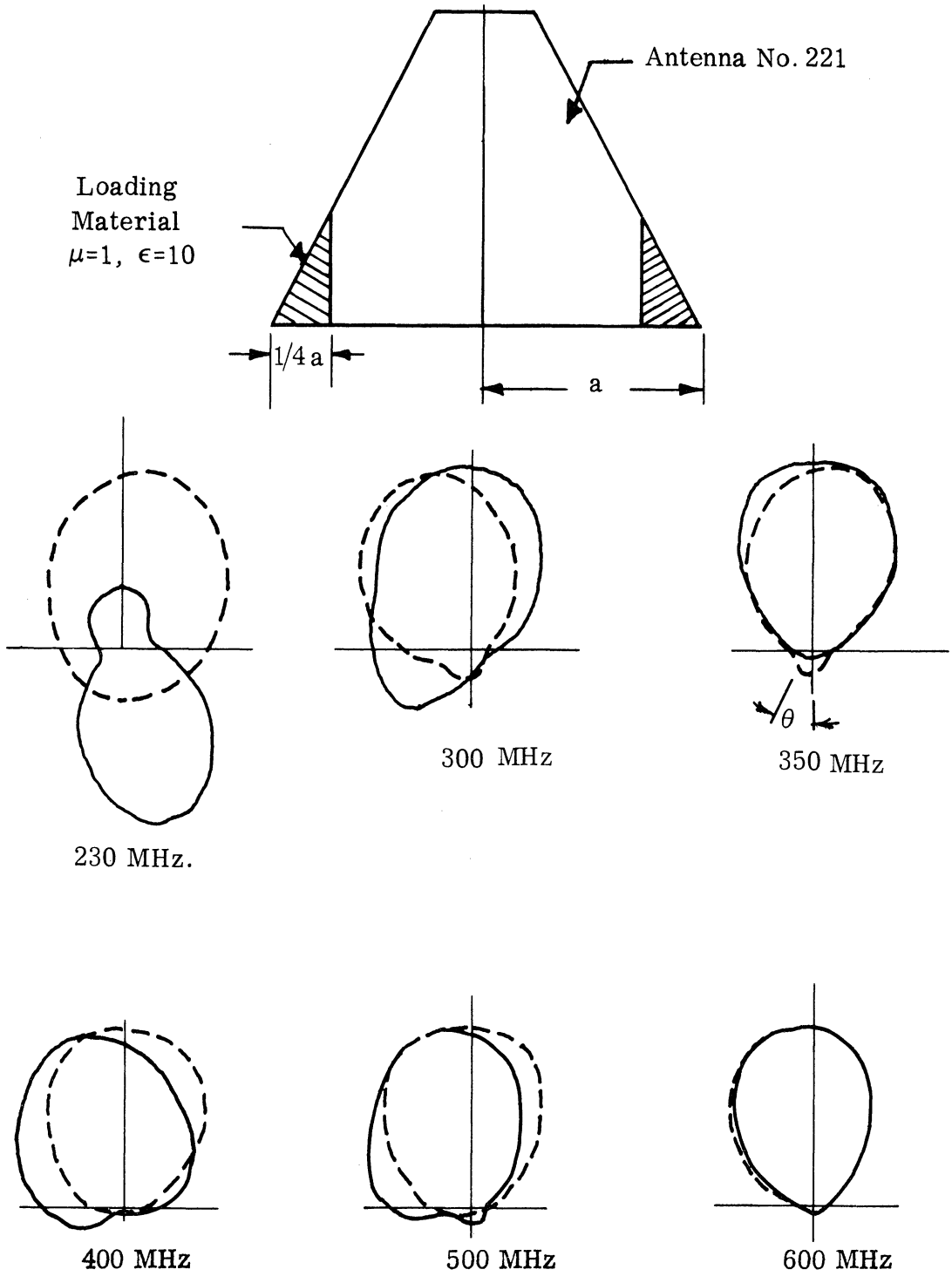

FIG. 6-11: TAPERED LOADING ON LOG-PYRAMIDAL HELIX NO. 221. — Unloaded, – – – Loaded, Plots of $|E_\phi|^2$.

A serious problem with loading first becomes evident in Fig. 6-10 at 500 - 600 MHz, where the fields are seen to be very erratic. Further insight into this problem will come from the near field measurements.

6.3.2 Near Field Measurements of Log-Pyramidal Helices

Near field amplitude and phase measurements are considerably more enlightening than far field plots for the conical helix antenna, because one can see the 'active' zone move with frequency and loading. Excellent examples of this also appear in Dyson (1964) and McClelland (1962) for the unloaded conical helix.

Figure 6-12, selected from a large amount of data (Wu, 1966), shows near field amplitude plots of Antenna 223 unloaded. Very similar plots resulted with Antenna No. 221. The active zones show up very well as increases in the near field amplitude, which move with changes in frequency; high frequencies have active zones near the tip, low frequencies (longer wavelength) have active zones near the large end of the cone.

By properly adjusting the probe height above the antenna (in this case to $\lambda/12$), the effects of wires (higher order space harmonics) are eliminated because these effects cling very closely to the antenna's surface. At a $\lambda/20$ to $\lambda/10$ distance from the surface, only the first space harmonic (n=-1) which causes the radiation has large amplitudes, clearly showing the active zone where the n=-1 harmonic is resonant. If a much closer probe spacing against the wire is used, current along the wire may be plotted. This position was used for phase measurements.

Figure 6-13 (Wu, 1966) shows the effects of loading with the dielectric layer, ϵ=10 (configuration shown in Fig. 6-10) upon the log-pyramidal helix. The near field at 500MHz has a large hump at approximately the position of the hump at 900 MHz for the unloaded case. However, several humps occur rather than one.

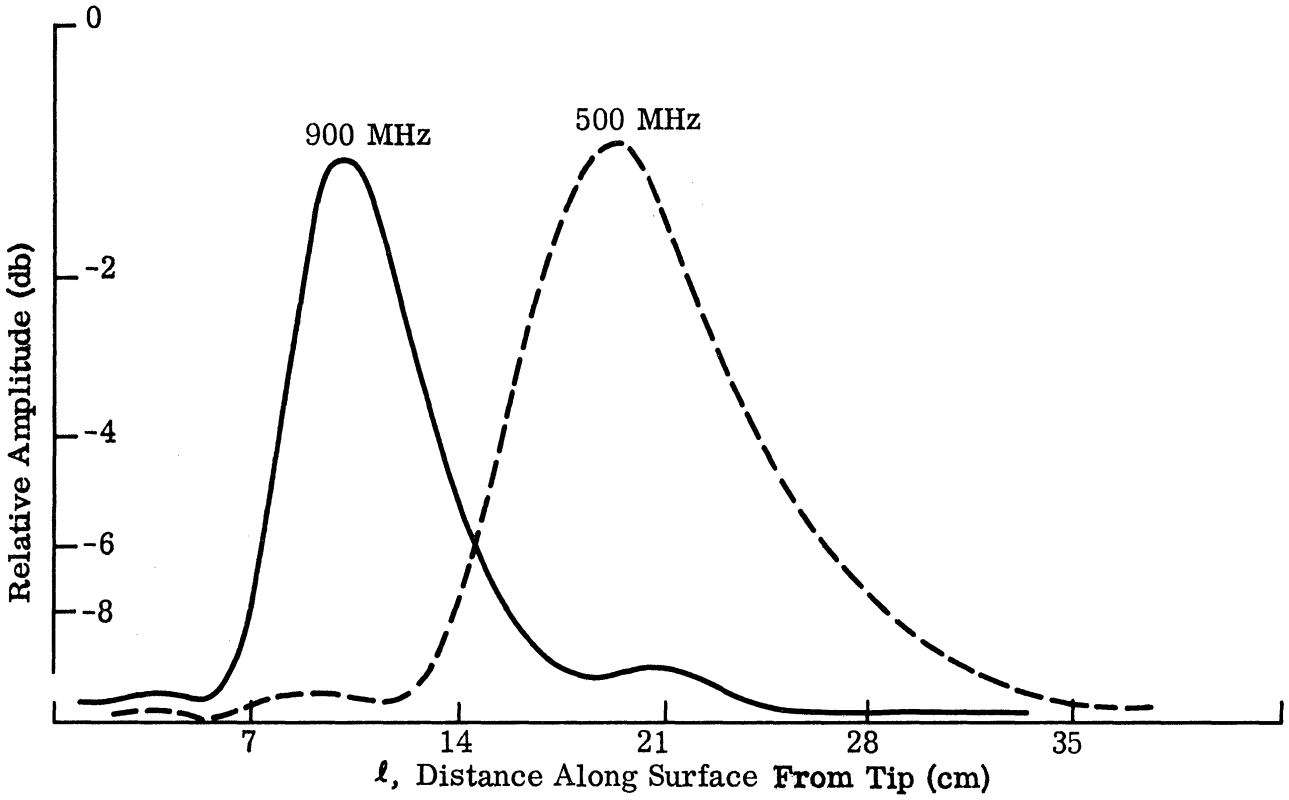

FIG. 6-12: DIELECTRIC LOADING OF LOG-PYRAMIDAL ANTENNA NO. 223: UNLOADED MODEL.

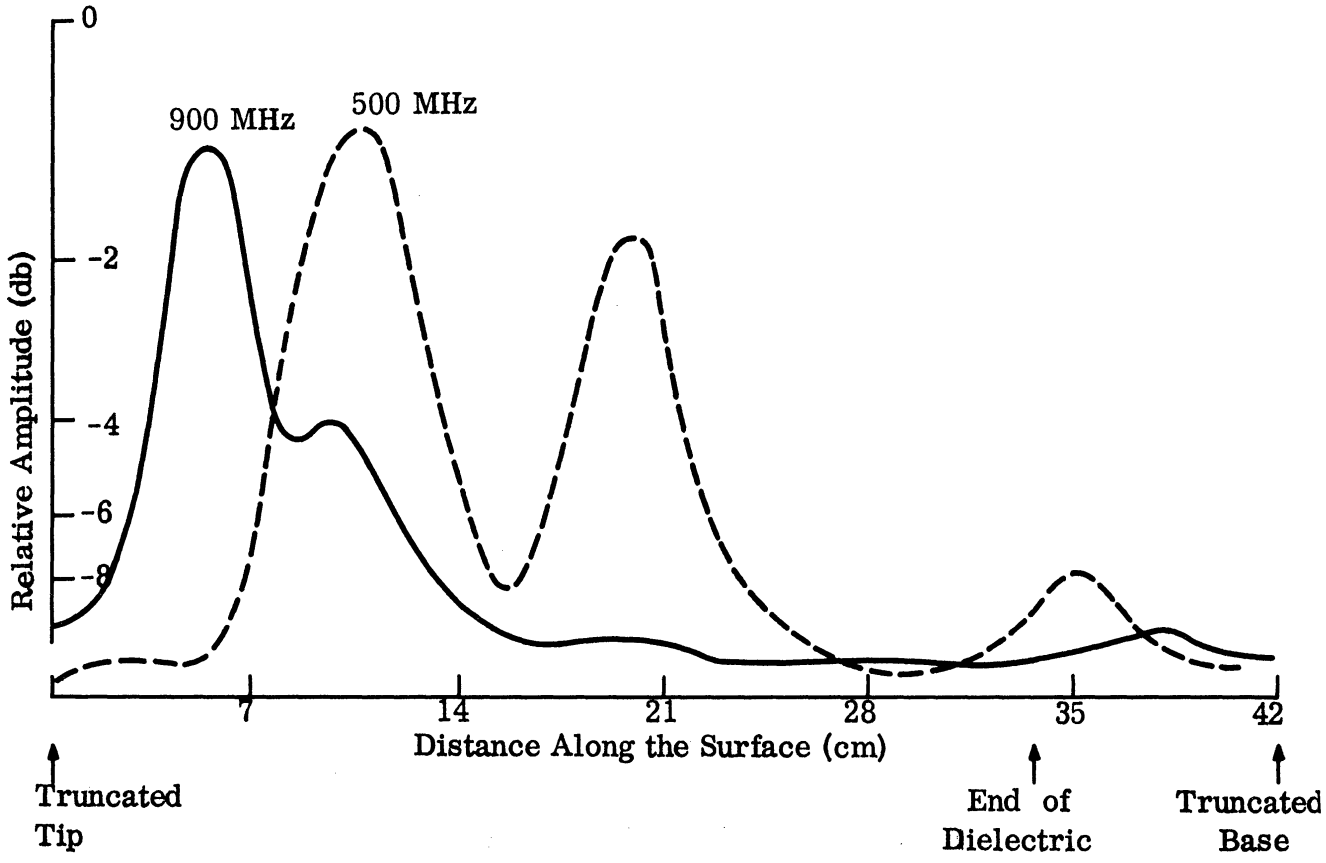

FIG. 6-13: DIELECTRIC LOADING OF LOG PYRAMIDAL ANTENNA NO. 223: LOADED MODEL. ϵ=10. Loading as in Fig. 6-10.

These humps may each correspond to a different active region. One might think that they are simply different space harmonics coming to resonance, wherein the first hump is the desired backward fire harmonic n = -1, and the others are n=-3, n=-5, etc., excited because some of the power was not radiated in the first active zone; however, the spacings are not 1 : 3 : 5 from the tip. Further, Wu has noted that the second hump appears to occur at the position of the unloaded active region. The theoretical tape solution as carried out so far gives no insight into this problem. Although few solutions have been carried out near the second hump, those that have do not indicate radiation, although the solutions do indicate the decreased radiation rate that allows power to get through the first region.

Results of current phase and amplitude measurements by the author on the log-pyramidal helix No. 223 fully loaded with a dielectric (ϵ=10) are shown in Figs. 6-14 and 6-15. In Fig. 6-14, the experimental phase measurements show excellent agreement with a line whose slope corresponds to the phase shift of a wave which has a phase velocity along the wire v_p= .425c, where c is the speed of light in a vacuum. The slope of a line corresponding to the phase shift of a wave going the speed of light along the wire is also shown. The factor .425 is the theoretical very narrow tape helix reduction factor from (3. 72)

$$\sqrt{(1+1/\mu)/(1+\epsilon)} = .425 = k_0/\beta_0 \sin\psi = v_p / c$$

where $\mu = 1$, $\epsilon = 10$ in this experiment. Thus, the formula for phase velocity reduction along the wire due to loading has strong confirmation. An additional verification of the phase velocity with the ferrite powder material inside Antenna 223 is also shown, along with data for the unloaded antenna.

The data for amplitude of the current wave along the wire, Fig. 6-15, shows the expected drop off due to radiation in the active zone. Also, the active zone clearly moves toward the tip of the antenna, displaying reductions of the size of the antenna at the start of the active zone of 0.56 for the ferrite loaded antenna and 0.49 for the dielectric loaded antenna. Also, the amplitude of the current decreases faster in the case of ferrite loading than dielectric loading. Actually the size reductions, computed from the positions where the

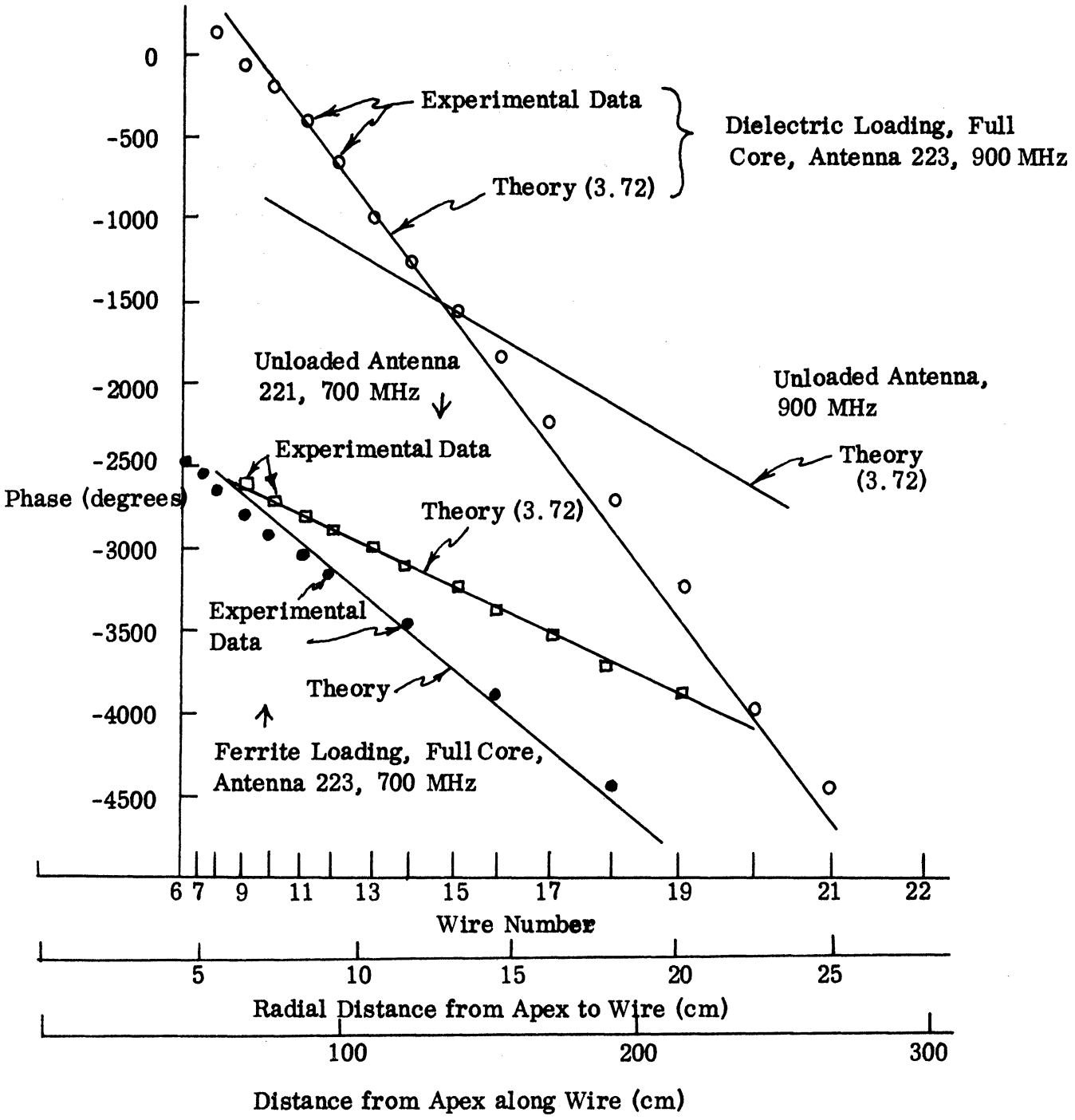

FIG. 6-14: MEASURED PHASE OF LOG-PYRAMIDAL HELICAL ANTENNAS NO. 221 and 223 WITH AND WITHOUT LOADING; v_p = phase velocity along wire, c = speed of light. Theoretical curves from (3.72), $k_o/\beta_w = v_p/c$; for dielectric loading with $\epsilon = 10$, $v_p/c \cong .425$; for ferrite loading with $\epsilon = 3.77$, $\mu = 2.2$, $v_p/c \cong .55$; for unloaded antennas, $v_p/c = 1$; $\beta_w = \beta_o \sin\psi$ = propagation parameter along the wire.

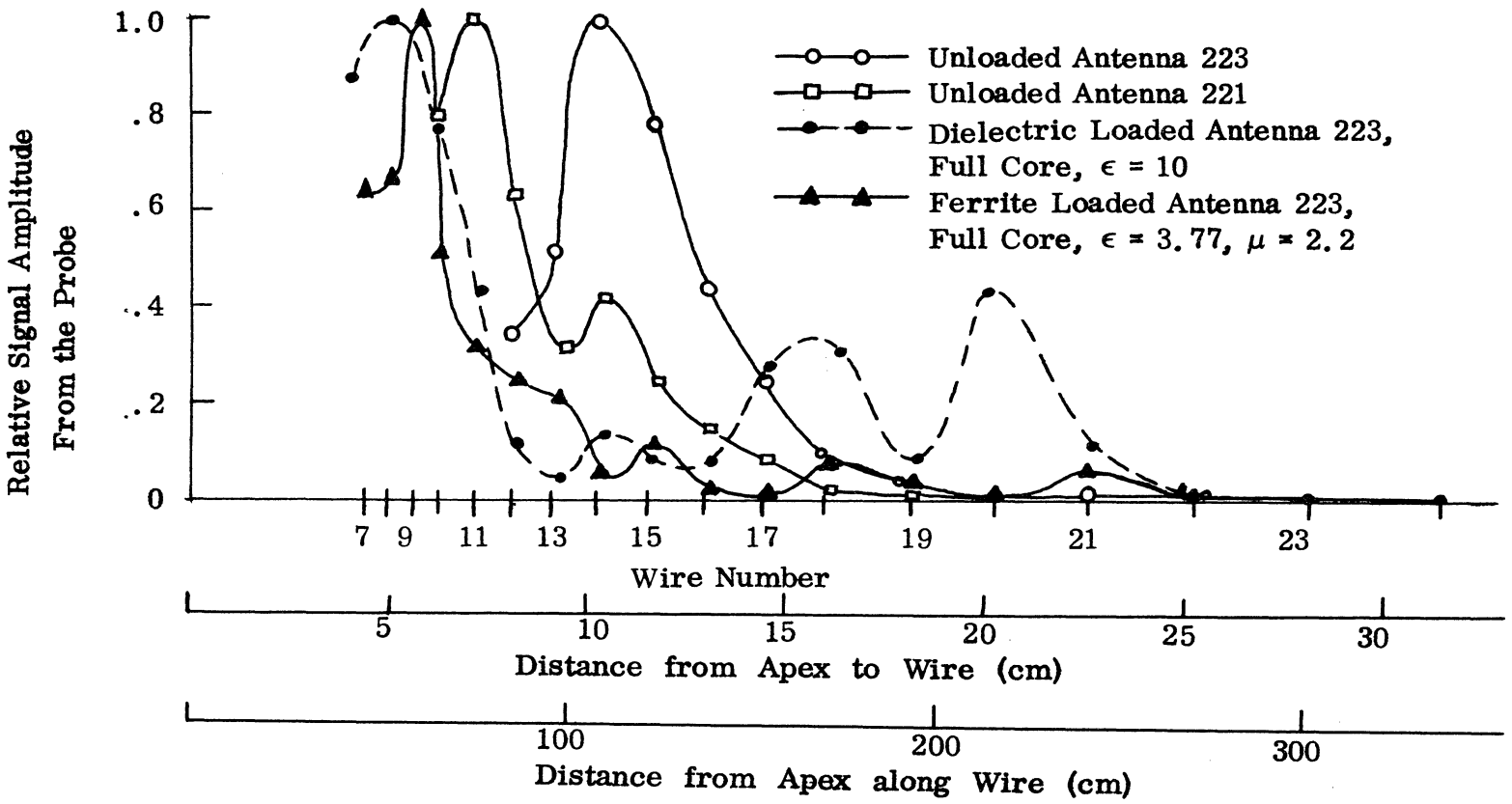

FIG. 6-15: MEASURED AMPLITUDE OF LOG-PYRAMIDAL HELICAL ANTENNAS NO. 221 AND 223 WITH AND WITHOUT LOADING. 700 MHz

current amplitude decreases to .1 of the peak value, are 0.56 for the ferrite case and 0.7 for the dielectric case, which indicates that the ferrite loading is better than dielectric loading for size reduction. If the increases in current amplitude near the base (Wire Nos. 17 and 19) are considered, the dielectric loaded case requires a larger antenna than the unloaded antenna, due to incomplete radiation in the first active zone. The rate of current attenuation for the unloaded case is approximately that predicted by Fig. 3-5. However, the rates of attenuation of the loaded cases are much larger than those predicted by Fig. 3-5 (dielectric case) and Fig. 3-6 (ferrite case), neglecting the peaks of current near the antenna base in the dielectric case. An envelope across the highest peaks in the dielectric case would show a much slower decay, as predicted theoretically in Fig. 3-5.

It should be noted that even with the loop probe touching the wire, there were indications, from the fall-off of signal amplitude near the tip of the cone, that the probe signal is not a good measure of current when the spacing between antenna wires approaches the size of the probe.

In conclusion, the data on the phase velocity of the antenna current confirms the theoretical prediction of a reduction in phase velocity due to material loading. Also, the amplitudes of the current, which indicate radiation rate, show a size reduction very close to that predicted from the simplified phase velocity reduction formula obtained from (3. 72). The current attenuation from the more exact tape-helix theory does not quantitatively predict the actual current attenuation in the two loaded cases checked. More cases with different loading materials must be checked experimentally for current attenuation, and the formation of the secondary peaks needs to be explained before accurate experimental attenuation values of current can be stated.

VII

SUMMARY

7.1 Conclusions

1) A reduction in the diameter of helical and conical helical antennas may be achieved by insertion of material of high ϵ and/or μ inside and close to the conductors. Active zone lengths are not reduced by the same amount, and may be increased by the use of dielectrics. Use of μ as well as ϵ (as in ferrites) holds promise of some active region length reduction.

2) The performance of backfire bifilar helix may be approximately analyzed using one current wave, the T_0 wave, with a complex propagation constant. The higher space harmonics are very important in determining the propagation constant. The numerical solution to the dispersion equation can also give the residue of the corresponding leaky wave pole in a simple gap-source problem. Extension of the solution to the tapered conical helix is relatively simple by established methods of gradually varying structures. An asymptotic, narrow-tape-helix diameter-reduction factor upon the addition of inside loading material is given by

$$\sqrt{\frac{1+\frac{1}{\mu}}{1+\epsilon}} \quad .$$

3) A sheath helix solution of the loaded helix accurately predicts the solution for the real part of the propagation parameter, β_0, of the loaded tape helix with a very narrow tape width (radiation) region by straight-line extrapolation on the k - β diagram from the slow wave solution to the fast wave. The close relation between the slow wave solutions and higher order harmonic solutions, not the dominance of one space harmonic on the tape helix, is the reason for the accuracy of the sheath solution. Layered loading solutions may be produced for the sheath helix, but the effect of layers on the higher harmonics of the tape helix will have to be considered, possibly also

using sheath solutions of the higher order harmonics. Since each higher space harmonic ($n > 1$) is more closely bound to the helix surface than the $n = -1$ harmonic, the layered sheath solution given should provide a lower bound for the effect of layer thickness.

4) Experimental studies of the near and far fields of both loaded helices and log-conical helices partially confirms the diameter reduction factor for the two materials used. A considerable range of material parameters and flexibility in measuring loaded and unloaded structures may be obtained using powdered materials rather than solid ones, with the retaining techniques developed. However, further experimental confirmation was restricted to the availability of materials having low loss for increased ranges of μ and ϵ values. Powdering of the materials precludes very high μ or ϵ .

5) Near field measurements of conical helices have proved very useful in interpreting the results of loading. For the rather large pyramidal cone angle used, loading produces several 'active zones' on the antenna and some interferences in the current distribution. The first active zone is moved toward the tip as theory predicts. The second active zone appears to occur at the unloaded active region position. This, and the other active regions are not yet understood. However, they can destroy the far field pattern, and should be eliminated by proper design of the first active zone to allow full radiation.

7.2 Original Work Done

To the best of the author's knowledge, the following parts of the above work are new and original:

1) The analysis of the fast wave solution of the tape helix fully loaded inside and operating in the backfire mode, including the asymptotic studies of the relative importance of the n=-1 space harmonic and the approximate sum of the rest of the harmonics; some interpretation in terms of a corresponding gap-source problem.

2) The asymptotic study of the full-core-loaded sheath helix, in the n= -1 mode, with application to helix antennas; the study of an inside layer-loaded sheath helix in the n= -1 mode,

3) Experimental work on the loading of helix and log-conical helix antennas, including both near and far field measurements; techniques of loading with material powders, using fiberglass and styrofoam retainers; interpretation of loaded helix measurements relative to their value to predicting loaded conical helix performance; verification of formulas for phase velocity reduction and size reduction.

7.3 Further Work

The progress attained in this research has shown some additional areas that might be profitably studied.

1) Mathematical investigation of all other possible single current wave modes of the loaded helix and the related source problems.

2) Possible application of coupled mode theory to the problem.

3) Effect of loading only the higher space harmonics, preparatory to discrete and layer loading analysis.

4) Experimental study of the effect of antenna parameters, particularly cone (taper) angle on loaded active zones.

5) Experimental study of the effect of other values of material parameters, particularly the theoretical prediction of the effect of high μ on β_i .

6) Experimental study of the higher active regions; possible use for higher gain in tapered structures.

APPENDIX A

SOLUTION OF TAPE HELIX AMPLITUDE CONSTANTS

The solution to (3.23) - (3.26) is a very straightforward solution to four simultaneous equations. In order to facilitate checking, as well as extensions to this work, some steps will be given.

The equations (3.23) and (3.26) are immediately used to eliminate a and b from (3.24) and (3.26). From (3.23)

$$\frac{n\beta}{a}\left[\frac{AK}{\Gamma^2} - \frac{a\,I}{\gamma^2}\right] + j\omega\left[B\frac{\mu_o K'}{\Gamma} - \frac{b\mu_1 I'}{\gamma}\right] = 0 \quad . \tag{A.1}$$

Substituting for a and b

$$A\frac{n\beta K}{a}\left[\frac{1}{\Gamma^2} - \frac{1}{\gamma^2}\right] + j\omega B\left[\frac{\mu_o K'}{\Gamma} - \frac{\mu\mu_o I'}{\gamma}\frac{K}{I}\right] + \frac{j\omega\mu\mu_o I'}{\gamma} - \frac{j\phi}{I} = 0 \quad . \tag{A.2}$$

Substituting,

$$C_{\gamma\gamma} = \left[1 - \frac{\Gamma^2}{\gamma^2}\right]; \qquad C_\mu = \left[\frac{\Gamma}{\gamma}\frac{K}{I} - \frac{1}{\mu}\frac{K'}{I'}\right]$$

$$C_\beta = \frac{n\beta}{a}; \qquad C_\gamma = \frac{\Gamma}{\gamma}$$

gives

$$\frac{j\omega A\, C_\beta C_{\gamma\gamma} K/I'}{\omega^2 \mu_1 \Gamma^2} + \frac{B}{\Gamma} C_\mu = \frac{-j\phi C_\gamma}{I\Gamma} \tag{A.3}$$

which is one of the two equations for A and B. For the other equation in A and B, from (3.25)

$$j\omega\left[\frac{\epsilon_o}{\gamma}\, I'a - \frac{\epsilon\epsilon_o AK'}{\Gamma}\right] + C_\beta\left[\frac{BK}{\Gamma^2} - \frac{bI}{\gamma^2}\right] = -j_z \qquad \text{(A. 4)}$$

Substituting for a and b yields,

$$\frac{j\omega A}{\Gamma}\left[\epsilon\,\frac{\Gamma}{\gamma}\,\frac{K}{I} - \frac{K'}{I'}\right] + \frac{C_\beta\, BK}{\epsilon_o I'}\left[\frac{1}{\Gamma^2} - \frac{1}{\gamma^2}\right] - \frac{j\omega C_\beta}{\epsilon_o \gamma^2 I'} = \frac{-j_z}{\epsilon_o I'} \quad . \qquad \text{(A. 5)}$$

Substituting

$$C_\epsilon = \left[\epsilon\,\frac{\Gamma}{\gamma}\,\frac{K}{I} - \frac{K'}{I'}\right]$$

as well as the other constants defined above, the other equation for A and B becomes

$$\frac{j\omega A C_\epsilon}{\Gamma} + \frac{BC_\beta C_{\gamma\gamma}}{\epsilon_o \Gamma^2}\,\frac{K}{I'} = \frac{-j_z}{\epsilon_o I'} + \frac{j\omega C_\beta C_\gamma^2}{\epsilon_o \Gamma^2 I'} \quad . \qquad \text{(A. 6)}$$

Solving (A.3) and (A.6) for B, then multiply (A.6) by

$$\frac{C_\beta C_{\gamma\gamma} K}{\omega^2 \mu_o \Gamma I'} = C_1$$

to get

$$j\omega A\left(\frac{C_\beta C_{\gamma\gamma} K}{\omega^2 \mu_1 \Gamma I'}\right) + B\,\frac{C_\beta^2 C_{\gamma\gamma}^2 K^2}{\omega^2 \mu\mu_o \epsilon_o \Gamma^3 C_\epsilon I'^2} = \frac{-j_z C_1}{\epsilon_o C_\epsilon I'} + \frac{j\omega C_\beta C_\gamma^2 C_1}{\epsilon_o C_\epsilon \Gamma^2 I'} \qquad \text{(A. 7)}$$

Subtract (A.7) from (A.3) to get

$$BC_\mu\left[1-\frac{C_\beta^2 C_{\gamma\gamma}^2 (K/I')^2}{\omega^2 \epsilon_o \mu\mu_o C_\epsilon C_\mu \Gamma^2}\right] = \frac{-j_\phi}{I}\left\{\left[C_\gamma + \frac{C_\beta^2 C_\gamma^2 C_{\gamma\gamma}}{k_o^2 \mu C_\epsilon \Gamma^2}\left(\frac{KI}{I'^2}\right) + \frac{j_z C_\beta C_{\gamma\gamma}\left(\frac{KI}{I'^2}\right)}{\epsilon_o \omega^2 \mu\mu_o C_\epsilon}\right]\right\} . \tag{A.8}$$

Substituting

$$C_{\mu\epsilon} = \frac{C_\beta^2 C^2 (K/I')^2}{k_o^2 \mu C_\mu C_\epsilon \Gamma^2} ; \qquad C_2 = \frac{C_\beta^2 C_\gamma^2 C_{\gamma\gamma}}{k_o^2 \mu C_\epsilon \Gamma^2}\left(\frac{KI}{I'^2}\right) = C_\beta C_\gamma^2 C_3$$

$$C_3 = \frac{C_\beta C_{\gamma\gamma}}{k_o^2 \mu C_\epsilon}\left(\frac{KI}{I'^2}\right) ; \qquad k_o^2 = \omega^2 \mu_o \epsilon_o .$$

There results the solution for B

$$B = \frac{1}{IC_\mu} \frac{-j_\phi (C_\gamma + C_2) + j_3 C_3}{(1-C_{\mu\epsilon})} . \tag{A.9}$$

Similarly, solving for A, multiply (A. 3) by

$$\frac{C_\beta C_{\gamma\gamma} K}{\epsilon_2 \Gamma}$$

to get

$$\frac{j\omega A}{\Gamma}\left[\frac{C_\beta^2 C_{\gamma\gamma}^2 K^2}{\omega^2 \epsilon_o \mu\mu_o \Gamma^2 I'^2}\right] + \frac{B}{\Gamma} \frac{C_\mu C_\beta C_{\gamma\gamma} K}{\epsilon_o \Gamma I'} = \frac{-j_\phi C_\gamma C_\beta C_{\gamma\gamma}}{I\Gamma^2 \epsilon_o} \frac{K}{I'} . \tag{A.10}$$

Multiply (A. 6) by C_μ, and subtract (A. 10) from it to get

$$\frac{j\omega A}{\Gamma}\left[C_\epsilon C_\mu - \frac{C_\beta^2 C_\gamma^2 (K/I')^2}{\omega^2 \epsilon_o \mu_o \mu \Gamma^2}\right] = \frac{-j_z C_\mu}{\epsilon_o I'} + j\phi\left[\frac{C_\beta C_\gamma^2 C_\mu}{\epsilon_o \Gamma^2 I'} + \frac{C_\beta C_\gamma C_{\gamma\gamma}}{I \epsilon_o \Gamma^2}\ \frac{K}{I'}\right] \quad \text{(A. 11)}$$

Substitute $C_{\mu\epsilon}$ as defined, after division by $C_\mu C_\epsilon$ to give

$$\frac{j\omega A}{\Gamma}\ (1-C_{\mu\epsilon}) = \frac{-j_z}{\epsilon C_o C_\epsilon I'} + \frac{j\phi}{\epsilon_2 I' C_\epsilon}\ \frac{C_\beta C_\gamma^2}{\Gamma^2}\ \left[1+\frac{C_{\gamma\gamma} K/I}{C_\mu C_\gamma}\right] \quad \text{(A. 12)}$$

which then gives

$$A = -j\ \frac{\Gamma}{k_o I' C_\epsilon}\ \sqrt{\frac{\mu_o}{\epsilon_o}}\left[\frac{-j_z + j\phi C_4}{1-C_{\mu\epsilon}}\right] . \quad \text{(A. 13)}$$

Thus, A and B are obtained.

APPENDIX B

NUMERICAL CALCULATION OF MODIFIED BESSEL FUNCTIONS OF COMPLEX ARGUMENT AND INTEGER ORDER

The numerical calculation of modified Bessel functions of complex argument but integral order has apparently not been completely explored. The few programs that have been made up are not generally available, and lack firm estimates on accuracy. They also appear to require double precision arithmetic while still being accurate for only a limited range of argument and order. In addition, complex numbers are not as easily handled in most computer languages as real numbers, thereby forcing step by step statements of some arithmetic operations.

Naturally, $I_n(z)$ and $K_n(z)$ could be expressed as functions of the Bessel function $J_n(z)$ and the Hankel functions $H_n^{(1)}(z)$ and $H_n^{(2)}(z)$, but suitable programs are still not readily available.

Briefly, the basic series for the modified Bessel function of complex argument is the ascending series, such as given in Abramowitz and Stegun (1964).

$$I_n(z)=\left(\frac{1}{2}z\right)^n \sum_{k=0}^{\infty} \frac{\left(\frac{1}{4}z^2\right)^k}{k!\,(n+k)!} \tag{B.1}$$

$$K_n(z)=\frac{1}{2}\left(\frac{1}{2}z\right)^{-n} \sum_{k=0}^{\infty} \frac{(n-k-1)}{k!}\left(-\frac{1}{4}z^2\right)^k + (-1)^{n+1}\,\ell n\left(\frac{1}{2}z\right) I_n(z)$$

$$+\frac{1}{2}\left(-\frac{1}{2}z\right)^n \sum_{k=0}^{\infty} \left\{\psi(k+1)+\psi(n+k+1)\right\} \frac{\left(\frac{1}{4}z^2\right)^k}{k!\,(n+k)!} \tag{B.2}$$

where

$$\psi(n) = -.57221 + \sum_{k=1}^{n-1} k^{-1}$$

$$\psi(1) = -.57721.....$$

This is a fairly good series to use for small arguments $z < 2\text{-}7$, n small, and with single precision arithmetic (8 digits). For larger arguments and orders, convergence gets much slower, and the series for $K_n(z)$ yields very poor accuracy, which can only be helped slightly ($z < 10 - 20$) by double precision arithmetic. The basic reason for this is that the series for $K_n(z)$ subtracts almost equal quantities, since

$$K_n \sim e^{-z}, \qquad I_n \sim e^{z} \qquad \text{(z large)}$$

and $I_n(z)$ is in the definition of $K_n(z)$. The same problem exists for $H_n^{(2)}(z)$. Harris and Pachares (1965) have worked out a double precision program with the subtraction problem reportedly eliminated by rearrangement of terms for $H_n^{(1)}(z)$ and $H_n^{(2)}(z)$. Even the ascending series for $I_n(z)$, $\theta \sim 90^o$ (i.e. $J_n(z)$) was found poor near the zeros for $z > 3$.

For large arguments, it is necessary to use the asymptotic series for large argument and order to supplement the ascending series. Unfortunately, the overlap of regions when using only single precision is rather small and quite dependent on the angle of the argument, so that much labor is necessary in checking accuracy in all regions to assure six significant figures of accuracy. This accuracy was felt essential because calculation of $L(\beta)$ in some regions causes subtraction of nearly equal quantities, as does the stepwise approximation for the derivative $dL(\beta)/d\beta$. Additional problems of accuracy checking exist for orders $n > 1$, because no tables are available.

The tables used to check n=0 and n=1 for $z < 10$ were by the National Bureau of Standards (1947, 1950) on $J_0(z)$, $J_1(z)$, $Y_0(z)$ and $Y_1(z)$, where $N_n(z)$ is commonly used for $Y_n(z)$. Even though these tables had great accuracy, as

many as 6 - 10 significant figures were often lost in the formulas relating $J_n(z)$ and $Y_n(z)$ to $K_n(z)$ (or $H_n^{(2)}(z)$). Thus, even double-precision programs for $J_n(z)$ and $Y_n(z)$ are inadequate for calculating $K_n(z)$ or $H_n^{(2)}(z)$ for $z > 10 - 15$, for some angles of the argument.

Several asymptotic series for large z were used in the regions $z > 2 - 7$ (depending on the angle) for calculation in this report for $n < 1$. The speed of computation is much better than for the ascending series using double precision, even where that is possible. Considerable care must be used in selecting the proper series. Although the asymptotic series are mathematically valid (as $z \to \infty$), they are not necessarily numerically accurate for moderate z. For instance, the series

$$I_n(z) \frac{e^z}{\sqrt{2\pi z}} \left\{ 1 - \frac{\mu - 1}{8z} + \frac{(\mu-1)(\mu-9)}{2!\,(8z)^2} + \ldots\ldots \right\} \qquad \text{(B. 3)}$$

where arg $z < \pi/2$, is given by Abramowitz and Stegun (1964); this series ignores terms of the form e^{-z} which may be found from the series for $J_n(z)$ found in the same reference. Thus, the series for $I_n(z)$ is very poor for (arg $z \sim \pi/2$). This has been checked numerically by the author. The series for $J_n(z)$ is more complete and should be used rather than the one for $I_n(z)$, although this was not checked by the author. Some difficulty in the asymptotic series for $J_n(z)$ was encountered for $\theta > 45^\circ$, where sines, cosines and exponentials of complex argument occur. The series $K_n(z)$ has to be written from the series for $J_n(z)$ and $Y_n(z)$, to assure accuracy.

There are polynomials that have been written to approximate the Bessel functions of a real variable , x, for $n \leq 1$, in various regions of x. These have been worked out essentially from the ascending series for small z, and from the asymptotic series for large z. They are given in Abramowitz and Stegun (1964) for the Bessel functions of real variable $I_n(x)$, $K_n(x)$, $J_n(x)$, $Y_n(x)$ for $n \leq 1$. They are particularly fast for computer use, since only six terms are

used, and these may be computed iteratively. They were investigated for use with complex variables by the author and found accurate in the general region $\theta < 45^{o}$ from the axis, although the accuracy and regions of use stated for x had to be revised. Some trouble assuring six significant figures for the small z polynomial forced use of the single precision ascending series for small z, whereas for large z, the polynomial approximations to the asymptotic series were used .

To summarize; the following formulas were used to compute $I_n(z)$, $K_n(z)$, $n \leq 1$, based on point by point numerical checks of single precision accuracy, where $z = x+jy=re^{j\theta}$.

1. For $I_n(z)$, $n \leq 1$

1.1 When $|z| < 2.9$ or ($|z|<6$ and $|y|<2|x|$) use the ascending series for $I_n(z)$.

1.2 Otherwise, use polynomials for large x from Abramowitz and Stegun (1964) for first quadrant variables with z replacing the real variable x given.

1.2.1 If $|y| > |x|$ use polynomial for $J_n(x)$, and then transform to $I_n(x)$.

1.2.2 If $|y| < |x|$, use polynomial for $I_n(x)$.

2. For $K_n(z)$, $n \leq 1$

2.1 When $|z| < 2.9$ or ($|z| < 3.9$ and $|y| > 2|x|$), use ascending series for $K_n(z)$.

2.2 Otherwise, use polynomials for large x for first quandrant variables, replacing x by z.

2.2.1 If $|y| > |x|$, use polynomial KS from $J_n(z)$ and $Y_n(z)$ (derived below).

2.2.2 If $|y| < |x|$, use polynomial for $K_n(z)$.

A simpler method, said to give 4 - 6 figure accuray for $H^{(2)}(z)$, but not checked by the author, uses the ascending series, $z < 5$, and the general asymptotic series for $J_n(z)$ and $Y_n(z)$, $z > 5$. The asymptotic series is carried out until the terms begin to increase. Dr. E. K. Miller, of the High Altitude Laboratory, The University of Michigan, has written a successful program using this method.

Polynomial KS

For deriving $K_n(z)$ for z large and almost purely imaginary, the asymptotic expansions and polynomials are invalid; the polynomials for $J_n(z)$ and $Y_n(z)$ must be used. These may be combined in the first quadrant to give,

$$K_n(z) = (-j)^{n+1} \frac{\pi}{2} H^{(2)}(-jz)$$

$$H_n^{(2)}(-jz) = J_n(-jz) - j\, Y_n(-jz) \quad .$$

But

$$J_n(x) \cong \frac{f_n(x)}{\sqrt{x}} \sin \theta_n(x)$$

$$Y_n(x) \cong \frac{f_n(x)}{\sqrt{x}} \cos \theta_n(x)$$

where $f_n(x)$ and $\theta_n(x)$ are polynomials given in Abramowitz and Stegun (1964). Generalizing the real variable x to the complex variable z in the limited range of the first quadrant z, $\theta < 45^\circ$, by analytic continuation

$$K_n(z) = -(-j)^n \frac{f_n(-jz)}{\sqrt{-jz}} e^{j\theta_o(-jz)} \quad .$$

This polynomial is accurate to approximately six significant figures or better in the given sector $|\theta| < 45^\circ$ for $|z| > 4$, as checked numerically at quite a few critical points by the author.

Using the conjugate relations

$$K_n(z^*)=K_n^*(z) \; ; \qquad I_n(z^*)=I_n^*(z)$$

and the 180^o rotation relations

$$I_n(ze^{\pi i})=(-1)^n I_n(z)$$

$$K_n(ze^{\pi i}) = (-1)^n K_n(z)-\pi i\, I_n(z)$$

the answers in the first quadrant may be transformed into any other quadrant.

Derivatives of the Bessel functions for n = 1 were calculated using recurrence relations in terms of the n = 0 and n = 1 order functions. The Bessel functions for larger orders may be obtained from the asymptotic series for large n, which have been programmed and found accurate for $n > 5$, over the sector $\theta < 45^o$. Another method often used for Bessel functions of real argument is the use of recurrence relations. Because of numerical stability problems, $I_n(x)$ may be calculated by recurrence for decreasing values of n, while $K_n(x)$ must be calculated for increasing values of n. A method for calculating $J_n(x)$ or $I_n(x)$ for increasing values of n is by using a recurrence method with the partial fraction expansion for $J_n(x)$. Whether recurrence methods work accurately numerically in the complex plane has not been found by the author, although some discussion appears in Harris and Pachares (1965). A possible problem is seen from the transformation of $K_n(z)$ through 180^o. For large z, $K_n(-z)$ then looks predominately like $I_n(z)$. Since recurrence must be done differently for $I_n(x)$ and $K_n(x)$, the question becomes what to do with 'in between' values of z. The large n asymptotic form for $I_n(z)$ and $K_n(z)$ supplemented by recurrence near the imaginary axis would probably give moderate accuracy.

Other programs for some of the Bessel functions, often not $H_n^{(2)}(z)$ or $K_n^{(2)}(z)$, are mentioned in Flesher (1961) and in the SHARE listings of IBM programs. New York University, particularly, has written several programs in SHARE; however, little information is available on the accuracy or the method of computation, and considerable knowledge of the computer is necessary to adapt these programs from SHARE to a particular computer system. Probably most of these programs use double-precision ascending series techniques valid for moderate arguments.

In this report, the asymptotic summation was used to eliminate the higher order Bessel function problem, as well as to make the analysis clearer.

APPENDIX C

APPROXIMATE SUMMATION OF A SERIES

The summation (3.69) can be approximated by means of a trick similar to Marcuvitz (1964, p.144). The series

$$s' = \frac{2}{\Delta^2} \sum_{\substack{n \text{ odd} \\ n=1,3,5,\ldots}}^{\infty} \frac{\sin^2 n\Delta}{n^3} \tag{C.1}$$

does not appear to be available in the literature. However, by differentiating with respect to Δ,

$$\frac{ds'}{d\Delta} = \frac{2}{\Delta^2} \sum_{n=1,3,5,\ldots}^{\infty} \frac{2 \sin n\Delta \cos n\Delta}{n^2} = \frac{2}{\Delta^2} \sum_{n=1,3,5..}^{\infty} \frac{\sin 2n\Delta}{n^2} \tag{C.2}$$

it can be put in a recognized form from Collin (1960, p. 580)

$$\text{Imag.} \sum_{n=1,3,5,..}^{\infty} \frac{e^{jnx}}{n^2} = \sum_{n=1,3,5,..}^{\infty} \frac{\sin nx}{n^2} = -\frac{x}{2} \ln \frac{x}{2} + \frac{x}{2} + \frac{x^3}{72} + \ldots \tag{C.3}$$

Replacing $x/2$ by Δ,

$$\frac{ds'}{d\Delta} = \frac{2}{\Delta^2} \sum_{n=1,3,5,..}^{\infty} \frac{\sin 2n\Delta}{n^2} = \frac{2}{\Delta^2} \left[-\Delta \ln \Delta + \Delta + \frac{\Delta^3}{9} + \ldots \right] \tag{C.4}$$

Integrating with respect to Δ to get s,

$$s' = \frac{2}{\Delta^2} \int (-\Delta \ln\Delta + \Delta + \frac{\Delta^3}{9} + \ldots) = \frac{2}{\Delta^2} \left[-\frac{\Delta^2}{2} \ln\Delta + \frac{3\Delta^2}{4} + \frac{\Delta^4}{36} + \ldots \right] \tag{C.5}$$

$$s' = \ln \frac{1}{\Delta} + \frac{3}{2} + \frac{\Delta^2}{18} + \ldots$$

which is the answer desired.

Actually, the resonant term n=(rn) should be subtracted from the sum in (C. 1) since it is calculated separately. It's contribution is approximately 1 for n small, thus

$$s = \frac{2}{\Delta^2} \sum_{\substack{n=1,3,5 \\ n \neq rn}}^{\infty} \frac{\sin^2 n\Delta}{n^3} \cong \ell n \frac{1}{\Delta} + \frac{1}{2} + \frac{\Delta^2}{18} + \ldots \cong \ell n \frac{1}{\Delta} \ (\Delta \text{small}) \quad . \tag{C. 6}$$

It is, however, interesting to note some of the other forms that might be encountered with different methods of solution for the differential equation. It can be seen that they are all very close together, for small Δ.

For the monofilar tape helix solution according to Sensiper's method of setting $E_{//}=0$ on the tape center line, the series used is (Sensiper, 1951)

$$s_s = \frac{1}{\Delta} \sum_{m=1}^{\infty} \frac{\sin n\Delta}{n^2} = \ell n \left(\frac{e}{\Delta}\right) = 1 + \ell n \frac{1}{\Delta} \quad . \tag{C. 7}$$

For the assumption of a non-uniform current across the tape, with peaks at the edges of an inverse square form (Sensiper, 1951)

$$s \cong \sum_{m=1}^{\infty} \frac{J_o(m x)}{m} \sim \ell n \frac{2}{\Delta} \cong .7 + \ell n \frac{1}{\Delta} \quad . \tag{C. 8}$$

Thus, the specific form of current or boundary condition applied to a narrow tape helix does not significantly affect the dispersion equation for small Δ. In any case, further accuracy should begin by using the true wire shape in a solution of some kind, probably with the developed helix model for the higher order modes.

REFERENCES

Abramowitz, M. and I. Stegun (1964), Handbook of Mathematical Functions, U. S. National Bureau of Standards, Department of Commerce, Washington, D. C.

Adams, A. T. (March 1964), "The Rectangular Cavity Slot Antenna with Homogeneous Isotropic Loading," The University of Michigan Cooley Electronics Laboratory Report No. 05549-7-T, AD 603657.

Adams, A. T. and R. M. Kalafus (January 1963), "Study and Investigation of a UHF-VHF Antenna," The University of Michigan Cooley Electronics Laboratory Report 03667-10-P.

Adams, A. T. and J. A. M. Lyon (June 1965), "Ferrite Loaded Antennas for Aerospace Applications," Supplement to IEEE Trans. Aerospace and and Electronic Systems, pp. 489-494.

Admiralty Services Weapons Establ. Gr. Br. "Dielectrically Loaded Electromagnetic Horns at S-band," AD 414430.

American Electronics Laboratory (November 1959), "Design and Development of Circularly Polarized Antennas," Final Report 57042-F for the U. S. Army Electronics Command, Fort Monmouth, N. J.

Angelakos, D. J. and M. M. Korman (October 1946), "Radiation From Ferrite Filled Apertures," Proc. IRE, 44, pp. 1463-1468.

Ash, E. A., et al. (April 1964), "Dispersion and Impedance of Dielectric Supported Ring and Bar Slow Wave Circuits," Proc. IEE, London, 3, No. 4, pp. 629-641.

Barnett, R. (1963), "An All Dielectric Waveguide and Antenna," Ph.D. Dissertation, Ohio State University, Columbus, Ohio.

Bernard, G. D. and A. Ishimaru (October 1963), "Pole Contributions to Electromagnetic Fields in the Light of a Modified Saddle Point Techniques," The University of Washington Technical Report No. 82.

Bevensee, R. M. (1964), Electromagnetic Slow Wave Systems, Wiley and Sons, New York.

Brillouin, L. (1946), Wave Propagation in Periodic Structures, McGraw-Hill Book Company, New York (or Dover Publications, Inc., 1953).

Brownell, F. B. and D. E. Kendall (1960), "Miniaturized Cavity Fed Slot Antennas, IEEE Wescon Record, Part 1, pp. 158-166.

Bulgakov, B. M. and V. P. Shestopalov (January, 1958), "Propagation of Electromagnetic Waves in Retarding Systems Consisting of Spirals and Dielectrics," Soviet Phys., Tech. Phys., 3, No. 1, pp. 167-177.

Bulgakov, B. M. et al (1960), "Symmetrical Surface Waves in a Helix Waveguide with a Ferrite Medium," Radio. i. Elek., 5, pp. 1818-1827.

Bulgakov, B. M. et al (July, 1961), "The Irreversible Propagation of Waves in a Helix Waveguide Place in a Ferrite Medium," Radio Eng. and Electr., 1, pp. 118-134.

Carrel, R. (May, 1957), "Experimental Investigation of the Conical Spiral Antenna," University of Illinois Technical Report 22, AD 144021.

Chodorow, M. and E. L. Chu (November 1954), "Cross Wound Twin Helices for Travelling Wave Tubes," Stanford University Hansen Laboratory of Physics, M. L Report No. 249, AD 51403.

Chu, C. M. (January, 1958), "Propagation of Waves in Helical Waveguides," J. Appl. Phys., 29, No. 1, pp. 88-99.

Collin, R. E. (1960), Field Theory of Guided Waves, McGraw-Hill Book Company New York.

Copeland, J. R. (September, 1960), "Radiation from the Balanced Equi-angular Spiral Antenna," Ohio State University Report 903-12.

Cruzan, O. R. (1959), "Radiation Properties of a Thin Wire Loop Antenna Embedded in a Spherical Medium," Trans. IEEE, AP-7, pp. 34-35.

DiFonzo, D. F. (December, 1964), "Reduced Size Log Periodic Antennas," Microwave J., pp. 37-42.

Dropkin, H. et al (1957), "VHF Ferrite Antenna-II: Radiation Measurements," IEEE-PGMIL Convention Record, pp. 175-182.

Dyson, J. F. (March 1964), "The Design of Conical Log-Spiral Antennas," IEEE International Convention Record, Part VI, pp. 259-273. See also, University of Illinois Antenna Laboratory Report, AD 465950, .

Flesher, G. T. (June 1961), "Propagation and Reflection of Plane Waves in a Plasma Having Inhomogeneity in One Direction," Bendix Systems Division Research Note 25, AD 268815

Fletcher, R. C. (August, 1952), "A Broadband Interdigital Circuit for Use in Travelling Wave Amplifiers," Proc. IRE, 40, pp. 951-958.

Fradin, A. Z. (1961), Microwave Antennas, Pergamon Press, New York.

Galejs, J. (October 1962), "Dielectric Loading of Electric Dipole Antennas," J. Res., NBS, 66D, No. 5, pp. 557-562.

Galejs, J. (August 1963), "Small Electric and Magnetic Antennas with Cores of Lossy Dielectric," J. Res., NBS, 67D, pp. 445-451.

General Precision, Kearfott Division (October 1962), "Broadband Antenna Study Program," Interim Study Report AD 293968.

Grimes, D. M. (1958), "Miniaturized Resonant Antennas Using Ferrites," J. Appl. Phys., 29, p. 401.

Hair, H. (December 1964), "Development of Helical Phase Shifters," General Electric H. M. E. D. Final Report prepared fot MIT-Lincoln Laboratory, Subcontract 250.

Hansen, R. C. (July 1966), "Microminiature Antennas," Microwave J., pp. 22-24.

Harris, J. H and J. Pachares (June 1965), "The Computation of Cylindrical Plasma Radiation Problems," Hughes Aircraft Company Report P65-79, AD 620251.

Harris, L. A. et al (January 1949), "Some Measurements of Phase Velocity Along a Helix with Dielectric Supports," Massachusetts Institute of Technology Report 93.

Harvey, A. F. (1963), Microwave Engineering, Academic Press, London.

Hellgren, C. (1953), "The Propagation of Electromagnetic Waves Along a Conical Helix with a Variable Pitch," Trans. Chalmers Univ. of Technology, Sweden, No. 130-pp. 4-12.

Herman, J. (April 1958), "Extended Theory of Thin Wire Loop Antenna With and Without a Spherical Ferrite Core," Diamond Ordnance Fuze Laboratories Technical Report 600, AD 201627.

Hildebrand, F. B. (1956), Introduction to Numerical Analysis, McGraw-Hill Book Company, New York.

Hong, S. (September 1965), "Size Reduction of Bifilar Helical Antennas by Loading with a Magneto-Dielectric Material," The University of Michigan Radiation Laboratory Internal Memorandum No. 7260-504-M.

Ingerson, P. G. and P. E. Mayes (May 1966), "Dispersion Properties of Linear Dipole Arrays," University of Illinois Antenna Laboratory Report No. 66-2, AFAL-TR-66-120.

Jasik, H. (1961), Antenna Engineering Handbook, McGraw-Hill Book Company, New York.

Johnson, C. (April 1959), "Impedance and Dispersion Characteristics of the Flattened Helix," Trans. IEEE, ED , pp. 189-195.

Johnson, H. R. et al (January 1956), "Wave Propagation on Multifilar Helices," Trans. IEEE, ED- , pp. 18-24.

Jones, E. M. T. (August 1950), "A Negative Dispersion Helix Structure," Stanford University Electronics Research Laboratory Report 27.

Jones, H. S., Jr. (1965), "Dielectric Loaded Waveguide Slot Arrays," Harry Diamond Laboratories Technical Report 1269.

Jones, J. et al (August 1960), "Design Techniques for a Light Weight High Power Spiral Antenna," IEEE National Convention Record, pp. 107-113.

Kantorovich, M. I. (1939), (title unknown), J. Exp. Theor. Phys. USSR, 9, p. 2195.

Karjala, D. S. and R. Mittra (October 1965), "Radiation from Some Periodic Structures Excited by a Waveguide," University of Illinois Antenna Laboratory Report 65-15, AFCRL-65-653.

Kirschbaum, H. S. (September 1959), "Characteristic Impedance and Phase Velocity of Shielded Helical Transmission Lines," AIEE Trans., 79, Pt. 1 No. 44, pp. 444-450.

Kiryushin, V. P. (1957), "The Influence of Dielectric on the Phase Constants of the Space Harmonics of a Helix," Radiotech. i. Elek., 2, No. 7, pp. 901-911.

Klock, P. (March 1963), "A Study of Wave Propagation of Helices," Ph. D Dissertation, University of Illinois. See also Antenna Laboratory Technical Report 68.

Klock, P. and R. Mittra (March 1963), "Complex Valued Phase Constants for the Sheath Helix and Their Relation to the Solutions for the Tape Helix," in the University of Illinois Quarterly Progress Report.

Kogan, S. Kh. (June 1949), "The Propagation of Waves Along an Endless Helix," Comp. Rend. Acad. Sci. S. R. S. S., 66, No. 5, p. 867; see also Wireless Engineer, XXVIII, p. A. 3, Item 30, January 1951.

Kogan, S. Kh. (April 1959), "Attenuation of Electromagnetic Waves Propagating Along a Helical Wire Line," Radio. Eng. and Electr., 4, No. 2, pp. 35-42.

Kogan, S. Kh. (November 1959), "Propagation of Symmetrical Magnetic Waves on Helical Lines," Radio. Eng. and Electr. 4, No. 11, pp. 171-183.

Kornhauser, E. T. (August 1949), "Electromagnetic Wave Propagation in Helical Structures," Harvard University Cruft Laboratory Report TR-88.

Knott, E. F. et al (1965), "A Surface Field Measurement Facility," Proc. IEEE, 53, pp. 1105-1107.

Kraus, J. (1950), Antennas, McGraw-Hill Book Company, New York.

Laxpati, S. and R. Mittra (February 1966), "A Study of the Equiangular Spiral Antenna," University of Illinois Antenna Laboratory Report TR-65-20, AFAL-TR-65-330.

Lee, W. C. (1960), "Analysis of a Non-Planar Equiangular Spiral Antenna," M. S. Thesis, Ohio State University Technical Report 903-15.

Lyon, J. A. M., et al (April 1965), "Study and Investigation of a UHF-VHF Antenna," The University of Michigan Radiation Laboratory Final Report 5549-1-F, AFAL-TR-65-64, AD 462895.

Lyon, J. A. M. et al (July 1965), 'Study and Investigation of a UHF-VHF Antenna," The University of Michigan Radiation Laboratory Interim Report 7140-1-T, AD 471835.

Lyon, J. A. M., et al (October 1965), "Ferrite Loading Effects on Helical and Spiral Antennas," 15th Annual Symp. USAF Antenna Res. and Dev., Monticello, Illinois. Paper RL-322.

Lyon, J. A. M., et al (July 1966), "Study and Investigation of a UHF-VHF Antenna," The University of Michigan Radiation Laboratory Final Report 7140-1-F, AFAL-TR-66-11.

Maclean, T. S. M. (1962), "The Helical Aerial, a Comparative Study of the Tape Helix Approach," University of Birmingham Electrical Engineering Department Memo 108.

Maclean, T. S. M. and W. Farvis (September 1962), "The Sheath Helix Approach to the Helical Aerial," Proc. IEE, London, V, 109, Part C, No. 16, pp. 548-555.

Maclean, T. S. M. and R. Kouyoumjian (December 1959), "The Bandwidth of Helical Antennas," Trans. IEEE, AP-7, pp. S379-386.

Marcuvitz, N. (1964), Waveguide Handbook, Boston Technical Publications, Lexington, Mass.

Marsh, J. A. (June 1951), "Current Distribution on Helical Antennas," Proc. IRE, 39, No. 6, p. 668

McClelland, O. (May 1962), "An Investigation of the Near Fields on the Conical Equiangular Spiral Antenna," The University of Illinois Technical Report 55, AD 276463.

Medved, D. B. (May 1957), "An Electronic Scan Using a Single Ferrite Aperture," Convair Report ZN-309, pp. 19-21.

Mei, K. K. (1965), "On the Integral Equations of Thin Wire Antennas," Trans. IEEE, AP-13, p. 374.

Mikazan, P. (1960), "Diffraction of Electromagnetic Waves at the Open End of a Helical Waveguide," Radio Eng. and Electr., 5, No. 3, pp. 69-81.

Mittra, R. and P. Klock (May 1966), "A Theoretical Study of the Conical Spiral Antenna," University of Illinois Antenna Laboratory Report 66-1, AFAL-TR-66-114.

Mittra, R. and S. Laxpati (April 1964), "Propagation in a Waveguide with Glide Reflection Symmetry," University of Illinois Antenna Laboratory Report 75.

Moizhes, B. Ia. (June 1958), "On the Theory of Electromagnetic Wave Propagation on a Helix," Soviet Phys. Tech. Phys., 3, No. 6, pp. 1196-1201.

Moore, R. and R. Beam (1963), "Small Antenna Arrays Utilizing Distributed Loading," IEEE Wescon Papers, 7, Pt. 1, No. 19. 4

Morgan S. P. and J. H. Young (1956), "Helix Waveguide," Bell Sys. Tech. J., 35, p. 1347.

Morse, P. and H. Feshbach (1953), Methods in Theoretical Physics, McGraw-Hill Book Company, New York

National Bureau of Standards (1947), Table of Bessel Functions $J_0(z)$ and $J_1(z)$ for Complex Arguments, Columbia Press, New York.

National Bureau of Standards (1950), Table of Bessel Functions $Y_0(z)$ and $Y_1(z)$ for Complex Arguments, Columbia Press, New York.

New, R. (June 1960), "Ferromagnetic Antennas," IEEE Milicon Papers, 4, pp 133-137.

Olving, S. (1955), "Electromagnetic Wave Propagation on Helical Conductors Embedded in a Dielectric Medium," Chalmers Univ. Technology Translation No. 156.

Page, L. (1946), "The Magnetic Antenna," Phys. Rev., 69, pp. 645-648

Patton, W. T. (September 1962), "The Backfire Bifilar Helical Antenna," Ph.D Thesis, University of Illinois, see also, Technical Report 61, AD 289084.

Phillips, R. (October 1950), "The Electromagnetic Field Produced by a Helix," Q. of Appl. Math., 8, No. 3, pp. 229-246.

Pierce, J. (1950), Travelling Wave Tubes, D. VanNostrand, New York.

Pierce, J. R. and P. K. Tien (September 1954), "Coupling of Modes in Helices," Proc. IRE, 42, pp. 1389-1396.

Polk, C. (December 1959), "Resonance and Supergain in Loaded Antennas," Trans. IEEE, AP-7, pp. 414-423.

Rumsey, V. and W. Weeks (1956), "Electrically Small Ferrite Loaded Loop Antennas," IEEE Nat. Conv. Rec., Part 1, p. 165.

Schroeder, K. (December 1964), "Miniature Slotted-Cylinder Antennas," Microwaves, 3, pp. 28-37.

Sensiper, S. (May 1951), "Electromagnetic Wave Propagation on Helical Conductors," MIT Research Laboratory of Electronics Technical Report 194.

Sensiper, S. (February 1955), "Electromagnetic Wave Propagation on Helical Structures: A Review and Survey of Present Progress," Proc. IRE, 43, pp. 149-161.

Serracchioli, F. and C. Levis (December 1959), "The Calculated Phase Velocity of Long Endfire Uniform Dipole Arrays," Trans. IEEE, AP-7, pp. S 424-434.

Shanks, H. and V. Galindo (1959), "Ferrite Excited Slots with Controllable Amplitude and Phase," IRE Nat. Conv. Record, 7, Pt. 1, pp. 88-92.

Sharp, E. D. and E. M. T. Jones (March 1962), "An Antenna Array of Longitudinally-Slotted Dielectrically Loaded Waveguides," Trans. IEEE, AP-10, pp. 179-187.

Shestopalov, V. P. et al (July 1961), "Theoretical and Experimental Investigations of Helix-Dielectric Aerials," Radio. Eng. and Electr. 6, No. 7, pp. 159-172.

Shestopalov, V. P. et al (March 1962), "Brief Communications, Electromagnetic Radiation by Helical Ferrite Antennas," Radio Eng. and Electr., 3, pp. 533-535.

Shestopalov, V. P. and B. Kondrat'ev (June 1960), "Spatial Resonance in a Helix in a Ferrite," Soviet Phys., Tech. Phys., 4, No. 12, pp. 1326-1345.

Shestopalov, V. P. and V. Slyusarskii (May1960), "Study of Helix-Anisotropic and Helix-Ribbed Structures in Slow Wave Systems," Soviet Phys., Tech. Phys., 4, No. 11, pp. 1212-1222

Shestopalov, V. P. and K. Yatsuk (1960), "The Use of Slow Surface Waves for Measuring the Dielectric Permittivity of Materials at High Frequency," Soviet Phys., Tech. Phys, Part I; 4, No. 7 (Jan 60) , Part II, 4, No. 9 (March 1960), Part III, 4, No. 11 (May 1960).

Sigelman R and A Ishimaru (May 1965), "Radiation from Periodic Structures Excited by an Aperiodic Source," Trans. IEEE, AP-13, pp. 354-364.

Smirnov, N. (1958), "Propagation of Electromagnetic Waves in Circular Waveguides with Periodic Slots," Soviet Phys., Tech. Phys., 28, p. 1494.

Stephenson, D. and P. Mayes (1963), "Log Periodic Helical Dipole Arrays," IEEE Wescon Papers, 7, Pt. 1, No. 19.3, 6 pp.

Stewart, J. (1957), "On Ferrite Loop Antenna Measurements," IRE Nat. Conv. Rec. pp. 42-48.

Suhl, H. and L. Walker (July 1954), "Topics in Guided Wave Propagation Through Gyrotropic Media, Part II: Transverse Magnetization and the Non-reciprocal Helix," Bell. Sys. Tech. J., 33, pp. 939-986.

Swift, D. and D. Hook (1958), "Dispersion Curves for a Helix in a Glass Tube," Proc. IEE London, 105B, Suppl. No. 11, p. 747.

Tamir, T. and A. Oliner (February 1963), "Guided Complex Waves," Proc. IEE, London, 110B, No. 2, pp. 310-335.

Tamir, T. and A. Oliner (February 1963), "The Spectrum of Electromagnetic Waves Guided by a Plasma Layer,". Proc. IEEE, 51, No. 2, pp. 317-332.

Tien, P. K. (November 1953), "Travelling Wave Tube Helix Impedance," Proc. IRE 41, No. 11, pp. 1617-1623.

Tien, P. K. (July 1954), "Bifilar Helix for Backward Wave Oscillators," Proc. IRE, 42, pp. 1137-1143.

Timirev, N. P. (1958), "A Conical Helix Antenna with a Constant Pitch Angle," Radio. i. elek., 13, No. 6, pp. 18-28.

Timirev, N. P. and A. Fedorenkov (April 1965), "Propagation of Non-symmetrical Waves Along a Conical Helix with Varying Parameters," Radio. Eng. and Electr., No. 4, pp. 646-648.

Tyras, G. and G. Held (1958), "Radiation from a Rectangular Waveguide Filled with Ferrite," Trans. IEEE, MTT-6, p. 268.

Unger, H. (November 1958), "Helix Waveguide Theory and Applications," Bell Sys. Tech. J., 37, No. 6, pp. 1599-1647.

Van Der Waerden, B. (1951), "On the Method of Saddle Points," Appl. Sci. Res., B2, pp. 33-45.

Wait, J. R. (June 1953), "The Receiving Loop with a Hollow Spheroidal Core," Can. J. Tech., 31, 132-137.

Walter, C. H. (1965), Travelling Wave Antennas, McGraw-Hill Book Company, New York.

Watkins, D. A. (1958), Topics in Electromagnetic Theory, John Wiley and Sons, New York.

Watkins, D. A. and E. Ash (June 1954), "The Helix as a Backward-Wave Circuit Structure," J. Appl. Phys., 25, pp. 782-790.

Wheeler, M. S. (January 1958), "Non-Mechanical Beam Steering by Scattering from Ferrites," Trans. IEEE, MTT-6, No. 1, pp. 38-42.

Whiteside, H. (October 1962), "Electromagnetic Field Probes," Harvard University Cruft Laboratory Technical Report 377, NRL Contract NR371-016.

Wong, J. Y. and R. S. Thomas (May 1959), "Bibliography on the Helical Beam Antenna," National Research Council of Canada, Radio and Electrical Engineering Division, Ottawa, Technical Report 5264.

Wong, J. Y. and R. S. Thomas (September 1959), "Effect of a Dielectric on the Bandwidth of a Helical Beam Antenna," National Research Council of Canada, Ottawa, Technical Report ERB-530.

Wu, P-R (April 1966), "The Effect of Dielectric Loading on the Near Field Amplitude for a Log Pyramidal Antenna, "The University of Michigan Radiation Laboratory Internal Memorandum 7260-517-M. See also U. S. Army Electronics Command Report ECOM-01263-4, AD 488 067, The University of Michigan Radiation Laboratory Report 7260-1-T.

Wu, P-R (1966), "Near Field Measurements," The University of Michigan Radiation Laboratory Internal Memorandum for Technical Report No. 7140-1-F, AFAL-TR-66-1-1.

Yakimenko, I. P. and V. Shestopalov (July 1962), "An Experimental Investigation of a Helix-Ferrite Waveguide," Radio Eng. and Electr. Phys., No. 7, p. 1047.

DISTRIBUTION LIST AF33(615)-3609 Proj. 07848

Destination	Number of Copies
Adams-Russell Company Library - Antenna Section 280 Bear Hill Road Waltham, Mass. 02154	1
Aero Geo Astro Security Officer Edsall and Lincolnia Blvd. Alexandria, Va.	1
Aerospace Corporation Robert C. Hansen 2400 E. El Segundo Blvd. Los Angeles, Calif. 90045	1
Cutler-Hammer Division, Airborn Instruments Labs. Librarian - Antenna Section Walt Whitman Road Melville, L.I., New York 11729	1
All Products Company Mr. James Buzbee Mineral Wells, Texas	1
Americal Electronic Laboratories, Inc. Antenna Section Box 552 Lansdale, Pa.	1
Andrew Alfred Consulting Engineers Librarian - Antenna Section 299 Atlantic Ave. Boston, Mass. 02110	1
AVCO Res. and Adv. Development Division Research Library 201 Lowell Wilmington, Mass. 01887	1
AVCO Electronic and Ordnance Division Technical Library 2630 Glendale-Milford Road Cincinnati, Ohio 45241	1
Bell Aircraft Corporation Technical Library - Antennas Buffalo, New York 14205	1
Bell Telephone Laboratories Inc. Technical Reports Library - Room 2A165 Whippany, New Jersey 07961	1

Bendix Radio Division
Technical Library - Dept. 462-4
East Joppa Road
Baltimore, Md. 21204 1

Bendix Research Laboratories
Technical Library
20800 10 1/2 Mile Road
Southfield, Michigan 48076 1

Boeing/Wichita - Antenna Systems Staff Unit
Technical Library
3801 South Oliver
Wichita, Kansas 67201 1

Boeing Aerospace Division
Technical Library - Antenna and Radomes
Box 3707
Seattle, Washington 98124 1

Bunker-Ramo Corporation, Defense Systems Div.
8433 Fall Brook Avenue
Canoga Park, California 91304 1

Canoga Electronics - Advanced Programs Dept
Box 2086
Canoga Park, California 91306 1

Chance-Vought Aircraft, Inc.
BuAer Representative
Technical Library - Antenna Section
Box 1500
Arlington, Texas 75222 1

Collins Radio Research Division
Technical Library
5200 C NE
Cedar Rapids, Iowa 52406 1

Collins Radio Corporation
Dr. Robert L. Carrel - Antenna Section
Dallas, Texas 75207 1

Dalmo Victor Company
Technical Library - Antennas
1515 Industrial Way
Belmont, California 1

Dorne and Margolin, Inc.
Technical Library - Antenna Section
29 New York Avenue
Westbury, L.I., N.Y. 11591 1

Douglas Aircraft MSSD Technical Library
Antenna Section
3000 Ocean Park Blvd.
Santa Monica, Calif. 90406 1

Dynatronics, Inc.
Technical Library - Antennas
Hwy 17 and 92 N. Castlebury
Orlando, Florida 1

Electronic Communications Research Division
Technical Library
1830 York Road
Timonium, Md. 1

Emerson and Cuminb, Inc.
E. J. Luoma
869 Washington St.
Canton, Mass. 02021 1

Fairchild Aircraft and Missiles Division
Technical Library - Antennas
Hagerstown, Maryland 1

Fairchild Hiller Corporation
Technical Library
1455 Research Blvd.
Rockville, Md. 20850 1

General Dynamics/Convair
Technical Library - Antennas
Grants Lane
P.O. Box 748
Fort Worth, Texas 76101 1

General Electric Electronics Laboratory
Technical Library
Electronics Park
Syracuse, New York 13201 1

General Electric Light Military Electronics Dept.
901 Broad Street
Utica, New York 13503 1

General Electric General Engineering Laboratory
Building 371, Room 478
Schenectady, New York 12305 1

General Electronics Laboratories, Inc.
Technical Library - Antennas
18 Ames Street
Cambridge, Mass 1

General Precision Laboratory
Technical Library - Antennas
63 Bedford Road
Pleasantville, N. Y. 1

Goodyear Aircraft Arizona Division
Antenna Department
Box. 85
Litchfield Park, Arizona 85340 1

Grumman Aircraft Engineering Corporation
Technical Library - Avionics Engineering
South Oyster Bay Road
Bethpage, N. Y. 1

Hallicrafters Company
Technical Library - Antennas
4401 West Fifth Avenue
Chicago, Illinois 60624 1

Hoffman Laboratories, Inc.
4501 North Arden Drive
El Monte, California 91734 1

Hughes Aircraft Corporation
Technical Library - Antennas
Centinela and Teale Streets
Culver City, California 90232 1

Hughes Aircraft Communications and Videosonics Div.
Antenna Section
1901 West Malvern Avenue
Fullerton, California 1

ITT Federal Laboratories
Technical Library - Antennas
500 Washington Ave.
Nutley, N. J. 07110 1

Laboratory for Electronics, Inc.
Antenna Department
1079 Commonwealth Avenue
Boston, Mass. 02115 1

Ling-Temco-Vought Military Electronics Div.
Librarian - Antennas
1200 Jupiter St.
Garland, Texas 1

Litton Systems, Amecom Division
Technical Library - Antennas
1140 E. W. Highway
Silver Spring, Md. 20910 1

Lockheed Marietta Division
South Cobb Drive
Marietta, Georgia 30061 1

Lockheed Electronic and Armaments System Office
P. O. Box 551
Burbank, California 91503 1

The Martin/Denver Division Headquarters
Antenna Laboratory Mail Nr. T-0453
P. O. Box 179
Denver, Colorado 80201 1

The Martin/Orlando Company
Technical Library - Microwaves
Box 5837
Orlando, Florida 1

The Martin/Baltimore Company
Technical Library - Antennas
Baltimore, Md. 21203 1

Maxon Electronics Corporation
Sunrise Highway
Great River, L. I., New York 11739 1

McDonnell Aircraft Corporation
Technical Library - Antennas
Box 516
St. Louis, Missouri 63166 1

Melpar, Inc.
Technical Library - Antennas
3000 Arlington Blvd.
Falls Church, Va. 22047 1

MITRE Corporation
Technical Library
Electronic Warfare Department D-21
Middlesex Turnpike
Bedford, Mass. 01730 1

Motorola Western Military Electronics Division
8201 E. McDowell
Scottsdale, Arizona 85252 1

North American Aviation, Inc.
Technical Library - Dept. 56
International Airport
Los Angeles, California 90009 1

North American Aviation, Autonetics Division
System Technology Department
3370 Miraloma Avenue
Anaheim, California 92803 1

North American Aviation/Columbus Division
Technical Library - Engineering Dept.
4300 E. Fifth Avenue
Columbus, Ohio 43216 1

Northrop/Norair Division
3901 West Broadway
Technical Information (3924-3)
Hawthorne, California 90250 1

Northrop/Ventura
Technical Information Center
1515 Rancho Conejo Blvd.
Newbury Park, Calfironia 91320 1

Philco Communications and Electronics
Government and Industrial Division
Technical Library - Antennas
4700 Wissachickon Ave.
Philadelphia, Pa. 19144 1

Radiation Systems, Inc.
Engineering Department
440 Swann Avenue
Alexandria, Va. 1

Radiation Products Division
Technical Library
Box 37
Melbourne, Fla. 31511 1

RCA Missile and Service Radar Division
Manager, Antenna Engineering Skill Center
Marne Highway
Moorestown, New Jersey 08057 1

Rantec Corporation
Librarian - Antenna Laboratory
24003 Ventura Blvd.
Calabasas, California 91302 1

Raytheon Equipment Division
Library - Mr. J. Portsch
P. O. Box 520
Waltham, Mass. 02154 1

Raytheon Missile Systems Division
Research Library
Hartwell Street
Bedford, Mass. 1

Raytheon Space and Information Systems Div.
528 Boston Post Road
Sudsbury, Mass. 1

Sanders Associates
Librarian - Antennas
95 Canal Street
Nashua, New Hampshire 1

Sichak Associates.
Mr. W. Sichak
518 Franklin Ave.
Nutley, New Jersey 1

HRB Singer Corporation
Attn: Library - Antennas
Box 60, Science Park
State College, Pa. 16801 1

Southwest Research Institute
Librarian - Antenna Laboratory
8500 Culebra Road
San Antonio, Texas 78206 1

Space Technology Laboratory
Research Library
One Space Park
Redondo Beach, California 90278 1

Sperry Gyroscope Division
Librarian - Antenna Laboratory
Great Neck, L. I., New York 11020 1

Sperry Microwave Electronics Division
Librarian - Antenna Laboratory
Box 1828
Clearwater, Florida 1

Stanford Research Institute
Librarian - Antennas
333 Ravenswood Street
Menlo Park, California 94025 1

Sylvania Electronic Products
Librarian - Antennas
Box 188
Mountain View, California 1

Sylvania Electronic Systems Division
Librarian - Antennas and Microwaves
40 Sylvan
Waltham, Mass 02154 1

Teledyne Communications System Division
12964 Panama Street
Los Angeles 66, California 1

Texas Instruments, Inc.
Librarian - Antennas
13500 N. Central Expressway
Dallas, Texas 75209 1

A. S. Thomas, Inc.
Librarian - Antennas
355 Providence Highway
Westwood, Mass. 02091 1

Westinghouse Aerospace Division
P. O. Box 746
Baltimore, Md. 21203 1

Wheeler Laboratories
Librarian - Antennas
Box 561
Smithtown, New York 11787 1

AFCRL C. J. Sletten CRD L G Hanscom Field Bedford, Mass. 01731	2
AFETRL - Technical Library Patrick AFB, Bla. 32925	1
AFMDC - Technical Library Holloman AFB, New Mexico 88330	1
APGC, Hq. 3208 Test Group Eglin AFB, Fla. 32542	1
ASD - ASEP B. Brooks Wright-Patterson AFB, Ohio 45433	1
RADC - EMATA, Griffiss AFB, New York 13442	1
RADC EMLT-1 Griffiss AFB, New York 13442	1
RADC EMIAD - R F Davis Griffiss AFB, New York 13442	1
SEG - SEAEM Mr. Mulligan Wright-Patterson AFB, Ohio 45433	1
SEG - SEACC Y. E. Stahler Wright-Patterson AFB, Ohio 45433	1
SEG - SEPIE Wright-Patterson AFB, Ohio 45433	1
AFSC - SCSE Andrews AFB, Wash. D. C. 20331	1
RTD - RTGS Bolling AFB, Washington, D. C. 20332	1
Hq, USAF, AFRDR, Lt. Col. B. Lieber Washington, D. C. 20330	1
Hq, USAF AFXSAI, Air Battle Analysis Center Dep. Dir. Plans for War Plans Washington, D. C. 20330	1
RTD RTHR Bolling AFB, Washington, D. C. 20332	1
FTD TD-EE Wright-Patterson AFB, Ohio 45433	1

U. S. Army Electronics Command
SIGRA/NAI
Ft. Monmouth, N J 1

U. S. Army White Sands Missile Range
Technical Library ORDBS-OM RR-312
White Sands, New Mexico 88002 1

Ballistic Research Laboratory
Technical Library - Antennas
Aberdeen Proving Ground, Md. 21005 1

Harry Diamond Laboratories
Connecticut Ave., and Vann Ness Street, NW
Attn: 240
Washington, D. C. 20438 1

U S Army Electronics R and D Activity
SELWS-ED
White Sands Missile Range, N. Mexico 88002 1

USAFSS
ESD/ESG Mr. A. Martinez
San Antonio, Texas 78241 1

Director, Surveillance Dept.
Evans Area
Technical Document Center
Belmar, New Jersey 1

ONR Branch Office
Box 39
FPO, New York 09510 1

Chief, Bureau of Ships
Code 312
Main Navy Building
Washington, D. C. 20360 1

Naval Research Laboratory
Code 5200
Washington, D. C. 20390 1

U S Naval Air Test Center
WSST-54, Antenna Section
Patuxent River, Md. 20910 1

Materials Laboratory
New York Naval Shipyard
Code 932
Brooklyn, N. Y. 11201 1

U. S. Navy Electronics Laboratory
Code 3220 - Library
San Diego, California 92152 1

U. S. Naval Ordnance Test Station
Mr. J. A. Mosko - Code 4021
China Lake, California 93557 1

U. S. Naval Ordnance Laboratory
Technical Library
Corona, California 91720 1

Office, Assist. Sec'y Def. R and D
Technical Library 3E1065, Pentagon
Washington, D. C. 20330 1

Air University Library
3T-AUL-59-30
Maxwell AFB, Alabama 36112 1

NASA Goddard Space Flight Center
Antenna Branch
Greenbelt, Md. 20771 1

V. DeSanti, Exchange Section DCD
Scientific/Technical Information Facility
P O Box 5700
Bethesda, Md. 1

GIT Engineering Experiment Station
Technical Library - Electronics Division
Atlanta, Ga. 30313 1

JHU Applied Physics Laboratory
8621 Georgia Avenue
Silver Springs, Md. 20910 1

JHU Carlyle Barton Laboratory
Charles and 34th Streets
Baltimore, Md. 22218 1

MIT-Lincoln Laboratory
Document Room
Box 73
Lexington, Mass. 02173 1

New Mexico State University
Antenna Department
Physical Science Dept.
University Park, New Mexico 1

Northeastern University
Dodge Library
Boston, Mass. 02115 1

Ohio University
Technical Library - EE Dept.
Athens, Ohio 1

Ohio State University Research Foundation
Technical Library - Antenna Laboratory
2024 Neil Ave.
Columbus, Ohio 43210 1

Ohio State University Antenna Laboratory
Technical Library
1320 Kinnear Road
Columbus Ohio 43212 1

PIB Microwave Research Institute
Professor A. A. Oliner
55 Johnson St.
Brooklyn, N. Y. 11201 1

Stanford Electronics Laboratory
Librarian - Antennas
Stanford, California 94025 1

Syracuse University
Dr. Jose Perihi - Electrical Engineering Dept.
Syracuse, N. Y. 13210 1

University of Dayton Research Institute
Professor Douglas Hanneman
300 College Park
Dayton, Ohio 45409 1

University of Southern California
W. V. Trusch - EE Dept.
University Park
Los Angeles, California 90007 1

University of Texas - EE Res. Lab.
Route 4
Box 189
Austin, Texas 1

AF 33(615)-3609 Proj. 07848

Cornell Aeronautical Laboratory Research Library Buffalo, New York 14221	1
University of Illinois EE Res. Laboratory Engineering Experiment Station Urbana, Illinois	1
Air Force Avionics Laboratory AVWE-3 Wright-Patterson AFB, Ohio 45433	5 +reproducible
Defense Documentation Center Alexandria Virginia 22314	20 + card
	163 + reproducible

UNCLASSIFIED

Security Classification

DOCUMENT CONTROL DATA - R&D

(Security classification of title, body of abstract and indexing annotation must be entered when the overall report is classified)

1. ORIGINATING ACTIVITY (Corporate author)
The University of Michigan Radiation Laboratory
Department of Electrical Engineering
Ann Arbor, Michigan 48108

2a. REPORT SECURITY CLASSIFICATION
UNCLASSIFIED

2b. GROUP

3. REPORT TITLE
Helical and Log Conical Helical Antennas Loaded with an Isotropic Material.

4. DESCRIPTIVE NOTES (Type of report and inclusive dates)
Quarterly Report No. 3. 1 August through 31 October 1966

5. AUTHOR(S) (Last name, first name, initial)
Rassweiler, George G.

6. REPORT DATE	7a. TOTAL NO. OF PAGES	7b. NO. OF REFS
November 1966	139	128

8a. CONTRACT OR GRANT NO.	9a. ORIGINATOR'S REPORT NUMBER(S)
AF 33(615)-3609	
b. PROJECT NO. 6278	7848-3-Q
c. Task 01	9b. OTHER REPORT NO(S) (Any other numbers that may be assigned this report)
d.	--

10. AVAILABILITY/LIMITATION NOTICES
Subject to special Export Controls (DoD Dir. 203. 4AFR400-10); not to be disseminated to OTS. Qualified requestors may obtain copies from DDC.

11. SUPPLEMENTARY NOTES	12. SPONSORING MILITARY ACTIVITY
	Air Force Avionics Laboratory Research and Technology Division, AFSC Wright-Patterson AFB, Ohio 45433

13. ABSTRACT

The determinental equation for a bifilar tape helix loaded inside with a full core of isotropic material is numerically solved for the complex propagation parameter of the primary current wave as a function of frequency. The results of the tape helix calculation are compared to a simplified slow-wave, inside-loaded sheath helix solution. Both methods show that such an antenna with a small pitch angle ψ has a diameter reduction factor for backward fire radiation of approximately $\sqrt{(1/\mu+1)/(\epsilon+1)}$ where μ and ϵ are the relative permeability and permittivity constants, respectively. Thus, the loading does achieve diameter reduction by slowing the phase velocity of the primary current wave. The log-conical helix is considered as a gradually tapered helix. The effect of dielectric loading is found theoretically to greatly reduce the radiation attenuation rate, making long active zones and small cone angles necessary for complete radiation of the power from the source. The addition of ferrite to the loading causes less reduction in the radiation attenuation, which allows some reduction in antenna length.

Experimental verification with antenna patterns, radiation efficiency, and near field amplitude and phase measurements verify the theoretical diameter and phase velocity reduction calculations; the calculated radiation attenuation rate of a loaded helix is not quantitatively verified experimentally.

DD FORM 1 JAN 64 1473

UNCLASSIFIED

Security Classification

14. KEY WORDS	LINK A		LINK B		LINK C	
	ROLE	WT	ROLE	WT	ROLE	WT
Helical Antennas Conical Spiral or Conical Helix Antennas Reduction of Antenna Size Dielectric Loading of Antennas Ferrite Loading of Antennas Theoretical Solutions of Antennas Experimental Investigations of Antennas						

INSTRUCTIONS

1. ORIGINATING ACTIVITY: Enter the name and address of the contractor, subcontractor, grantee, Department of Defense activity or other organization *(corporate author)* issuing the report.

2*a*. REPORT SECURITY CLASSIFICATION: Enter the overall security classification of the report. Indicate whether "Restricted Data" is included. Marking is to be in accordance with appropriate security regulations.

2*b*. GROUP: Automatic downgrading is specified in DoD Directive 5200.10 and Armed Forces Industrial Manual. Enter the group number. Also, when applicable, show that optional markings have been used for Group 3 and Group 4 as authorized.

3. REPORT TITLE: Enter the complete report title in all capital letters. Titles in all cases should be unclassified. If a meaningful title cannot be selected without classification, show title classification in all capitals in parenthesis immediately following the title.

4. DESCRIPTIVE NOTES: If appropriate, enter the type of report, e.g., interim, progress, summary, annual, or final. Give the inclusive dates when a specific reporting period is covered.

5. AUTHOR(S): Enter the name(s) of author(s) as shown on or in the report. Enter last name, first name, middle initial. If military, show rank and branch of service. The name of the principal author is an absolute minimum requirement.

6. REPORT DATE: Enter the date of the report as day, month, year; or month, year. If more than one date appears on the report, use date of publication.

7*a*. TOTAL NUMBER OF PAGES: The total page count should follow normal pagination procedures, i.e., enter the number of pages containing information.

7*b*. NUMBER OF REFERENCES: Enter the total number of references cited in the report.

8*a*. CONTRACT OR GRANT NUMBER: If appropriate, enter the applicable number of the contract or grant under which the report was written.

8*b*, 8*c*, & 8*d*. PROJECT NUMBER: Enter the appropriate military department identification, such as project number, subproject number, system numbers, task number, etc.

9*a*. ORIGINATOR'S REPORT NUMBER(S): Enter the official report number by which the document will be identified and controlled by the originating activity. This number must be unique to this report.

9*b*. OTHER REPORT NUMBER(S): If the report has been assigned any other report numbers *(either by the originator or by the sponsor)*, also enter this number(s).

10. AVAILABILITY/LIMITATION NOTICES: Enter any limitations on further dissemination of the report, other than those imposed by security classification, using standard statements such as:

(1) "Qualified requesters may obtain copies of this report from DDC."

(2) "Foreign announcement and dissemination of this report by DDC is not authorized."

(3) "U. S. Government agencies may obtain copies of this report directly from DDC. Other qualified DDC users shall request through _____."

(4) "U. S. military agencies may obtain copies of this report directly from DDC. Other qualified users shall request through _____."

(5) "All distribution of this report is controlled. Qualified DDC users shall request through _____."

If the report has been furnished to the Office of Technical Services, Department of Commerce, for sale to the public, indicate this fact and enter the price, if known.

11. SUPPLEMENTARY NOTES: Use for additional explanatory notes.

12. SPONSORING MILITARY ACTIVITY: Enter the name of the departmental project office or laboratory sponsoring *(paying for)* the research and development. Include address.

13. ABSTRACT: Enter an abstract giving a brief and factual summary of the document indicative of the report, even though it may also appear elsewhere in the body of the technical report. If additional space is required, a continuation sheet shall be attached.

It is highly desirable that the abstract of classified reports be unclassified. Each paragraph of the abstract shall end with an indication of the military security classification of the information in the paragraph, represented as *(TS)*, *(S)*, *(C)*, or *(U)*.

There is no limitation on the length of the abstract. However, the suggested length is from 150 to 225 words.

14. KEY WORDS: Key words are technically meaningful terms or short phrases that characterize a report and may be used as index entries for cataloging the report. Key words must be selected so that no security classification is required. Identifiers, such as equipment model designation, trade name, military project code name, geographic location, may be used as key words but will be followed by an indication of technical context. The assignment of links, rules, and weights is optional.